



Návrh a ověření měřicí tratě pro výzkum supersonických ejektorů

Diplomová práce

Studijní program: N2301 – Mechanical Engineering
Studijní obor: 2302T010 – Machines and Equipment Design
Autor práce: **Anjelynn Mae Saligao Guanlao**
Vedoucí práce: doc. Ing. Václav Dvořák, Ph.D.





TECHNICAL UNIVERSITY OF LIBEREC
Faculty of Mechanical Engineering ■

Design and verification of a test rig for research of supersonic ejectors

Diploma thesis

Study programme: N2301 – Mechanical Engineering
Study branch: 2302T010 – Machines and Equipment Design
Author: **Anjelynn Mae Saligao Guanlao**
Supervisor: doc. Ing. Václav Dvořák, Ph.D.



DIPLOMA THESIS ASSIGNMENT

(PROJECT, ART WORK, ART PERFORMANCE)

First name and surname: **Anjelynn Mae Saligao Guanlao**
Study program: **N2301 Mechanical Engineering**
Identification number: **S14000516**
Specialization: **Machines and Equipment Design**
Topic name: **Design and verification of a test rig for research of supersonic ejectors**
Assigning department: **Department of Power Engineering Equipment**

R u l e s f o r e l a b o r a t i o n :

1. Perform a literature review of supersonic ejector and methodologies for measuring static pressure and mass flow using orifices and nozzles.
2. Study the test track of subsonic ejectors in laboratories.
3. Design a test rig for experimental research of supersonic ejectors, solve measurement of static and stagnation pressures and mass flows, propose adjustments for optical measuring.
4. Design all components and create drawings.
5. Design a simple ejector for verification of the test rig.
6. Verify the test rig by analytical and numerical computations and by experiments, process and describe the results.
7. Formulate conclusions.

Scope of graphic works: **20 pages**

Scope of work report
(scope of dissertation): **40 pages**

Form of dissertation elaboration: **printed**

Language of dissertation elaboration: **English**

List of specialized literature:

[1] **DVOŘÁK, V., 2010.** *Research and optimization of ejectors, habilitation work.* **Technická univerzita v Liberci.**

[2] **DVOŘÁK, V., 2013.** *Flow processes in ejectors, Ph.D. work.* **Technická univerzita v Liberci.**

Tutor for dissertation: **doc. Ing. Václav Dvořák, Ph.D.**
Department of Power Engineering Equipment

Dissertation Counsellor: **Ing. Jan Kracík**
Department of Power Engineering Equipment

Date of dissertation assignment: **18 November 2015**

Date of dissertation submission: **18 February 2017**


prof. Dr. Ing. Petr Lenfeld
Dean




doc. Ing. Václav Dvořák, Ph.D.
Head of Department

Liberec, dated: 18 November 2015

Prohlášení

Byla jsem seznámena s tím, že na mou diplomovou práci se plně vztahuje zákon č. 121/2000 Sb., o právu autorském, zejména § 60 – školní dílo.

Beru na vědomí, že Technická univerzita v Liberci (TUL) nezasahuje do mých autorských práv užitím mé diplomové práce pro vnitřní potřebu TUL.

Užiji-li diplomovou práci nebo poskytnu-li licenci k jejímu využití, jsem si vědoma povinnosti informovat o této skutečnosti TUL; v tomto případě má TUL právo ode mne požadovat úhradu nákladů, které vynaložila na vytvoření díla, až do jejich skutečné výše.

Diplomovou práci jsem vypracovala samostatně s použitím uvedené literatury a na základě konzultací s vedoucím mé diplomové práce a konzultantem.

Současně čestně prohlašuji, že tištěná verze práce se shoduje s elektronickou verzí, vloženou do IS STAG.

Datum: 27. 05. 2016

Podpis: 

ACKNOWLEDGEMENT

First of all, I would like to thank my thesis advisor doc. Ing. Václav Dvořák of the Department of Power Engineering Equipment at Technical University of Liberec. His valuable advice and guidance throughout the course of conducting this thesis helped me a lot in understanding and figuring out solutions to several problems encountered. He has been very patient and understanding especially during times when I was feeling so lost.

I would also like to thank my counsellor Ing. Jan Kracík of the Department of Power Engineering Equipment at Technical University of Liberec. He has helped me a lot with understanding a lot of things and encouraged me when the future seemed to be so bleak.

I would also like to thank the Czech Government, and the people involved in selecting recipients of the Czech Government Scholarship for Developing countries for giving me this amazing opportunity. Without the scholarship, none of these will be possible. I have learned and experienced so much in the past two years that totally changed me.

And finally, I would like to thank my family and my boyfriend. From the start of my study here, I have put the image of them in the finish line, cheering me on. The ride was long and tough, but we saw it through. I dedicate this work to my mother, Melita Guanlao. Making you proud is one of my main purposes in life.

Anjelynn Mae S. Guanlao
Author

Table of Contents

1.	Nomenclature	3
2.	Introduction	5
3.	Review of Related Literature	6
3.1	Supersonic ejector.....	6
3.1.1	One-dimensional analysis of supersonic ejectors	8
3.1.2	Numerical Analysis	11
3.1.3	Experimental Setup.....	12
3.2	Pressure measurement methods	13
3.2.1	Pressure measurement by wall tapping	14
3.3	Mass flow measurement methods.....	16
3.3.1	Pressure Differential Flow Meters.....	16
3.3.1.1	Orifice plates	16
3.3.1.2	Design standards based on ISO 5167-2 2003	19
4.	Test Rig Design.....	28
4.1	Design Requirements	28
4.1.1	Primary air inlet, chamber, and nozzle	28
4.1.2	Secondary air inlet, chamber, and nozzle	29
4.1.3	Mixing chamber.....	29
4.1.4	Diffuser and outlet pipe	29

4.2	Proposed design	30
4.3	Recommendation for optical measurements	37
5.	Analytical Solution.....	38
5.1	One-dimensional analysis	38
5.2	Losses.....	42
5.2.1	Losses in nozzles	43
5.2.2	Loss in constant-area section.....	45
5.2.3	Losses in diffusers	46
6.	Numerical Solution	48
7.	Results and Discussion.....	51
8.	Conclusion.....	61
9.	References	63

1. Nomenclature

The following nomenclature is used in this thesis.

a	Speed of sound	[m/s]
A	Cross-sectional area	[m ²]
c	Velocity	[m/s]
C	Coefficient of Discharge	[1]
c_p	Constant pressure specific heat	[J/kg K]
d, D	Diameter of duct/pipe/hole	[m]
e, E	Orifice plate thickness	[m]
f	Coefficient of friction	[1]
h	Specific enthalpy	[J/kg]
k	Turbulence kinetic energy	[J/kg]
l_s	Orifice depth	[m]
l_1, l_2	Pressure tap spacing	[m]
M	Mach number	[1]
\dot{m}, q_m	Mass flow rate	[kg/s]
p	Pressure	[Pa]
$q(\lambda)$	Aerodynamic function of mass flow	[1]
r	Specific gas constant	[J/kg K]
Ra	Surface roughness	[μ m]
Re	Reynolds number	[1]
s	Specific entropy	[J/kg K]
T	Temperature	[K]
v	Specific volume	[m ³ /kg]
x_c, y_c	Geometric constant for secondary nozzle	[m]
$z(\lambda)$	Aerodynamic function	[1]
α	Orifice plate bevel angle	[°]
β	Orifice to pipe diameter ratio	[1]
Γ	Entrainment ratio	[1]

ε	Expansibility factor/ dissipation	[1]
η	Efficiency	[1]
θ	Included half angle of secondary nozzle	[°]
Θ_{21}	Ratio of secondary and primary total temperatures	[1]
κ	Isentropic exponent	[1]
λ	Laval number	[1]
μ_{τ}	Friction velocity	[m/s]
ρ	Density	[kg/m ³]
τ_w	Wall shear stress	[Pa]
ψ	Flow coefficient	[1]
ω	Specific dissipation rate	[1/s]

Subscripts

() ₀	Stagnation conditions
() _{1,2,3,4,etc}	Static condition at section 1, 2, 3, 4, etc.
() _{01,02,03,04,etc}	Stagnation condition at section 1, 2, 3, 4, etc.
() _{cr}	Critical conditions
() _D	Diffuser
() _E	Ejector, primary nozzle exit
() _N	Nozzle
() _{max}	Maximum condition
() _{min}	Minimum condition

Superscripts

()'	Primary stream
()''	Secondary stream

2. Introduction

Supersonic ejectors are mechanical devices which are used in various industries for compression, transport, vacuum, and other purposes. Although it has been used for quite a long time, researchers still has a lot of work in their hands in accurately defining ejector characteristics, especially the mixing phenomenon occurring at the mixing chamber due to its complexity. Various factors must be taken into account such as wall friction, viscous effects of two streams mixing together, shockwaves occurring in the mixing chamber, and other losses. In this regard, designing and constructing a test rig for supersonic ejector is an important contribution to the research of these devices. Being able to change necessary parts as quickly and conveniently as possible brings an opportunity to increase the research capacity of the department.

This thesis focuses on the design and construction of a test rig for the purpose of supersonic ejectors. It will look at the various techniques that can be employed in measuring pressure and mass flow. The current design will use metallic materials which are opaque but adjustments to accommodate optical measuring will be proposed. The test rig shall be verified by analytical and numerical solutions.

3. Review of Related Literature

3.1 Supersonic ejector

A supersonic ejector is a mechanical device which uses a high pressure fluid to entrain another low-pressure fluid. It is used in various applications such as in refrigeration, vacuum technology, material transport, mixing of two streams, ventilation and air conditioning, and others. Although it can be found in different applications, the principle of operations is still the same in each case. Research involving ejectors, its different types, applications, and different approaches in analysis and characterizing its performance has been summarized in a review done by Sun and Earnes [1]. The principle of operation of a typical ejector is characterized by a high-pressure fluid transferring part of its energy to a low-pressure fluid and the resulting mixture is discharged at a pressure that lies between the primary fluid pressure and the suction pressure. The efficiency and performance of the ejector is based on the ability of the two inlet streams to mix and exchange energy. Figure 1a shows a typical ejector setup.

The high-pressure primary fluid accelerates to supersonic speed by passing through a convergent-divergent nozzle, converting pressure energy to kinetic energy, thus, producing a high velocity jet. At the end of the nozzle, the primary air is already at a pressure p'_1 , which is much lower than that of the secondary air. This causes the entrainment of the secondary air into the mixing chamber. The secondary stream is typically drawn from the atmosphere; therefore, its stagnation pressure is equivalent to atmospheric pressure. At section 1, as shown in Figure 1b, both streams should start to mix and have a mean static pressure equivalent to p_1 . In the mixing chamber, the primary and secondary streams combine. During the mixing of these two streams,

some part of the kinetic energy of the primary stream is transferred to the secondary stream,

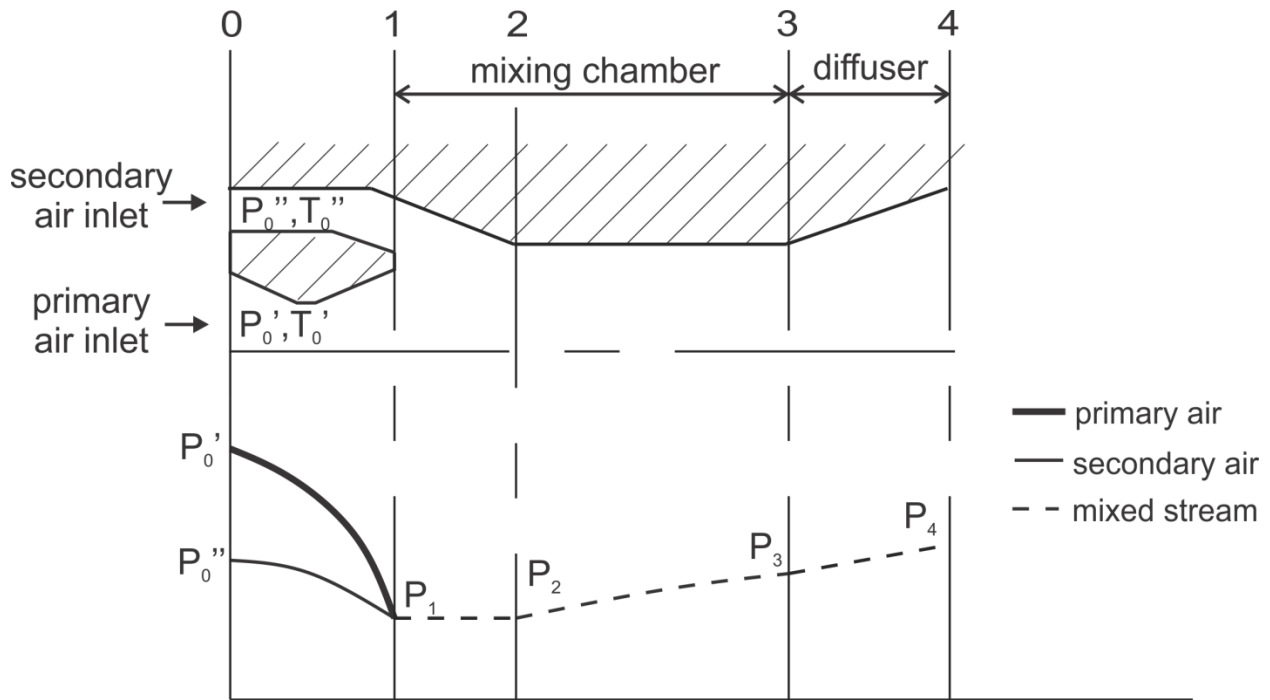


Figure 1. Typical ejector set-up. a) structure scheme, b) pressure variation along the ejector.

causing the secondary stream to increase its velocity. The other part of the kinetic energy of the primary stream is converted to pressure energy, increasing the pressure of the flow along the mixing chamber. And finally, a part of the kinetic energy of the mixed flow of the two streams is dissipated and converted into heat energy due to friction on the walls and viscous mixing. This process ideally ends at the end of the mixing chamber length where the two streams are assumed to be completely mixed and with the resulting static pressure of p_3 . At the end of the mixing chamber, a subsonic diffuser may be located which facilitates a re-compression process of the resulting stream to reach the back-pressure at the diffuser outlet, p_4 . Figure 2 shows us the enthalpy-entropy diagram of the process in the supersonic ejector. In this diagram, we show an idealized isentropic case, not showing losses in the nozzles and diffuser. However, the increase in entropy in the mixing chamber, between sections 2 and 3, is shown as Δs_m . This demonstrates that the mixing is assumed to be an irreversible adiabatic process.

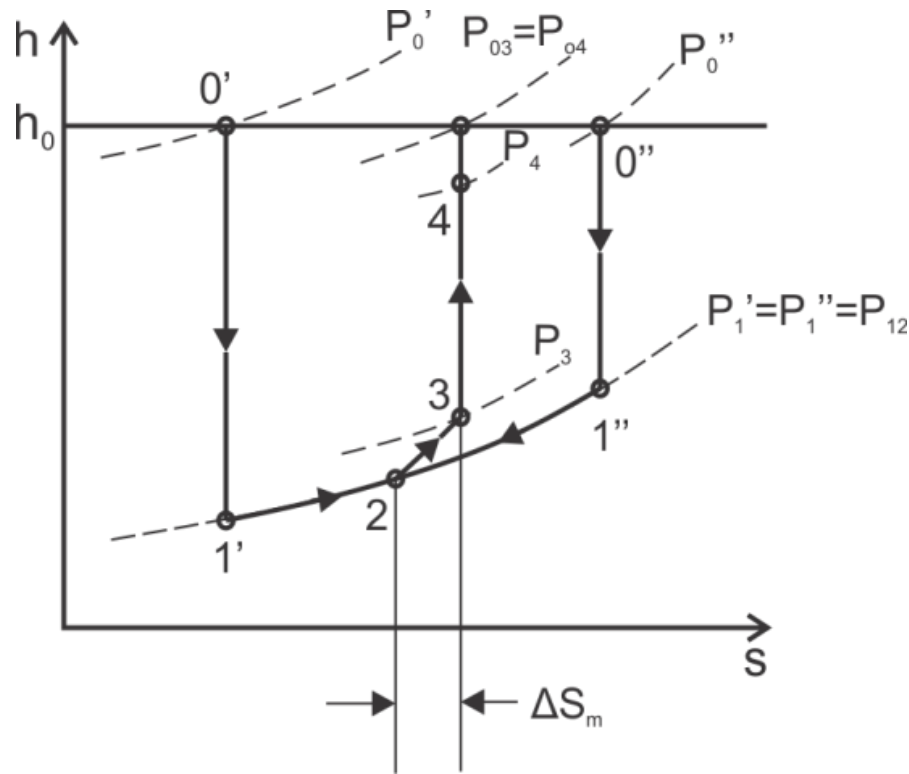


Figure 2. Enthalpy-Entropy diagram of the process in a supersonic ejector.

The main advantage of using supersonic ejector is the simplicity of the mechanical design, which involves no moving parts. This makes it relatively easy to install, operate, and maintain. However, one major drawback is the low efficiency. This is a huge opportunity for research and development to investigate ways to optimize the design and increase the efficiency of the ejector.

3.1.1 One-dimensional analysis of supersonic ejectors

Several researches have focused in the one dimensional analysis of supersonic ejectors. Keenan and Neumann [2] proposed a method of analysis of a simple air ejector with no subsonic diffuser after the mixing chamber. The simple air ejector is constructed as an axisymmetric ejector where the primary nozzle is at the same axis as the secondary inlet and the mixing chamber, as shown in Figure 1. The ejector is designed such that the mixing of the primary and secondary streams occurs in the constant cross-sectional area of the mixing chamber. They

calculated the performance of an ejector using one-dimensional continuity, momentum, and energy equations. The results of the simplified analysis were consistent and had a good comparison with the experimental results. Further into their research, Keenan et.al. [3] have identified two types of mixing: the constant-pressure and the constant-area mixing which is illustrated in Figure 3. They proposed an analysis considering both types of mixing occurring in the mixing chamber. Although the analytical solution proposed did not consider losses in the nozzles and diffusers and losses due to friction along the constant area mixing chamber, and it disregarded the fact that certain geometry of the constant-pressure mixing chamber is required for an actual constant-pressure mixing to occur, they have found a relatively good agreement between analytical and experimental results.

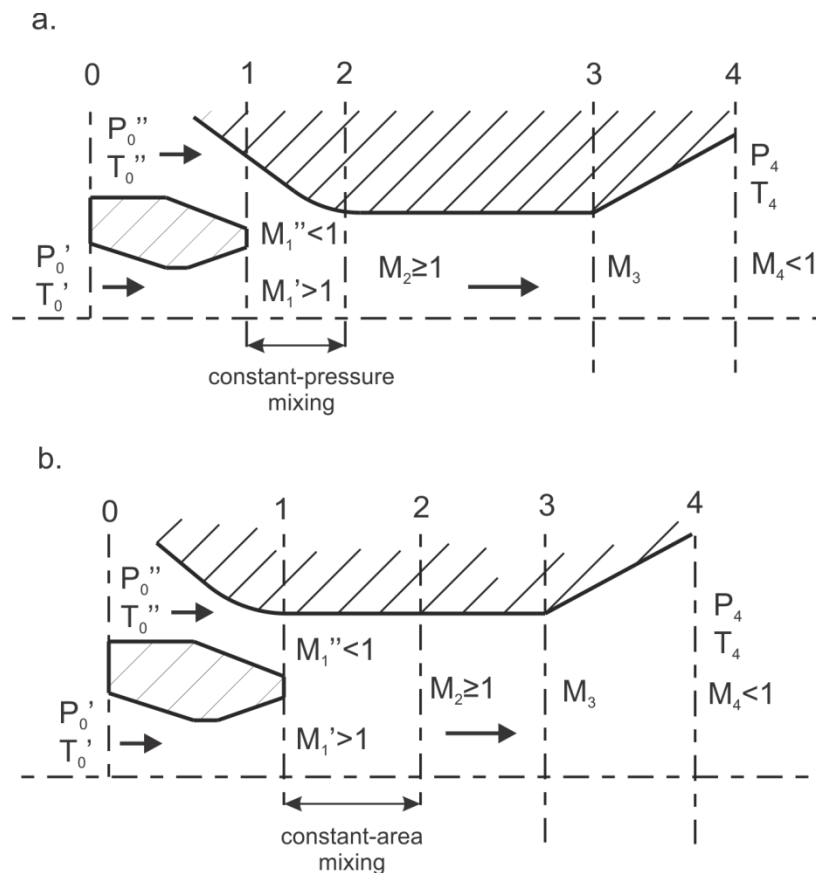


Figure 3. a) Constant-pressure mixing, b) Constant-area mixing

Dutton and Mikkelsen [5] investigated a constant area supersonic-supersonic ejector. They conducted a one-dimensional theoretical analysis of the constant area section and assumed inviscid mixing in the interaction region of the two streams. Comparing to the experimental results, they have found that such theoretical approach overpredicts the maximum compression ratios by as much as 15-22% higher. This error may be attributed to the simplicity of the approach employed to a very complex mixing phenomenon occurring in real life. The theoretical approach did not take into account mixing of the primary and secondary stream, boundary layer growth and separation, and shock wave/boundary layer/mixing layer interactions. They also found that the ejector is at high risk of flow separation of the secondary stream at the point of flow merging of the primary and secondary streams.

In the paper published by Kracik and Dvorak [6], they outlined a one-dimensional analytical method for predicting the flow in a supersonic ejector. Although the case discussed is attempted for application on an ejector with twelve supersonic annular primary nozzles, the basic isentropic equations are valid to an axisymmetric ejector with one primary nozzle placed in the axis of the mixing chamber. Losses in the primary and secondary nozzles were taken into account by obtaining a coefficient from the numerical solution. It was recommended to further study the friction and other losses due to mixing to have a better agreement between the analytical results and the experimental data.

A similar solution is discussed by Dvorak in his textbook [7]. For an axisymmetric ejector configuration as shown in Figure 3b, a one-dimensional analysis is performed and the end result is obtaining the entrainment ratio of a given ejector. The entrainment ratio, Γ , is defined as the ratio of the mass flow rates of the primary (\dot{m}') and secondary (\dot{m}'') streams at the respective inlets.

$$\Gamma = \frac{\dot{m}'}{\dot{m}''} \quad (2.1)$$

Several important assumptions have been made in order to simplify the analytical solution. The flow was considered to be steady and one-dimensional. It was assumed that no heat transfer occurs between the flow and the walls bounding it, making the case adiabatic. The primary and secondary streams of air was considered to be identical and to behave as an ideal gas, therefore, values of κ and c_p were considered to be constant and equal for the two inlets and the outlet stream. The stagnation conditions (pressure and temperature) were assumed to be constant at the primary inlet, secondary inlet, and the outlet of the mixing chamber and diffuser. Isentropic relations were used for calculations, and occurrence of shock waves was not considered.

3.1.2 Numerical Analysis

The first attempt into computational fluid dynamics (CFD) by ejector researchers was made by Hedges and Hill when they developed a finite-difference scheme to model the flow process inside an ejector. The development of solution schemes in CFD has been becoming easier due to reduction of computer cost relating to advancements in technology. Although time required setting up the correct mesh and the specialist knowledge required to set-up solutions is still a big drawback since convergence is quite difficult to achieve especially for cases with supersonic flow.[1]

In the paper by Bartosiewicz et.al.[4], the performances of six well-known turbulence models (k- ϵ , Realizable k- ϵ , RNG-k- ϵ , k- ω , k- ω -SST, and Reynolds stress model (RSM)) were evaluated for the study of supersonic ejectors. The validation focused on the shock location, shock strength, and the average pressure recovery prediction. The results of the numerical simulations were validated using axial pressure measurements with a capillary probe. Laser

tomography pictures were used to evaluate the non-mixing length. The results showed that the $k-\omega$ -SST model agrees best with experiments.

The same turbulence model is verified in the study conducted by Kolar and Dvorak[9] by comparing numerical results with experimental Schlieren color pictures and pressure measurements using pneumatic transducers. In their study, they utilized the Reynolds Averaged Navier-Stokes equation for the supersonic flow involving high Reynolds number. The study discussed in detail the turbulence model and analytically obtained model constants, which will be used later on to improve the accuracy. It has also detailed the boundary conditions and solver settings made using ANSYS Fluent.

3.1.3 Experimental Setup

In the paper of Keenan, et.al. [3], the experimental set-up of a test ejector is described and can be seen in Figure 4. Primary air is supplied from a compressor through a large receiver, which reduces fluctuations in the flow and a strainer to filter-out solid or liquid particles carried in the air flow. The high pressure primary air then passes through a length of straight pipe to further reduce disturbances in the stream before it enters the primary nozzle. There is a provision for the primary nozzle position to be adjusted, which is attached to the outside wall of the secondary chamber. The secondary air enters the mixing chamber through a pipe with straightening vanes, which has a control valve and a sharp edge orifice to measure secondary air mass flow.

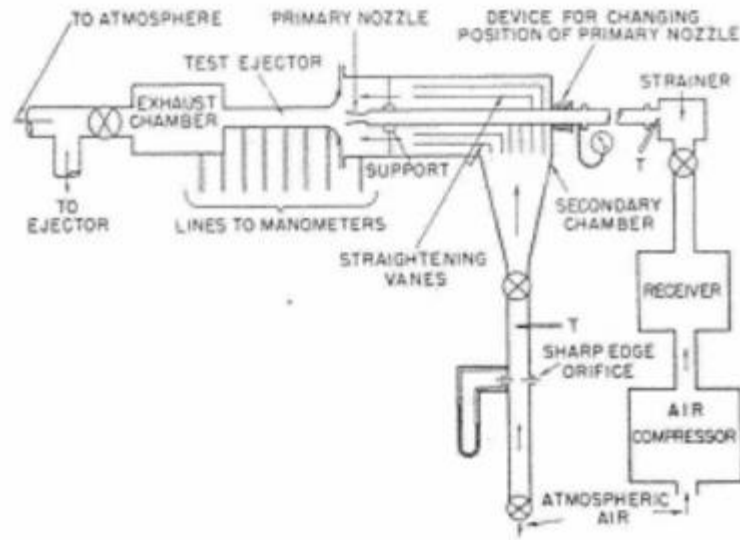


Figure 4. Diagram of test apparatus by Keenan et al.

Dutton, et al. [5], constructed a similar experimental apparatus where they tested five ejector configurations with varying Mach numbers and primary-to-secondary area ratios. The mixing chamber was designed such that mixing length can be varied for different tests.

3.2 Pressure measurement methods

Pressure measurement in fluid flow is essential in investigating flow properties. It may be required in order to determine several different flow parameters such as the thermodynamic properties, forces applied on a body due to the pressure distribution in the surface of the body, dynamic pressure and flow velocity, and others. By definition, pressure is a scalar quantity representing the molecular activity in a given fluid. This molecular activity is considered to be non-directional. Thus, pressure measurement must be done by a measuring device which is stationary relative to the flow. In fluid dynamics, we can classify pressure measured into two types: total or stagnation and static.[12]

Pressure is commonly measured both at the walls and in the freestream using different types of measurement devices shown in Figure 5 connected to a transducer of suitable sensitivity and range.[12] For the purpose of our study, we shall focus on pressure measurements using wall tapping since this is more suitable for the application.

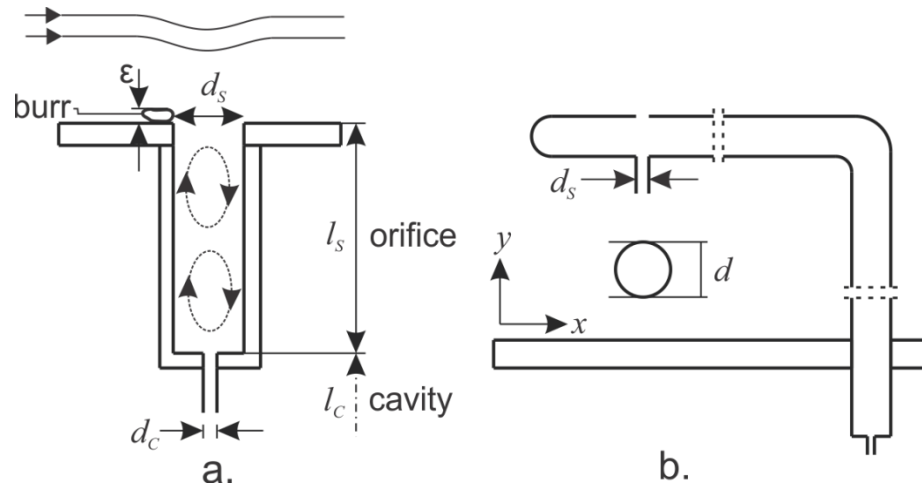


Figure 5. Static pressure measurement methods. a) Wall tapping b) Static probe.

Figure 5 shows us two possible methods of determining static pressure. First is by wall tapping, and second by a static tube. For the purposes of this study, we shall focus on the details of pressure measurement by wall tapping.

3.2.1 Pressure measurement by wall tapping

Wall tapping is a simple method of obtaining pressure at the wall, p_{wall} , of bounded flow. Although, care must be taken especially for more complicated flows like in the case of supersonic flows. The presence of the tapping affects the wall-bounded flow such that the streamlines are deflected into the hole and a system of eddies, also called cavity vortices, occurs within the orifice cavity. As a result, the recorded pressure at the wall is higher than the actual pressure value at the wall. Figure 5a shows us the typical geometry of a wall tapping.[13]

The restriction in the geometry of the wall tapping may be dictated by manufacturing capabilities or response time constraints. Some complication arises when the tapping diameter is larger than the boundary-layer thickness which may cause some changes in the flow field such as cavity vortices mentioned above, and thus, causes inaccuracies in the measurement. The finite size of tapping that can be conveniently manufactured may be large enough to affect some amount of error in the measured pressure, such that

$$p_{wm} = p_w + \Delta p_w, \quad (2.17)$$

where p_{wm} is the pressure measured at the wall, p_w is the actual pressure on the wall, and Δp_w is the error in the measured pressure. Performing a dimensional analysis, it is shown that, for a pressure tapping of given geometry in a zero-pressure-gradient flow, or in the case where the diameter of the pressure tap is much smaller compared to the scale of pressure variation along the wall, the non-dimensionalized Δp with respect to the wall shear stress τ_w is a function of the condition of the wall-bounded flow (laminar or turbulent) and of the following variables:

$$\pi = \frac{\Delta p}{\tau_w} = f\left(\frac{d_s u_\tau}{\nu}, \frac{d_s}{D}, M, \frac{l_s}{d_s}, \frac{d_c}{d_s}, \frac{\epsilon}{d_s}\right), \quad (2.18)$$

where d_s is the tapping diameter, $u_\tau = \sqrt{\tau_w/\rho}$ is the friction velocity, D is the flow lengthscale or the pipe diameter, M is the Mach number, l_s is the depth of the orifice, d_c is the diameter of the cavity behind the orifice connecting to the pressure sensor, ϵ is the root-mean-square height of the burrs on the edge of the tapping orifice, ρ is the fluid density, and ν is the kinematic viscosity. The actual pressure on the wall is, therefore, given by

$$p_w = p_{mw} - \pi \tau_w. \quad (2.19)$$

The complexity of the flow occurring near the pressure tapping means that analytical and numerical solutions currently available for the pressure error are only valid for very low

Reynolds number and /or two-dimensional geometries. From experiments conducted, majority of the data obtained are for turbulent flow over the orifice, and the comparisons of experiments show a quantifiable scatter between results. This can be observed in the results of the investigation on static pressure correction in high Reynolds number fully developed turbulent flow in pipes conducted by McKeon and Smits[13]. In the results, they have concluded that further studies and flow visualization may still be needed to clearly specify the dependence of the static pressure correction on the ratio of the pressure tap diameter and the pipe diameter. This may be due to the complicated nature of the experiments where the pressure error is the same order as the experimental uncertainty which also makes the quantification of the pressure error difficult.

3.3 Mass flow measurement methods

3.3.1 Pressure Differential Flow Meters

Flow meter techniques used for measuring mass flow rate in bounded flow are usually based on pressure difference measured across some change in the flow cross section area. These devices include orifice plates, venture tubes, and nozzles. These three devices work on the same principle and are only differentiated by the specific purpose or requirement of usage. For the purpose of this study, we will dive into more detail of the orifice plate, its principle and construction.

3.3.1.1 Orifice plates

This flow measuring device is implemented by obstructing the flow with a plate containing a round hole in the middle. The pressure difference between the upstream and downstream side of the plates is measured and the Bernoulli principle is employed to calculate the resulting mass

flow. The solution using the Bernoulli principle is only valid when the flow is subsonic. The solution assumes that the flow is incompressible and laminar. These assumptions are not all valid in real life, therefore losses due to flow turbulence are accounted for by the flow coefficient, C_f . The flow coefficient is an experimentally found value which is normally available in reference books. The value of the flow coefficient depends on the orifice and pipe diameters, and the flow's Reynolds number. Figure 6 shows a schematic of an orifice plate based on the ISO 5167 standard.[15]

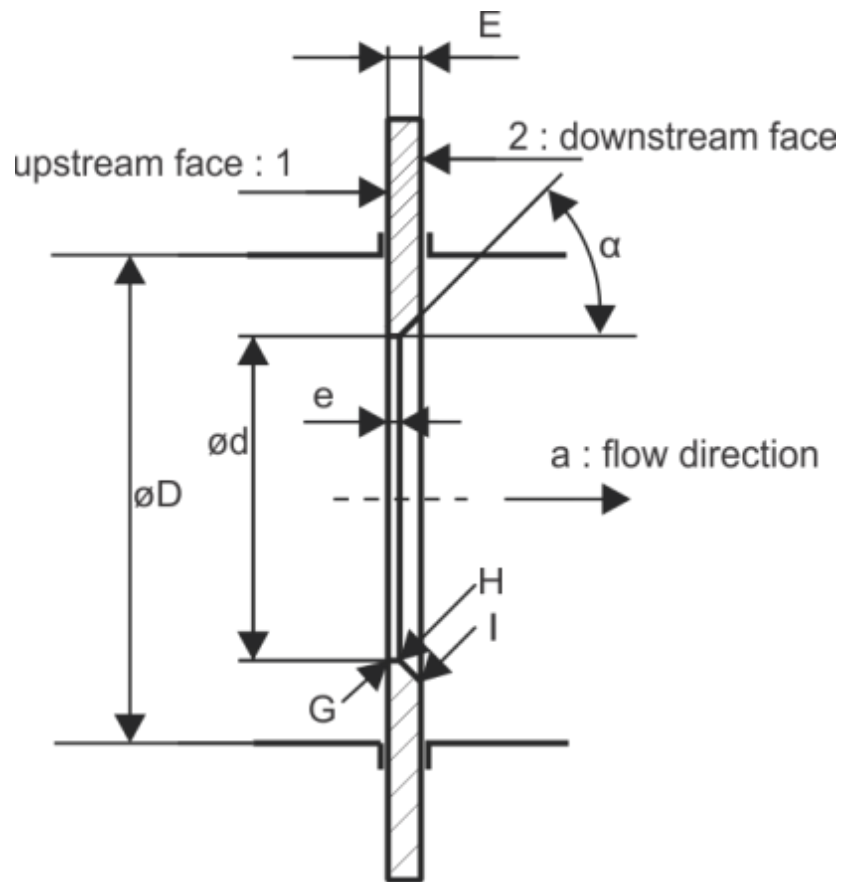


Figure 6. Orifice plate geometry based on ISO 5167

The mass flow rate, q_m , is given by

$$q_m = \frac{C}{\sqrt{1 - \beta^4}} \varepsilon \frac{\pi}{4} d^2 \sqrt{2\Delta p \rho_1} , \quad (2.20)$$

where C is the coefficient of discharge which is dependent on the Reynolds number, Re , and is given by the equation

$$\begin{aligned} C = & 0.5961 + 0.0261\beta^2 - 0.216\beta^8 + 0.000521 \left(\frac{10^6 \beta}{Re_D} \right)^{0.7} \\ & + (0.0188 + .00063A)\beta^{3.5} \left(\frac{10^6}{Re_D} \right)^{0.3} \\ & + (0.043 + .080e^{-10L_1} - 0.123e^{-7L_1})(1 - 0.11A) \frac{\beta^4}{1 - \beta^4} \\ & - 0.031(M'_2 - 0.8M'^{1.1}_2)\beta^{1.3} , \end{aligned} \quad (2.21)$$

where $D < 71.12$ mm, an additional term which is specified below shall be included to equation (2.21)

$$+0.011(0.75 - \beta) \left(2.8 - \frac{D}{25.4} \right),$$

where Re_D is the Reynolds number calculated with respect to the pipe diameter D , L_1 is the non-dimensional length of the distance of the upstream tapping equivalent to l_1/D , L_2 is the non-dimensional length of the distance of the downstream tapping equivalent to l_2/D , which is also consequently dependent on q_m , β is the diameter ratio d/D , d is the orifice hole diameter, Δp is the measured pressure difference between the upstream and downstream side of the orifice, ρ_1 is the density of the fluid being measured at the upstream side, ε is the expansibility factor given by

$$\varepsilon = 1 - (0.351 + 0.256\beta^4 + 0.93\beta^8) \left[1 - \left(\frac{p_2}{p_1} \right)^{\frac{1}{k}} \right]. \quad (2.22)$$

Note that the above equation is only applicable for values of $p_2/p_1 \geq 0.75$.

The advantage of using orifice plates to measure mass flow is its simplicity. However, main disadvantage is the relatively large pressure loss experienced when the flow passes through the plate. This loss is not recoverable; therefore, care should be taken so that it will be applied to applications where the pressure loss generated shall not influence the behavior of the flow being investigated.

3.3.1.2 Design standards based on ISO 5167-2 2003

The design guidelines have been described in high detail in the ISO 5167-2 2003. The standard includes guidelines for geometry, material, quality, inspection, and installation.

3.3.1.2.1 Orifice Plate

The standard orifice plate, as shown in Figure 6, is a circular plate with a concentric hole placed inside a pipe. The centerline of the pipe must coincide with the centerline of the plate. The upstream and downstream faces of the plate shall always be flat and parallel. Special attention should be done in designing and installing the plate such that the buckling and elastic deformation of the plate, caused by a certain magnitude of the differential pressure across the plate or any other forces, external or otherwise, shall not cause the flatness to exceed the limits set in the standard. This limit shall be discussed more in detail in the next sections.

3.3.1.2.1.1 Flatness and surface quality

We can identify the plate with its two surfaces: upstream face labelled as A, and downstream face labelled as B, as shown in Figure X. When possible, a distinctive mark to differentiate these two surfaces is recommended.

The upstream face A of the plate shall be flat when installed in the pipe with zero differential pressure across it. Measuring the flatness can be done with the plate removed from the pipe provided it can be proven that the method of mounting in the pipe does not, in any way, distort the plate. The flatness criterion that should be fulfilled is the measure of the maximum gap between the plate and a straight edge of length D laid across any diameter of the plate. This is demonstrated by Figure X. The gap, which is labelled “5” in figure X, should be less than $0.005(D - d)/2$. Alternatively, the maximum slope of the tangent line of the curvature of the plate should be less than 0.5% when the plate is uninstalled, and less than 1.0% under working conditions.

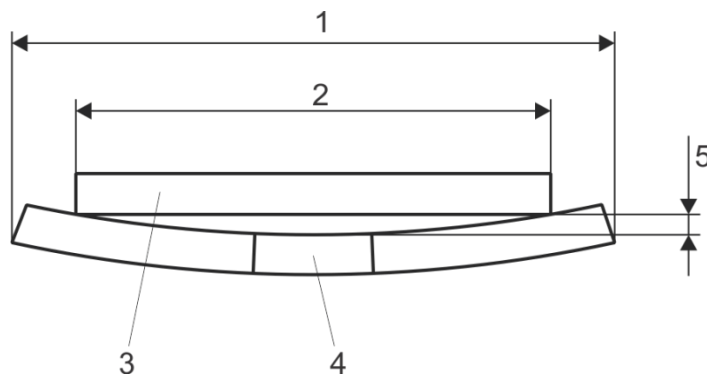


Figure 7. Orifice plate flatness measurement based on ISO 5167. 1) outside diameter of the orifice plate, 2) inside diameter of pipe, 3) straight edge, 4) orifice, 5) flatness deviation measured at the edge of orifice.

Surface quality criterion of upstream face A of the orifice plate shall satisfy $Ra < 10^{-4}d$ within a circle boundary with diameter not less than pipe diameter D , with center located at the

center of the orifice plate. Note that the roughness of the upstream face A of the orifice plate shall not, in all cases, affect the edge sharpness measurement of the orifice hole. In the event that the face does not satisfy the specified surface quality criterion during normal operation, it is recommended to re-polish or clean the surface within the diameter of at least D .

On the downstream face B, it is required to ensure that it is flat and parallel with the upstream face A. It is, however, unnecessary to manufacture the downstream face B in the same surface roughness quality as the upstream face A. Ultimately, the surface criteria for this side of the plate is not very strict that visual inspection is enough unless plate will be used to measure reversed flow as well.

3.3.1.2.1.2 Thickness E and e

The thickness criterion for e shall be $0.005D < e < 0.02D$ with a difference between e values measured at any two points within the plate not exceeding $0.001D$. The thickness of the plate E shall be $e < E < 0.05D$. For pipe diameters with size $50\text{mm} \leq D \leq 64\text{mm}$, orifice plate thickness E of up to 3.2 mm is acceptable. Also, do not forget to consider deflection requirements as stated in the last section.

For pipe diameters $D \geq 200$ mm, the difference of measured E between two points within the plate shall not be greater than $0.001D$. For pipe diameters $D < 200$ mm, the difference of measured E between two points within the plate shall not be greater than 0.2 mm.

3.3.1.2.1.3 Angle of bevel α

The downstream side of the orifice plate shall be beveled in the case when the thickness E of the plate exceeds the thickness e of the orifice. The angle of the bevel α shall be equal to $45^\circ \pm 15^\circ$.

3.3.1.2.1.4 Orifice edge quality

The upstream edge labeled G in Figure X shall be sharp and square. Edge radius shall not be greater than $0.0004d$ for the edge to be considered as sharp. For orifice with diameter $d \geq 25$ mm, the edge radius requirement can be satisfied by visual inspection. However, in the case when $d < 25$ mm, visual inspection is not sufficient. In any case, if there is doubt as to whether the edge sharpness requirement is met, measuring the edge radius is recommended. The upstream edge G should also be kept clear of wire-edges or burrs.

For the edge to be considered square, the angle between the orifice bore and the upstream face of the orifice plate should be $90^\circ \pm 0.3^\circ$. The orifice bore is the surface between edges G and H.

Strict requirements of the edge and surface quality are employed for this part of the orifice plate since it is in direct contact with the flow and we want to minimize external effects of non-conformity to the flow. However, the downstream edges H and I are within the separated flow region. Therefore, these edges do not have the same strict requirements as the upstream edges and surfaces.

3.3.1.2.1.5 Orifice diameter d

The lower limit for the diameter d shall be, in all cases, greater than 12.5 mm. The diameter ratio, $\beta = d/D$, shall always be $0.10 \leq \beta \leq 0.75$.

Measurements should be taken as the mean of at least four sampling diameters at approximately equal angles to each other. The orifice shall be cylindrical, such that, the maximum deviation from the mean diameter shall not exceed 0.05% of the mean diameter. As mentioned above, the surface quality of the cylindrical orifice bore shall not, in any way, affect the edge sharpness measurement of upstream edge G.

3.3.1.2.1.6 Bidirectional plate

Orifice plates can be designed such that, it can be also used to measure reversed flow. If so, certain requirements shall be fulfilled. Firstly, the plate shall not be beveled. Second, the two faces of the orifice plate shall comply to the surface and edge quality requirements of the upstream surface A and edge G, as mentioned previously. Third, the plate thickness E shall be equal to the orifice thickness e and so, it may be necessary to limit the differential pressure across the plate to prevent plate distortion. And lastly, for orifice plates with D and $D/2$ tappings, which will be discussed in the next section, measurements of pressure should still follow the upstream and downstream direction flow. Therefore, there should be D and $D/2$ pressure taps available on both sides of the orifice, and measurements will be taken depending on the direction of the flow.

3.3.1.2.1.7 Material

The plate may be manufactured from any type of material as long as the material will be suitable as to be able to satisfy all criterion stated above during normal operating conditions.

3.3.1.2.2 Pressure Tapping

For each orifice plate installed in a pipe, there should be at least one pressure tapping located at the upstream side of the orifice, and another one located at the downstream side. In the case of multiple tapping in one side of the orifice, the tapping shall be offset by 30° from each other. This is to minimize the effect of the flow disturbance of each tapping to the pressure measurements obtained by the subsequent pressure taps along the flow. The types of standard orifice meter are classified by the location of the pressure tapping: D and $D/2$, flange, or corner tapping. Limitation of each type is detailed in ISO 5167. For our purpose, we shall use the corner tapping with annular slot

3.3.1.2.2.1 Corner Tapping with annular slot

Corner taps with annular slot is another type of tapping location. The taps can be located in the flange. Figure 8 shows the schematic for this kind of tapping. Table 1 summarizes the design requirements for the corner tapping with annular slots.

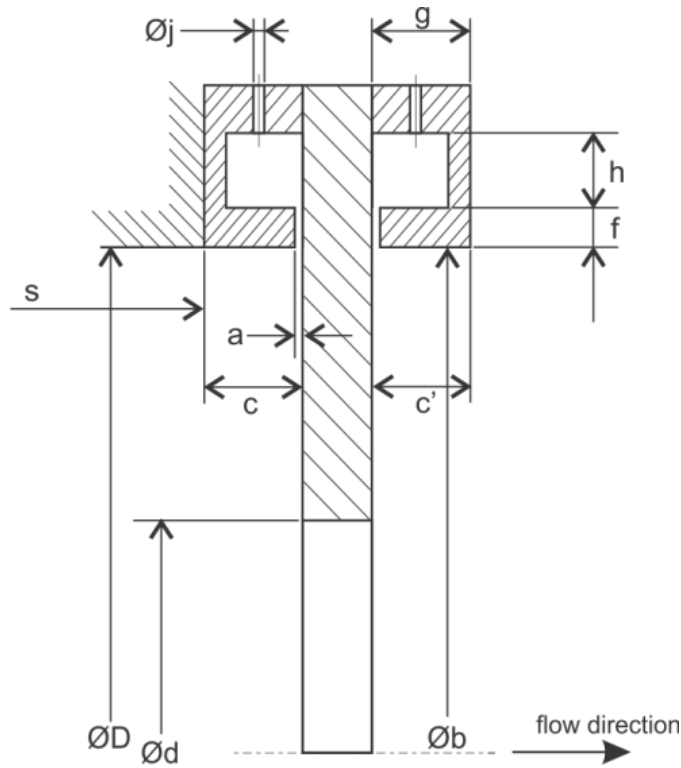


Figure 8. Corner tapping.

Table 1. Summary of design requirements for corner tapping with annular slot.

Symbol	Description	Requirement
a	Width of annular slot	<p>The minimum diameter is determined in practice and should be small enough to prevent accidental blockage and give satisfactory reaction time.</p> <p>For $D < 100mm$, a maximum value of $a = 2mm$ is acceptable for any β.</p> <p>The annular slot shall be continuous over the entire perimeter. Otherwise, four openings at equal angles apart shall connect the flow to the annular chamber. The each opening area is at least $12 mm^2$.</p>

b	Internal diameter of carrier rings	It shall be greater than or equal to diameter of the pipe D . Make sure that they do not protrude into the pipe, but $b \leq 1.04D$ is the maximum limit.
c, c'	Length of upstream and downstream rings	$c, c' < 0.5D$ It should also satisfy the following condition $\frac{b-D}{D} \times \frac{c}{D} \times 100 < \frac{0.1}{0.1 + 2.3\beta^4}$
$\emptyset D, \emptyset d$	Diameter of pipe, and orifice	
f	Thickness of the slot	$f \geq 2a$
g, h	Dimensions of annular slot	$gh \geq \frac{af}{2}$
$\emptyset j$	Diameter of pressure tapping	$4mm \leq j \leq 10mm$
s	Pipe length upstream	Refer to Table 3 of reference [15] for complete details.

3.3.1.2.2.2 Tapping conditions

The pressure tapping hole should be circular with a diameter less than $0.13D$ and less than 13 mm. There is no restriction on the minimum diameter of the pressure tapping, only that it should be small enough to prevent accidental blockage and to give satisfactory dynamic performance. Upstream and downstream tapping shall have equal diameters. The depth of the hole shall be at least 2.5 times the pressure tapping diameter, measured from the inner wall of the pipe.

The hole shall be cylindrical, with its centerline intersecting the pipe centerline within a perpendicularity of 3° . The hole shall be circular at break-through point. The edges shall be flush

with the surface of the pipe wall and shall be as sharp as possible. This means that no burrs or wire edges are allowed. These may be eliminated by rounding the edges, although radius of edge rounding must be kept as small as possible. If possible to measure, it shall not exceed 0.10 times the tap hole diameter. Conformity to cylindricity, perpendicularity, and edge quality may be evaluated through visual inspection.

The centerlines of the pressure tapping may be located in any axial plane around the pipeline. The axes of the upstream and downstream tapping may be located in different axial planes, but is normally located on the same axial plane.

4. Test Rig Design

4.1 Design Requirements

In this section, we identify the design requirements for each part of the test rig. These parts are identified as the primary air inlet, primary air chamber, primary air nozzle, secondary air inlet, secondary air chamber, secondary air nozzle, mixing chamber, diffuser, and outlet pipe. It is also important to discuss the requirements for the pressure and mass flow measurements in the various parts of the ejector. In all parts, ease of manufacturing, installation, and adjustment, where necessary, is primarily considered.

4.1.1 Primary air inlet, chamber, and nozzle

The primary air chamber shall be connected to the compressed air line using a standard connection. The compressed air is delivered into a chamber which shall be designed to withstand a maximum pressure of 3 MPa without bursting. At the primary air chamber, flow shall be conditioned or directed to deliver a uniform flow into the primary nozzle. Material should be able to withstand repeated usage, preferably with corrosion and wear resistance properties. In the primary air chamber, stagnation pressure shall be measured. The primary initial nozzle geometry is adapted from an existing design by [18]. It is intended to use the test rig for testing other nozzle geometry. The design shall include a provision for adjusting the horizontal position of the primary nozzle with respect to the mixing chamber. This feature shall be easy to operate. Air leaks shall be prevented where necessary.

4.1.2 Secondary air inlet, chamber, and nozzle

For the secondary air inlet, measurement of mass flow shall be done. The design shall include a provision for measuring the stagnation pressure of the secondary air before entering the mixing chamber. The design shall also include a mechanism for causing reduction in pressure at the secondary inlet.

4.1.3 Mixing chamber

The mixing chamber shall be connected directly to the secondary air chamber. The design shall provide access to the flow for static pressure measuring along the length of the chamber. The design shall be flexible to allow easy variation in the mixing chamber length. Design should also allow room for modifications for future development to allow optical measurement methods to be used.

4.1.4 Diffuser and outlet pipe

The design shall allow provisions to measure static pressure along the length of the diffuser. It shall also allow ease of change of this part to accommodate different possible designs and configuration of the diffuser. The design of the outlet pipe shall include a provision to measure the total mass flow rate at the outlet. The design shall also provide a mechanism to cause a pressure reduction at the outlet of the pipe, or also known as the backpressure.

4.2 Proposed design

Figure 9 illustrates the schematic diagram of the proposed test rig set up.

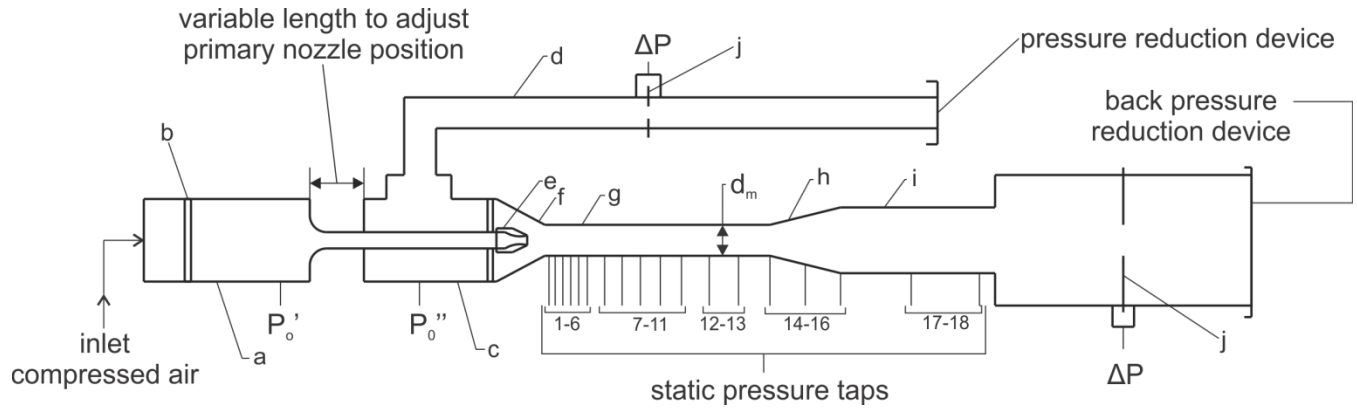


Figure 9. Proposed supersonic test rig set-up. a) primary air chamber, b) flow conditioner, c) secondary air chamber, d) secondary inlet duct, e) primary nozzle, f) secondary nozzle, g) mixing chamber, h) diffuser, i) outlet duct and j) orifice for mass flow measurement.

Compressed air up to 3MPa will be introduced into the primary air chamber, passing through a perforated plate acting as flow conditioner. The flow conditioner aims to condition the flow such that it will be uniform coming into the primary nozzle. Stagnation pressure of the primary air is measured in the primary air chamber. The secondary air is drawn from the atmosphere. A perforated plate may be attached at the inlet as a pressure reduction device. Secondary mass flow rate is measured using an orifice plate before coming in to the secondary air chamber, where the stagnation pressure of the secondary air is measured. The secondary flow is then directed into the mixing chamber where it mixes with the primary stream. Static pressure is measured along the length of the mixing chamber at given length intervals. The mixed flow then proceeds into the diffuser. Mass flow rate of the outlet stream is measured with an orifice plate. Finally, the outlet stream is released into the atmosphere. A similar perforated plate as the

one employed in the secondary inlet will be used as a back pressure reduction. The position of the nozzle can be adjusted by moving the secondary air chamber along the horizontal direction.

The tables shown below detail the design requirements for each segment of the ejector and the proposed solution.

Table 2 Design requirements and solutions for the primary air inlet, chamber, and nozzle

Primary air inlet, chamber, and nozzle	
<i>Design Requirements</i>	<i>Solution</i>
1. Connection to the compressed air line.	British Standard Straight Pipe thread G1/2.
2. Primary air chamber must withstand 3 MPa of internal pressure without bursting.	<p>The minimum thickness of the pipe wall to withstand bursting is calculated from the equation $T = \frac{S_f P D_I}{2S}$ where S_f is the safety factor, P is the internal pressure in Pascals, D_I is the pipe internal diameter in meters, and S is the yield strength of pipe material. The internal pipe diameter is chosen to be 0.03m. The ultimate strength of free-cutting brass is given in the range of 338-469 MPa [17].</p> <p>The minimum thickness of the pipe with a factor of safety of 5 is 0.5mm. The design is ensured to not have sections thinner than this value. Please refer to attached drawings of parts PRT0001, PRT0002, and PRT0009 contained in the Appendix.</p>
3. Provision for flow conditioning of	A plate with numerous holes was designed to

primary inlet stream.	condition the flow of the incoming high pressure air. This plate can be detached and replaced by a different configuration, if necessary. Please refer to attached drawing of part PLATE1.
4. Measurement of stagnation pressure.	An annular chamber is designed to measure the stagnation pressure of the primary air. The chamber has four air access holes around the perimeter for primary air to enter. It is designed such that the flow will ideally be at zero velocity at pressure measurement.
5. Establish a standard connection for primary nozzle.	The initial design is based on the nozzle used in [18]. Standard threaded attachment of M14x1 is chosen. For specific dimensions, please refer to attached drawing of part PRT0012.
6. Provision for horizontal adjustment of primary nozzle position with respect to mixing chamber.	Secondary air chamber (PRT0003) is designed such that it will be able to slide along PRT0012, which is the holder of the primary nozzle. PRT0003 is held in place by four set screws.

Table 3. Design requirements and solutions for secondary air inlet, chamber, and nozzle.

Secondary air inlet, chamber, and nozzle	
<i>Design Requirements</i>	<i>Solution</i>
1. Secondary inlet mass flow rate should be measured.	An orifice plate designed based on ISO 5167 standard is currently available in the laboratory. This can be reused and flange with tapping and ducts are necessary to be designed and manufactured.
2. Secondary stagnation pressure should be measured.	Similar to the experimental set up of [3] and [5], the wall pressure tap is located at the wall opposite the incoming secondary air flow.
3. Provision for pressure reduction at secondary inlet.	A cheap and easy way to regulate the pressure at the inlet of the secondary air is by attaching a perforated plate into the inlet of the duct. This may be designed by referencing the works of Gan and Riffat[20] and Malavasi, et al.[21]. A pressure loss coefficient given by $k = \frac{\Delta P}{1/2\rho c^2}$ is provided which is verified through experiments and numerical simulation.

Table 4. Design requirements and solutions for mixing chamber

Mixing chamber	
<i>Design Requirements</i>	<i>Solution</i>
<p>1. Static pressure measurement along the length of the mixing chamber. Reduce possible measurement error by minimizing the effect of flow disturbance caused by successive pressure taps.</p>	<p>Static pressure wall taps are manufactured into the mixing chamber wall. To reduce possible measurement error along the wall, the pressure taps were placed at radial axes 60° apart. In this way, flow disturbance caused by one pressure tap will not affect the next pressure tap along the line, but would rather get a chance to normalize before encountering the next pressure tap. Please refer to drawings of parts PRT0017 and PRT0018 for more details.</p>
<p>2. Mixing chamber shall be easy to install and design should provide for flexibility in the mixing chamber length.</p>	<p>The design of the mixing chamber is modular such that, the mixing chamber is a separate part from the secondary nozzle and diffuser. The length of the mixing chamber can easily be modified by taking out or adding additional parts. The geometry is simple. More details on design outline may be seen in Appendix X.</p>
<p>3. Design must provide room for future development of optical measurement.</p>	<p>The design may be easily adapted to suit transparent material like glass for optical measurement. Parts concerned will be parts PRT0005, PRT0017, PRT0018, and PRT0020.</p>

Table 5. Design requirements and solutions for diffuser and outlet duct

Diffuser and outlet duct	
<i>Design Requirements</i>	<i>Solution</i>
1. Static pressure measurement along the length of the diffuser. Reduce possible measurement error by minimizing the effect of flow disturbance caused by successive pressure taps..	Static pressure wall taps are manufactured into the diffuser wall. To reduce possible measurement error along the wall, the pressure taps were placed at radial axes 60° apart, similar to the scheme in the mixing chamber. Please refer to drawing of part PRT0027 for more details.
2. Diffuser must be easy to assemble and provide a possibility to change the configuration.	The diffuser is designed as a separate part from the mixing chamber. This makes it easier to manufacture and provides the possibility to change the design without manufacturing a new mixing chamber. Please refer to the drawing of part PRT0027 for more details.
3. Mass flow of the outlet flow shall be measured.	The orifice designed for the mass flow measurement of the secondary inlet stream is used. Take note that direction of flow is important and care must be taken to install the orifice in the correct direction.
4. Provision for back pressure reduction at the end of the outlet duct.	The same mechanism for pressure reduction employed in the secondary air inlet is used to reduce the back pressure.

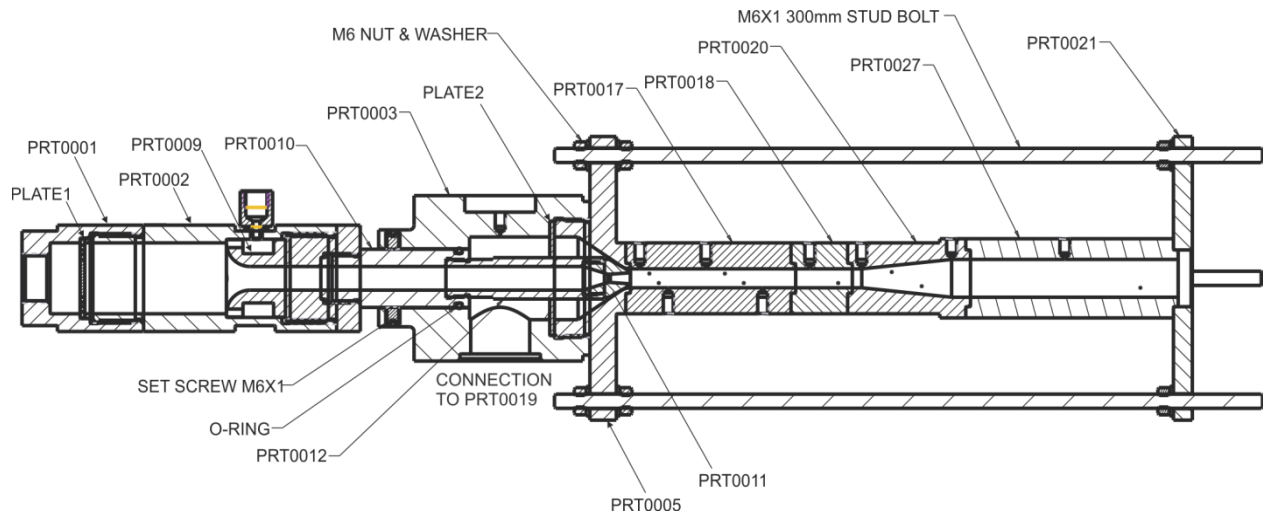


Figure 10. Section view of main part of test rig.

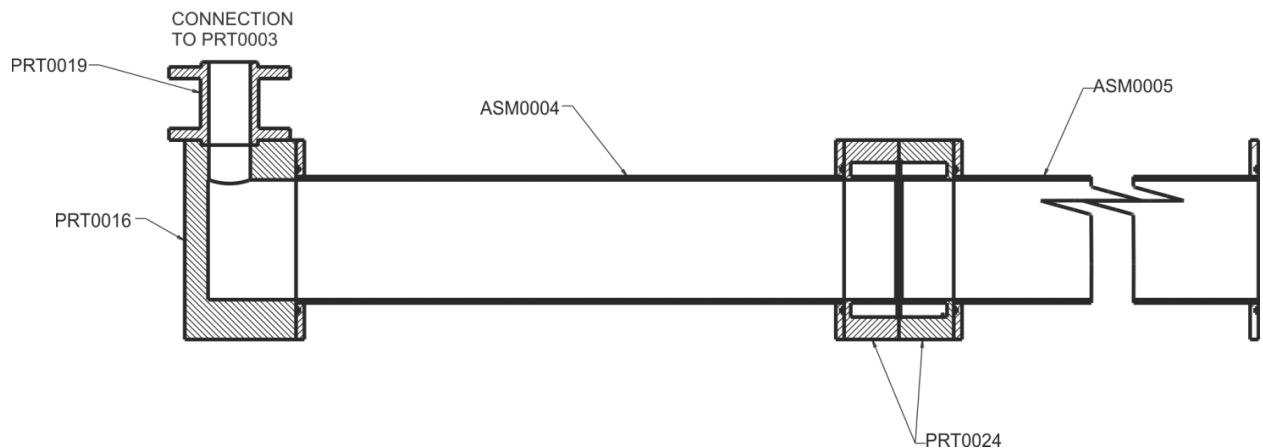


Figure 11. Section view of secondary inlet duct.

Figure 10 shows the section view of the main part of the test rig composed of the primary chamber, secondary chamber, mixing chamber and the diffuser. The primary chamber composed of PRT0001, PRT0002, PRT0009, PRT0010 and PLATE1 are permanent parts. The secondary chamber labeled PRT0003 with PLATE2, including the secondary inlet duct with orifice mass flow measurement, shown in Figure 11, are also permanent parts. Parts PRT0005, PRT0011, PRT0012, PRT0017, PRT0018, PRT0020, and PRT0027 are parts that may be customized to suit other ejector configuration desired. The mixing chamber section is conveniently held together by four M6 stud bolts which allow the variation in the length of the mixing chamber and diffuser

parts. PRT0021, which holds the mixing chamber and attaches it to the outlet duct with another orifice mass flow measurement, is a permanent part.

Appendix contains part drawings and assembly drawings. This is important reference for future work in the test rig.

4.3 Recommendation for optical measurements

The test rig has been designed with a modular approach, such that, the whole mixing chamber can be easily uninstalled and replaced. The constant-area section is also modular such that adjustments in lengths can easily be done. The converging part of the secondary air chamber is a separate part which can be redesigned to suit a transparent material such as glass.

5. Analytical Solution

The analytical solution followed the method proposed by Kracik and Dvorak[6] and Dvorak[7] although some modifications were made to account for the losses due to wall friction in the constant area mixing chamber. The flow is analyzed in the critical operation regime where the flow is assumed to be choked in the secondary nozzle. Figure 12 shows that this regime lies along pressures of $p_4 \leq p_{cr}$.

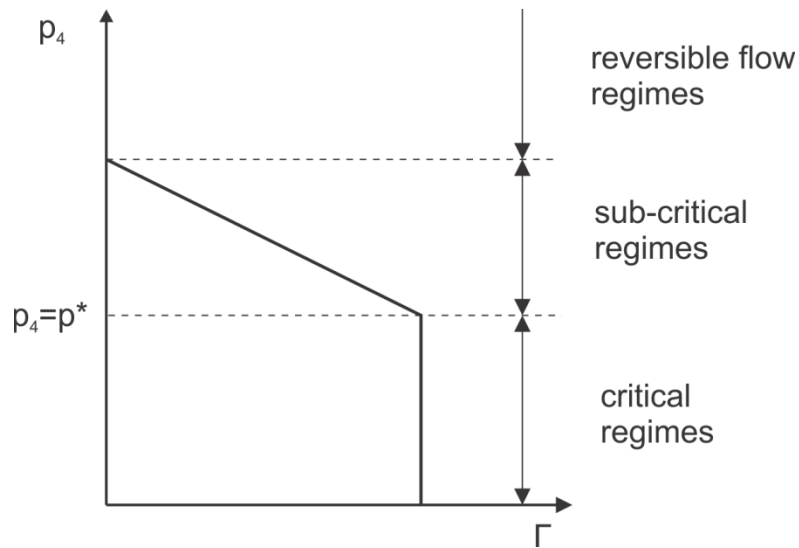


Figure 12. Regimes of operation of a supersonic ejector.

5.1 One-dimensional analysis

The analysis done closely follows procedures indicated in the work of Dvorak[7]. Although some adjustments are made since we are considering the area of the secondary stream is dependent on the location of the primary nozzle located at some distance x from the start of the constant-area mixing. The three basic conservation equations are considered. First, the continuity equation which is expressed as

$$c'_1 \rho'_1 A'_1 + c''_1 \rho''_1 A''_1 = c_3 \rho_3 A_3, \tag{5.1}$$

where, A'_1 is the cross-sectional area at the outlet of the primary nozzle, A''_1 is the cross-sectional area of the secondary air inlet at the same section as the outlet of the primary nozzle, and A_3 is the cross-sectional area of the mixing chamber. The relation between the areas can be expressed as

$$A'_1 = \frac{\pi d_{E,INNER}^2}{4}, \quad (5.2)$$

$$A''_1 = \frac{\pi (d_s^2 - d_{E,OUTER}^2)}{4},$$

$$d_s = d_M + 2[y_c + (x - x_c) \tan \theta],$$

$$A_2 = A_3,$$

where x_c , y_c , and θ are quantities based on the geometry of the ejector, as shown in Figure 13. For the current design, values are $x_c = 3.5\text{mm}$, $y_c = 1.22\text{mm}$, and $\theta = 34^\circ$. Note that equation (5.2) is valid for $x \geq x_c$.

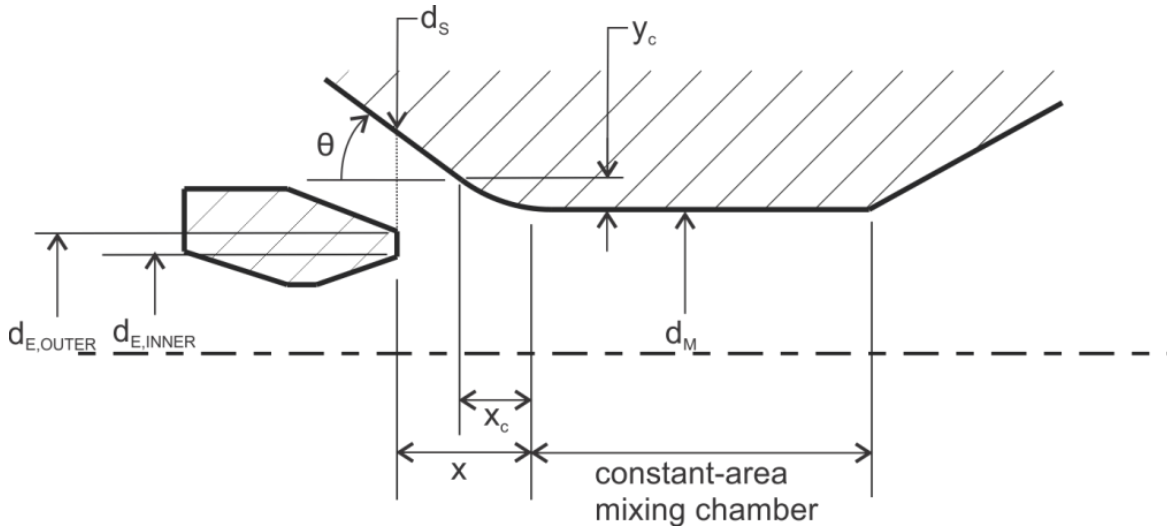


Figure 13. Ejector geometry.

Quantities c and ρ represents the flow velocity and density, respectively, at the specified sections on the ejector.

The second equation considered is the momentum conservation equation given by

$$\dot{m}'c'_1 + p'_1A'_1 + \dot{m}''c''_1 + p''_1A''_1 = (\dot{m}' + \dot{m}'')c_3 + p_3A_3. \quad (5.3)$$

And the third is the conservation of energy given by

$$\dot{m}'\left(c_{p'}T'_1 + \frac{c'^2_1}{2}\right) + \dot{m}''\left(c_{p''}T''_1 + \frac{c''^2_1}{2}\right) = (\dot{m}' + \dot{m}'')\left(c_{p_3}T_3 + \frac{c_3^2}{2}\right). \quad (5.4)$$

Using the assumption stated above regarding the equality of the isobaric heat capacities ($c_{p'} = c_{p''} = c_{p_3}$) and the heat capacity ratio ($\kappa_1 = \kappa_2 = \kappa_3$) between the primary, secondary, and outlet stream, the conservation equations were simplified to express the state of the gas at the end of mixing. The total pressure of the outlet stream p_{03} can be expressed as:

$$p_{03} = p'_0 \frac{\sqrt{(1 + \Gamma)(1 + \Gamma\Theta_{21})} q(\lambda_1)}{1 + \frac{p'_0}{p''_0} \Gamma \sqrt{\Theta_{21}} \frac{q(\lambda_1)}{q(\lambda_2)}}, \quad (5.5)$$

where Γ is the entrainment ratio obtained from equation 2.1, Θ_{21} is the ratio of the static temperatures of the primary and secondary stream expressed as

$$\Theta_{21} = \frac{T''_0}{T'_0}, \quad (5.6)$$

and $q(\lambda)$ is the aerodynamic function of the mass flow rate given by

$$q(\lambda) = \frac{\rho c}{(\rho c)_{cr}} = \left(1 - \frac{\kappa - 1}{\kappa + 1} \lambda^2\right)^{\frac{1}{\kappa - 1}} \left(\frac{\kappa + 1}{2}\right)^{\frac{1}{\kappa - 1}} \lambda, \quad (5.7)$$

where λ is the dimensionless speed, also known as the Laval number, given by

$$\lambda = \frac{c}{c_{cr}}, \quad (5.8)$$

where c and c_{cr} represents the flow velocity and the critical flow velocity, respectively, at a given cross section.

The total temperature at the end of mixing, T_{03} , is derived from the conservation of energy, and we obtain

$$T_{03} = T'_0 \frac{1 + \Gamma \Theta_{21}}{\Gamma + 1}, \quad (5.9)$$

The dimensionless velocity at the end of mixing, λ_3 , is obtained from the equation

$$z(\lambda_3) = \frac{z(\lambda_1) + \Gamma \sqrt{\Theta_{21}} z(\lambda_2)}{\sqrt{(1 + \Gamma)(1 + \Gamma \Theta_{21})}}, \quad (5.10)$$

where $z(\lambda)$ is the aerodynamic function given by

$$z(\lambda) = \lambda + \frac{1}{\lambda}, \quad (5.11)$$

When solving for the value of the dimensionless number at the end of mixing using equation (2.9), two solutions can be found: one indicates subsonic flow, and the other indicates supersonic flow at the end of mixing. It is physically possible to obtain both subsonic and supersonic flows at the end of mixing, depending on the initial flow conditions and the dimensions of the ejector.

Using the relations above, we can completely calculate the values of all significant variables for the resulting flow in the supersonic ejector without taking into account losses. The operating characteristics of an ejector is determined through the working pressure, Δp , which is defined as the difference between the secondary inlet stagnation pressure and the backpressure, given by

$$\Delta p = p_4 - p''_0, \quad (5.12)$$

and also the mass flow at the secondary inlet, \dot{m}'' , or the total mass flow at the outlet, \dot{m}_3 . The efficiency of the ejector is given by

$$\eta_E = \frac{\dot{m}_2 \left(\frac{p_4}{p_{02}} \right)^{\frac{\kappa-1}{\kappa}} - 1}{\dot{m}_1 \left(1 - \left(\frac{p_4}{p_{01}} \right)^{\frac{\kappa-1}{\kappa}} \right)} \frac{T_{02}}{T_{01}}. \quad (5.13)$$

Dynamic functions for isentropic flow of ideal gas are used to obtain characteristic properties of the flow inside an ejector. This is a simplified way since it only depends on the Mach number of the flow at the section being investigated. The dynamic functions for temperature, pressure, density, cross-section area, and the conversion between Mach number and Laval number are given by the following equations, respectively

$$\frac{T}{T_0} = \left[1 + \frac{\kappa-1}{2} M^2 \right]^{-1}, \quad (5.14)$$

$$\frac{p}{p_0} = \left[1 + \frac{\kappa-1}{2} M^2 \right]^{\frac{\kappa}{1-\kappa}}, \quad (5.15)$$

$$\frac{\rho}{\rho_0} = \left[1 + \frac{\kappa-1}{2} M^2 \right]^{\frac{1}{1-\kappa}}, \quad (5.16)$$

$$\frac{A}{A_{cr}} = \frac{\psi_{max}}{\psi} = \frac{1}{M} \left[\left(\frac{2}{\kappa+1} \right) \left(1 + \frac{\kappa-1}{2} M^2 \right) \right]^{\frac{\kappa+1}{2(\kappa-1)}}, \quad (5.17)$$

5.2 Losses

The ejector is divided into four parts, as shown in Figure 1. In the first part, we consider the losses occurring in the primary and secondary nozzle. In the second part, losses caused by the mixing of two streams shall be neglected. In the third part, the losses due to friction in constant

area ducts are considered. And finally, in the fourth part, the losses due to the diffuser are accounted.

5.2.1 Losses in nozzles

Some losses in the primary and secondary nozzles must be taken into account since the initial assumption made is that the process in these nozzles is isentropic.

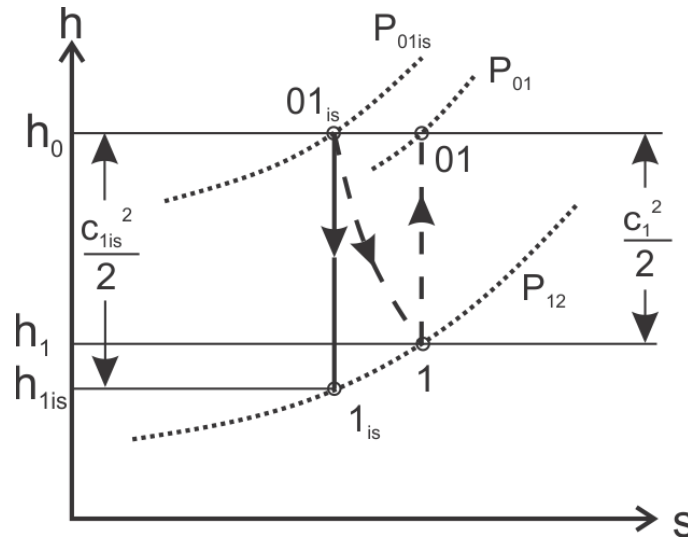


Figure 14. h-s diagram of expansion in nozzle.

Figure 14 shows us the h-s diagram for the isentropic and real expansion in nozzles. From the diagram, the energy equation can be derived as

$$h_0 = h_{1is} + \frac{c_{1is}^2}{2} = h_1 + \frac{c_1^2}{2}. \quad (5.18)$$

The efficiency of the nozzle is defined as

$$\eta = \frac{h_0 - h_1}{h_0 - h_{1is}}. \quad (5.19)$$

We consider that the specific heat is constant so equation (5.19) can be transformed into

$$\eta = \frac{T_0 - T_1}{T_0 - T_{1is}}. \quad (5.20)$$

And finally, using the isentropic relationship between temperature and pressure, we can derive an equation for the nozzle efficiency in terms of the stagnation and static pressures.

$$\eta_1 = \frac{1 - \left(\frac{p_{12}}{p_{01}}\right)^{\frac{\kappa-1}{\kappa}}}{1 - \left(\frac{p_{12}}{p_{01is}}\right)^{\frac{\kappa-1}{\kappa}}}. \quad (5.21)$$

Similarly, for the secondary nozzle, the efficiency may be expressed as

$$\eta_2 = \frac{1 - \left(\frac{p_{12}}{p_{02}}\right)^{\frac{\kappa-1}{\kappa}}}{1 - \left(\frac{p_{12}}{p_{02is}}\right)^{\frac{\kappa-1}{\kappa}}}. \quad (5.22)$$

The efficiency of the nozzles for primary and secondary stream is obtained from the numerical calculation. The mass-weighted average for the stagnation and static pressures are obtained from the result of the numerical simulation to compute the efficiency of the primary and secondary nozzles. This is then used to find the corrected stagnation pressure of both streams.

The following equations are used

$$p_{01} = p_{12} \left\{ 1 - \eta_1 \left[1 - \left(\frac{p_{12}}{p_{01is}}\right)^{\frac{\kappa-1}{\kappa}} \right] \right\}^{\frac{\kappa}{1-\kappa}}, \quad (5.23)$$

$$p_{02} = p_{12} \left\{ 1 - \eta_2 \left[1 - \left(\frac{p_{12}}{p_{02is}}\right)^{\frac{\kappa-1}{\kappa}} \right] \right\}^{\frac{\kappa}{1-\kappa}}. \quad (5.24)$$

5.2.2 Loss in constant-area section

In this part we take into account the effect of wall friction in the flow of compressible gas in constant-area ducts. We shall assume that no heat is transferred to and from the stream, making the process adiabatic for short lengths of the duct, as in our case. We also assume one-dimensional steady flow along the constant area duct, where no external heat exchange and shaft work is produced. The change in potential energy due to elevation is negligible compared to the effect of friction.

The energy equation for steady flow is expressed as

$$h_{02} = h + \frac{c^2}{2}, \quad (5.25)$$

where h and c are the enthalpy and velocity of the fluid at any section of the duct, respectively.

The continuity equation in the control volume between sections 2 and 3 is given by

$$c_2 \rho_2 A_2 = c_3 \rho_3 A_3 = \text{constant}, \quad (5.26)$$

where the quantity on the left side of the equation is equivalent to the equation (5.1) because at this point we still assume that the two streams have not started to mix.

The momentum equation between the sections 2 and 3 is given by

$$\dot{m}_2 c_2 + p_2 A_2 = \dot{m}_3 c_3 + p_3 A_3 + 4f \frac{c_3^2 L}{2D} \rho_3 A_3, \quad (5.27)$$

where the term $4f \frac{c_3^2 L}{2D} \rho_3 A_3$ represents the effect of wall friction to the flow at the end of the mixing chamber. The friction factor f is defined by using the Darcy friction factor which is a

function of the flow Reynolds number, Re , and the relative roughness, Ra/D , where D is the pipe diameter. The viscosity is computed using the Sutherland's formula given by

$$\mu = \mu_0 \frac{T_0 + C}{T + C} \left(\frac{T}{T_0} \right)^{3/2}, \quad (5.28)$$

where, for air, the constants are given as $\mu_0 = 18.27 \mu Pa \cdot s$, $C = 120 K$, and $T_0 = 291.15 K$.

For turbulent flow, which is characterized by Reynolds number between the values $5000 \leq Re \leq 10^8$, and a relative roughness between $10^{-6} \leq \frac{Ra}{D} \leq 10^{-2}$, the friction factor may be computed as

$$f = \frac{0.0625}{\left[\ln \left(\frac{Ra}{3.7D} + \frac{5.74}{Re^{0.9}} \right) \right]^2}. \quad (5.29)$$

We can express the right side of equation (5.27) in terms of the critical speed and Laval number at section 3.

$$\dot{m}_3 a_{cr3} \frac{\kappa + 1}{2\kappa} \left[\lambda_3 \left(1 + \frac{4fL}{D} \frac{\kappa}{\kappa + 1} \right) + \frac{1}{\lambda_3} \right] = \dot{m}_3 a_{cr3} \frac{\kappa + 1}{2\kappa} z(\lambda_3). \quad (5.30)$$

Combining with equation (5.10), we can obtain λ_3 with the effect of wall friction.

5.2.3 Losses in diffusers

At the diffuser, we assumed a one-dimensional, steady flow, isentropic compression. In reality, some loss is incurred caused by several factors such as viscous dissipation, wall friction, etc. Figure 15 shows the $h - s$ diagram for the compression in the diffuser, both the isentropic and the real case. If we assume that the kinetic energy at end of the diffuser is not completely lost, the efficiency may be expressed as

$$\eta_D = \frac{\Delta h_4 + \frac{c_4^2}{2}}{\frac{c_4^2}{2}} = \frac{h_{04} - h_{4'}}{h_{03} - h_3}. \quad (5.31)$$

For ideal gas, c_p is constant. We can now express the efficiency in terms of temperatures

$$\eta_D = \frac{T_{04} - T_{4'}}{T_{03} - T_3} = \frac{1 - \frac{T_{4'}}{T_{04}}}{1 - \frac{T_3}{T_{03}}}, \quad (5.32)$$

and using the isentropic relationship between temperature and pressure, the final form of the diffuser efficiency can be expressed as

$$\eta_D = \frac{1 - \left(\frac{p_3}{p_{04}}\right)^{\frac{\kappa-1}{\kappa}}}{1 - \left(\frac{p_3}{p_{03}}\right)^{\frac{\kappa-1}{\kappa}}}, \quad (5.33)$$

where $p_3 = p_{4'}$, based on Figure 15.

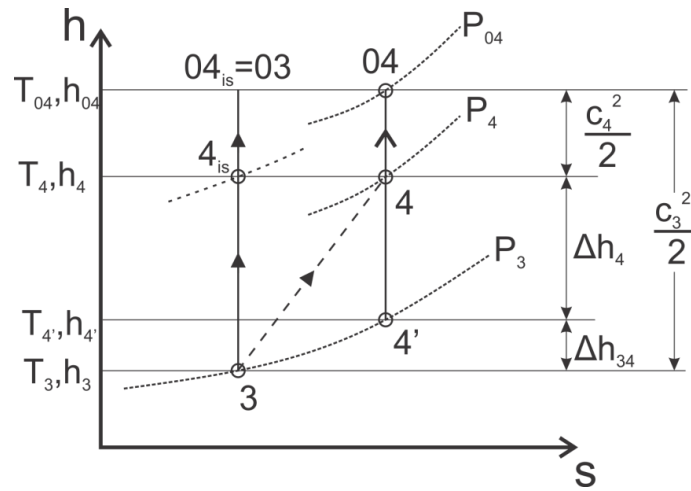


Figure 15. h-s diagram of compression in a diffuser with losses.

For our purposes, the efficiency of the diffuser is obtained from the numerical solution. The stagnation and static pressures are obtained by finding the mass-weighted average of these values

at the specified cross-section. This is then used to compute for the efficiency of the diffuser. To be able to find p_{04} equation (5.34) is used.

$$p_{04} = p_3 \left\{ 1 - \eta_D \left[1 - \left(\frac{p_3}{p_{03}} \right)^{\frac{\kappa-1}{\kappa}} \right]^{\frac{\kappa}{1-\kappa}} \right\}. \quad (5.34)$$

6. Numerical Solution

The numerical solution is obtained using ANSYS Fluent. The geometry of the one-fourth section of the ejector is created using DesignModeler. A structured mesh is generated using the ANSYS Meshing software. The geometry was split into surfaces so a quadrilateral face mesh can be applied. The mesh is further refined using edge sizing functions with a bias of finer mesh near the walls. Figure 16 shows the mesh created in the primary nozzle and secondary inlet part. The quality of the mesh generated is reported in Table 6.

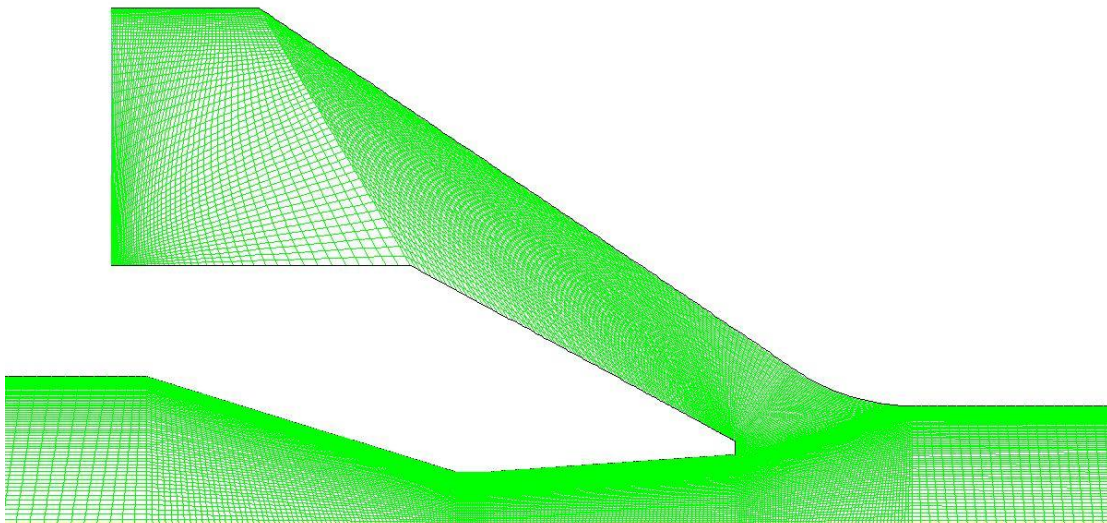


Figure 16. Mesh generated.

Table 6. Mesh quality values and criteria.

Parameter	Value	Criterion
Orthogonal quality	0.933	Worst – 0; Best – 1
Skewness (average)	0.146	Good – 0; Bad – 1
Aspect ratio (average)	6.03	Good - <5

The stated criteria in Table 6 are based on good mesh quality suggested in the ANSYS Fluent Users Guide [23]. From the above values, we can say that the mesh is not the best. For a mesh of this quality, the computational cost will be high as the convergence will be difficult to reach.

The solution used a 2D, steady flow, axisymmetric, density-based solver. The solution formulation is Implicit Roe-FDS, and second order upwind discretization is used for the flow, turbulent kinetic energy, and specific dissipation rate. The turbulence model used is the k- ω SST model on the basis of the studies conducted by [4] and [9].

The boundary conditions are stated in Table 7.

Table 7. Boundary conditions

Boundary condition	Value
Primary pressure inlet	300 000 Pa
Secondary pressure inlet	0 Pa
Outlet pressure/back pressure	0 – 70 000 Pa
Operating pressure	97 000 Pa

The calculation was run for different back pressures to be able to obtain a characteristic curve of the ejector efficiency and the relative back pressure against the entrainment ratio.

It is very difficult to obtain convergence with cases involving supersonic compressible flows, especially one involving turbulence, free shear layers, shockwaves, etc. The convergence criteria considered for the results is the mass balance. The error must be less than 0.01% of the smallest inlet mass flow. This is represented by the following equation.

$$|(\dot{m}' + \dot{m}'') - \dot{m}_3| < 0.0001\dot{m}_{min}. \quad (5.30)$$

7. Results and Discussion

Parts designed for the test rig were successfully manufactured according to drawing specifications. Some issues were encountered, but these are easily re-workable. Shown below is a photo of the manufactured assembly and the individual components manufactured. Refer to Appendix for complete engineering 2D and assembly drawings.

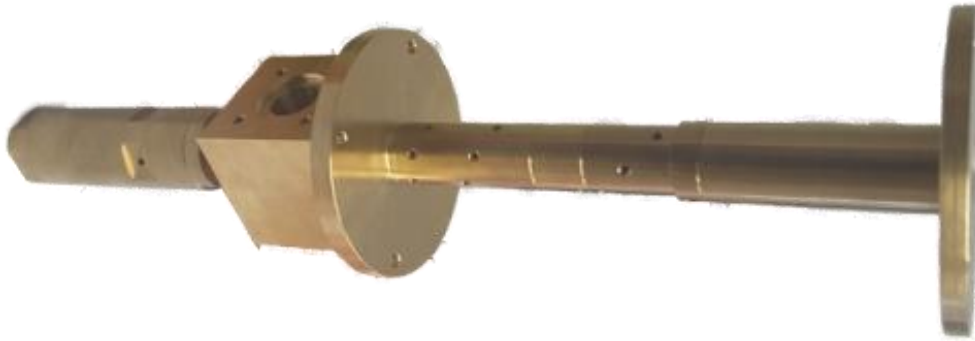
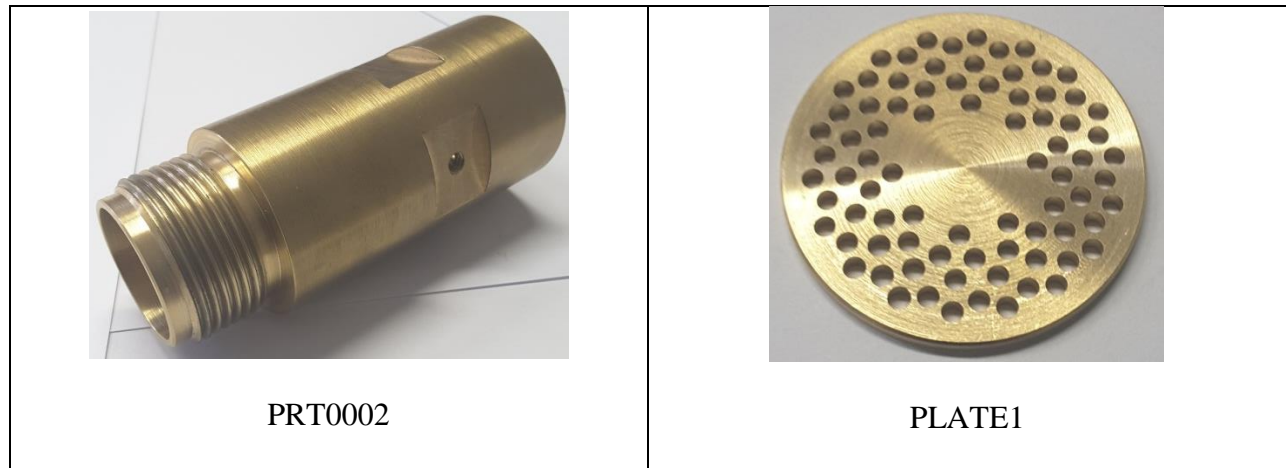


Figure 17. Manufactured assembly





PRT0009



PRT0010



PRT0012



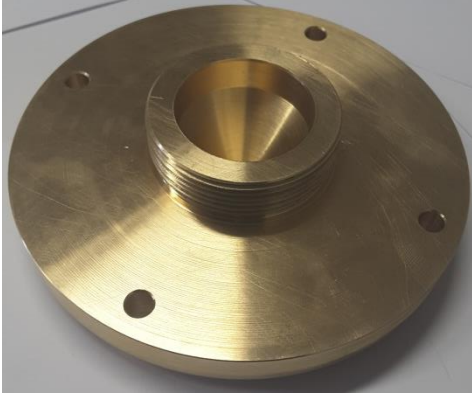
PRT0011



PRT0003



PLATE2



PRT0005



PRT0017



PRT0018



PRT0020



PRT0027



PRT0021

Figure 18 shows the ejector characteristic curve obtained using the analytical solution.

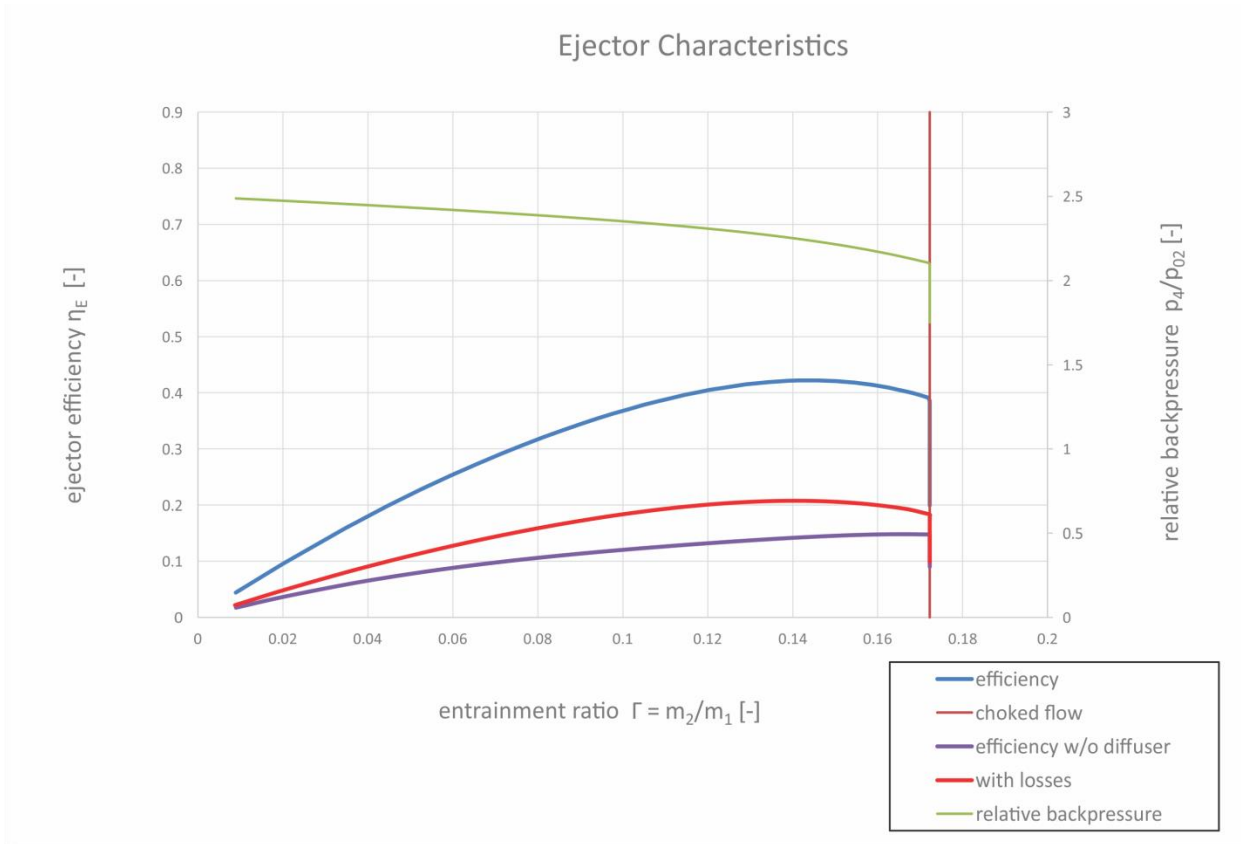


Figure 18. Ejector characteristic by analytical solution

For the case where no losses were taken into account, the efficiency of the ejector can reach a value of 43%. Taking into account the losses, the efficiency becomes significantly lower. Choking occurs at entrainment ratio equal to 0.1723. This means that the secondary mass flow is choked and further decrease in relative back pressure will only decrease the ejector efficiency.

Figure 18 also shows the curve of the relative back pressure p_4/p_{02} . If we compare it to Figure 12, it shows that the critical regime of operation starts at relative back pressure equal to 2.0962.

The results from the numerical solution show contours of Mach number, static pressure distribution along ejector wall, turbulence kinetic energy, and dissipation rate. The characteristic curve is also shown.

The simulation was run several times varying the back pressure from 0 to 70 000 Pa. However, no convergence was met in the case of zero back pressure. This data has been excluded from the analysis. In the case when the back pressure set was equal to 60 000 Pa, the solution diverged very quickly resulting from reversed flows at the secondary inlet. This indicates that at back pressures above 60 000 Pa approximately, the ejector is operating in the reversed flow regime and we can say that it is not functioning as intended.

The characteristic curve of the ejector generated using numerical results is presented in Figure 19. It shows us that maximum entrainment ratio is approximately 0.97 and the critical relative backpressure is approximately 1.3. Comparing to the curve generated by analytical solution shown in Figure 18, there is a significant difference between the results. It must be noted that the analytical solution proposed did not take into account the phenomena of shockwaves and choking in the mixing chamber. Therefore, it is expected to see some difference between the results.

Figure 19 also shows the operation regime of the ejector. For relative back pressure less than 1.3 approximately, the ejector operates at critical regime. It means that both the primary and secondary stream are choked and the entrainment ratio is, therefore, not dependent on the value of the backpressure. This operation regime is often referred to as “on-design”. For relative back pressures greater than 1.3 approximately, the ejector operates in the subcritical regime and the

secondary mass flow rate is dependent on the backpressure, assuming that the primary stream is choked, which is true in this case.

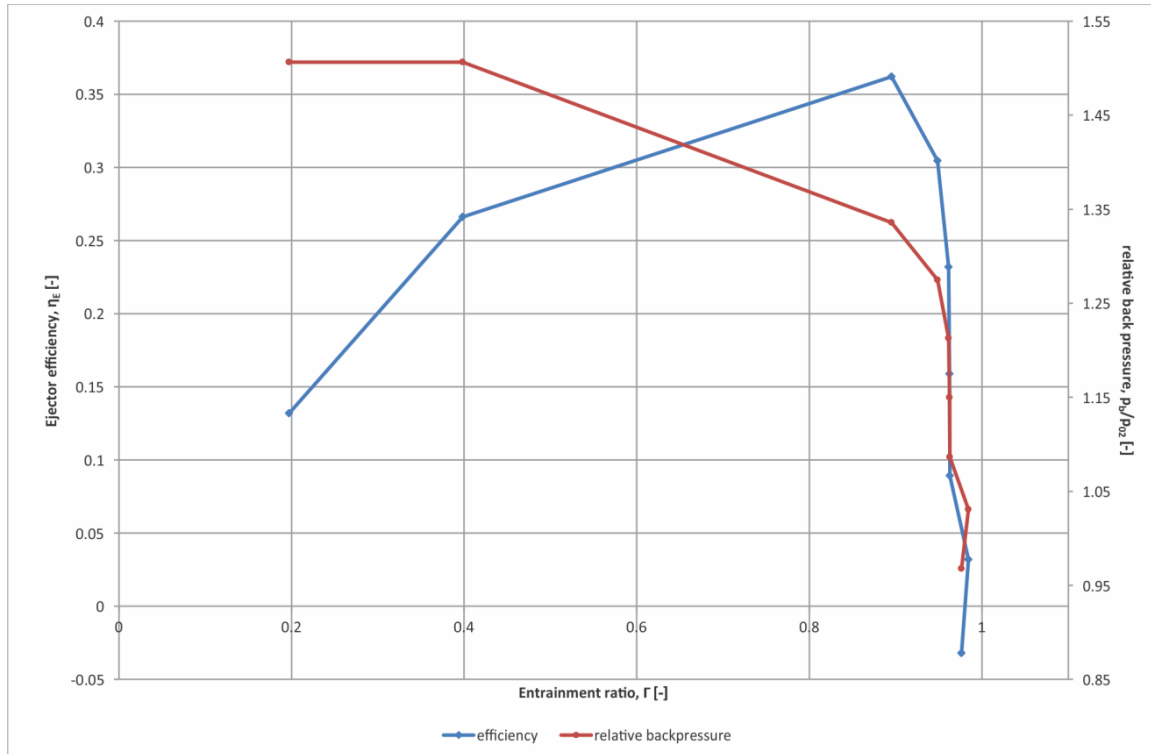


Figure 19. Characteristic curve of the ejector obtained using numerical results.

Figure 20 shows the contour of Mach number for back pressure equal to 5000 Pa. A normal shock wave can be observed at the exit of the primary nozzle followed by what Matsuo, et al. [24] has described as a shock train, which is composed of a combination of oblique and normal shock waves. A shock train is a type of boundary layer interaction where the Mach number before the shock wave is greater than 1.5. This is true in our case. As the two streams flow along the constant area mixing chamber, the pressure of the primary stream is adjusted with the secondary stream to attenuate the shocks until they disappear.[4] From Figure 23, we can observe that the shock train is shorter for higher back pressures. The difference in backpressure does not influence the existence of a normal shock wave and boundary layer separation at the end of the primary nozzle.

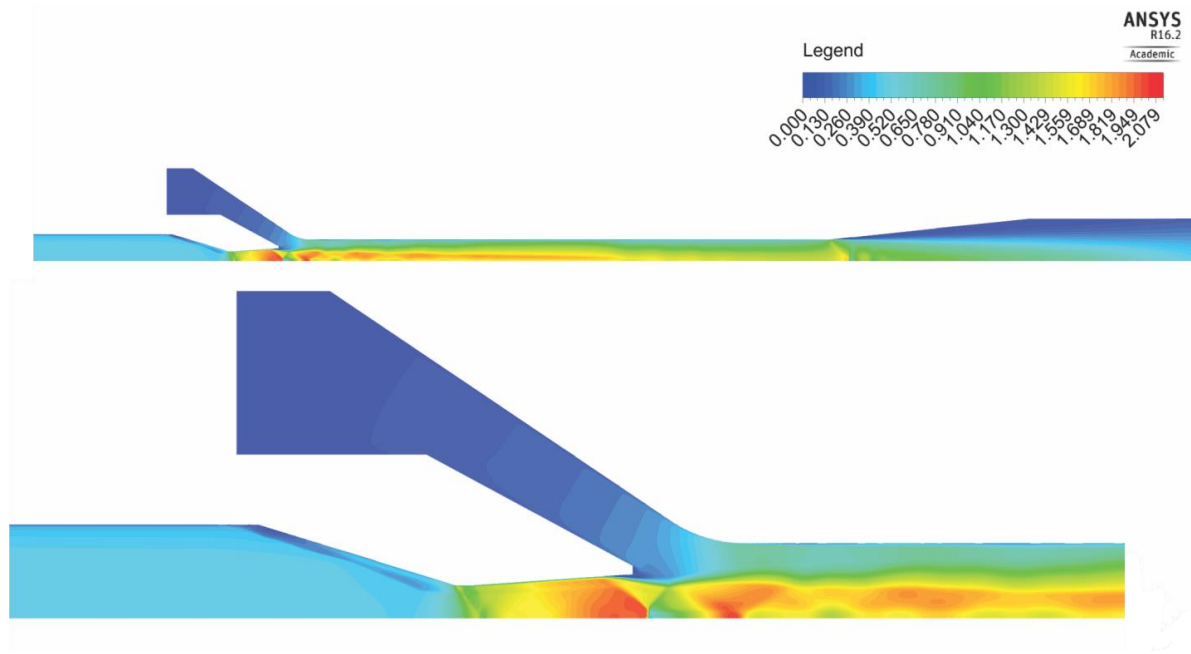


Figure 20. Contour of Mach number for pb=5000 Pa

The shock wave occurring at the exit of the primary nozzle for all backpressures is strong enough to cause a boundary layer separation towards the end of the divergent part of the primary nozzle. Boundary layer separation may also indicate that the geometry of the divergent part of the primary nozzle is not suitable. Further investigation is necessary to clearly determine the cause.

Figure 21 shows the wall static pressure distribution along the mixing chamber for the different back pressures calculated. This clearly illustrates the phenomena of the shock train as reflected to the static pressure. At the entrance of the mixing chamber, an oscillating behavior is observed. This is in good agreement with the theories in [24]. In the mixing chamber, static pressure is recovered through the influence of shockwaves, shear layers and wall friction. A similar static pressure oscillation can be observed towards the end of the mixing chamber for

flows with back pressure from 5000 to 20000 Pa. Referring to Figure 23a – f, some weak shock train can be observed towards the end of the mixing chamber and at the beginning of the diffuser.

Figure 22 gives us a closer view of the shock waves occurring at the beginning of the diffuser. A more defined shock wave occurs at lower backpressures.

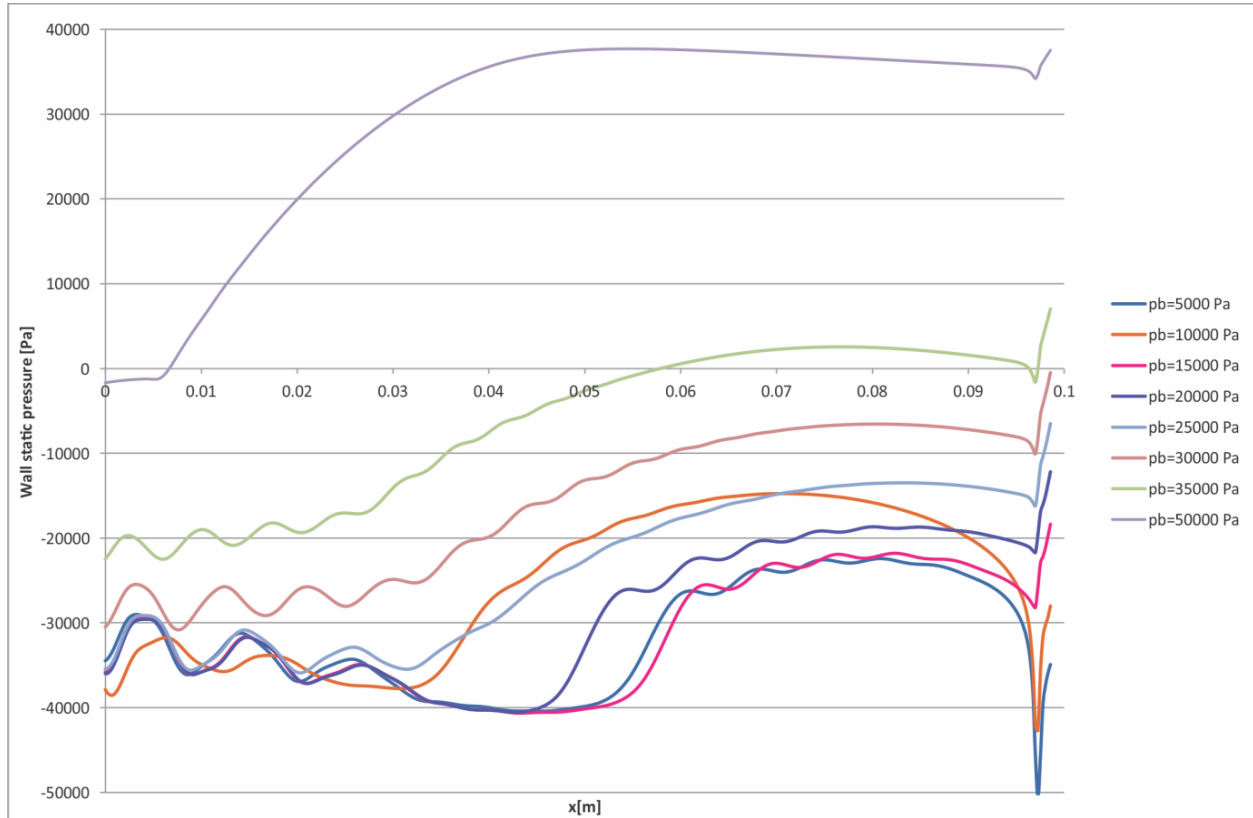


Figure 21. Wall static pressure along the mixing chamber.

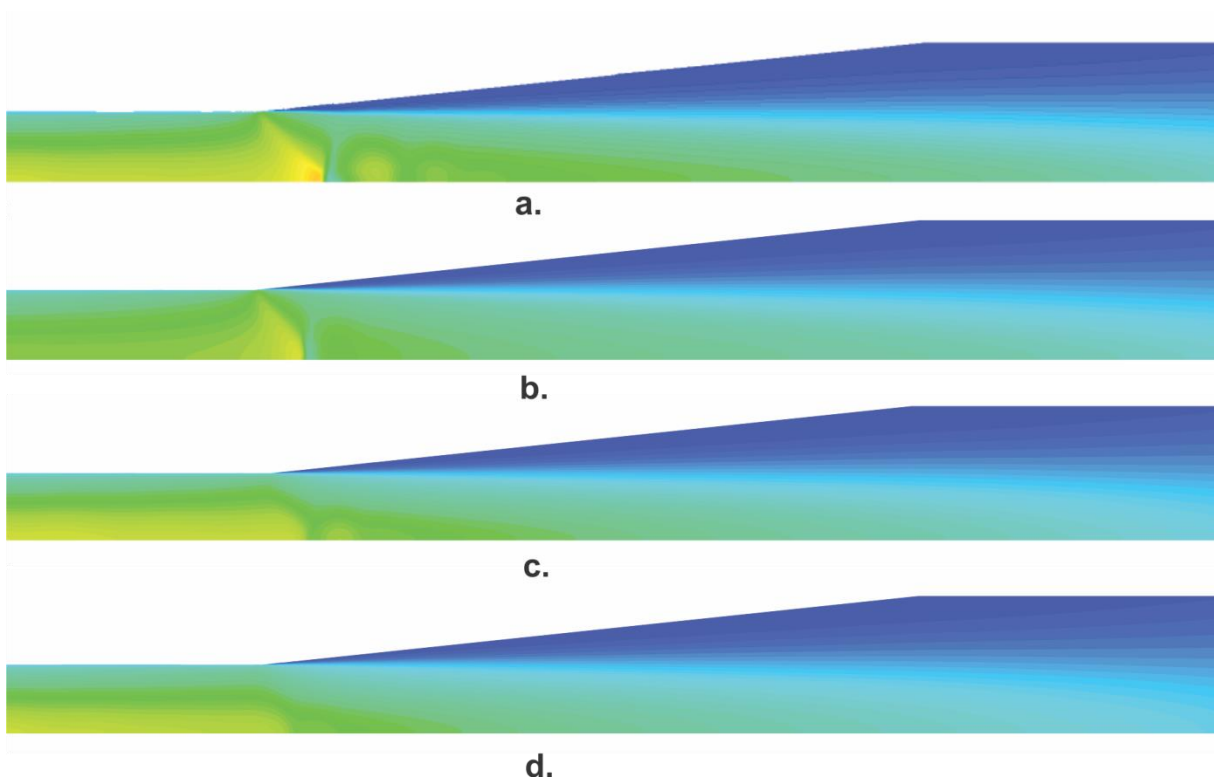


Figure 22. Closer view at Mach number contours with shock wave occurring at the beginning of the diffuser for backpressures a) $p_b=5000$, b) $p_b=10000$, c) $p_b=15000$, d) $p_b=20000$.

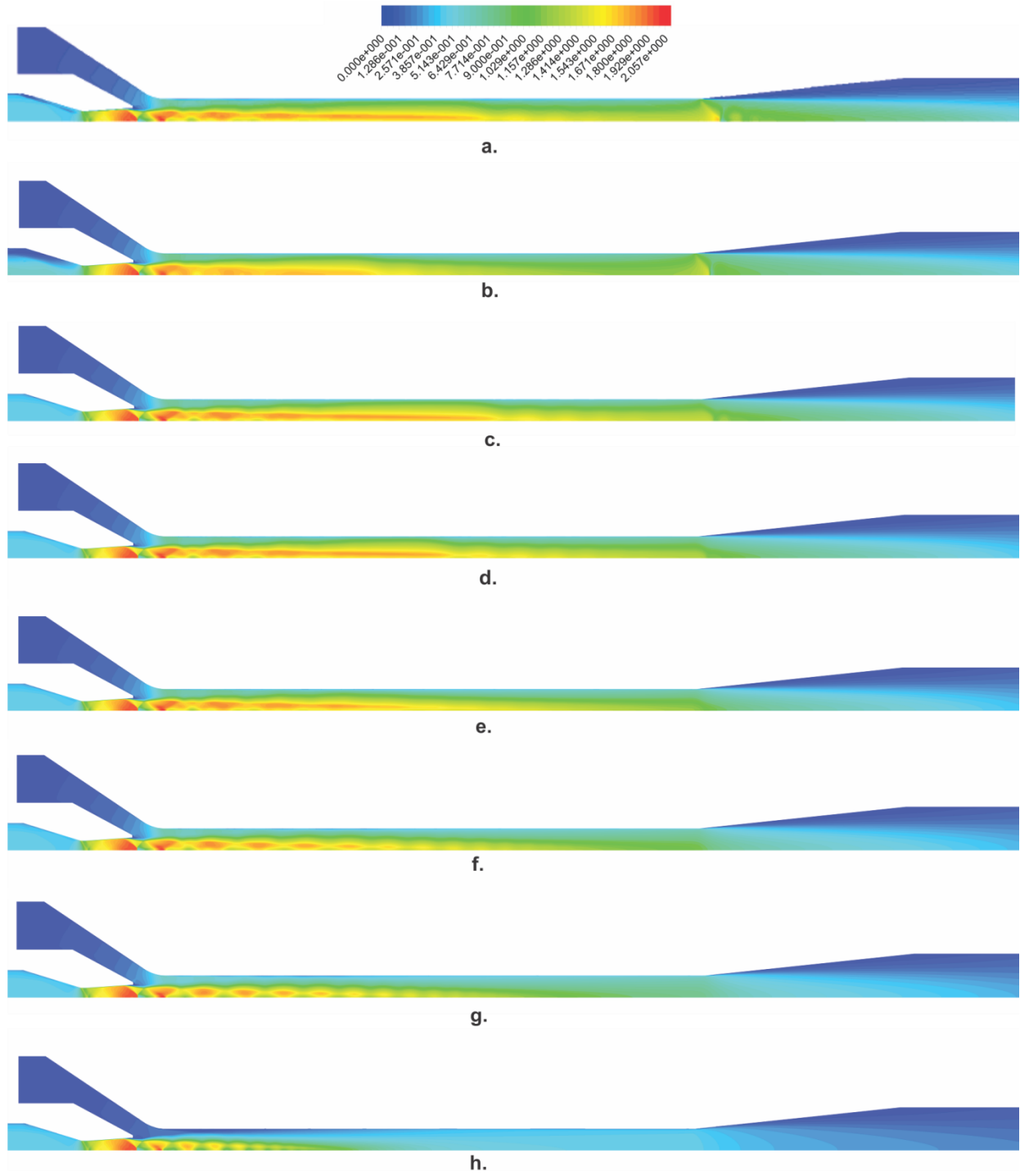


Figure 23. Contour of mach number for different back pressures. a) pb=5000, b) pb=10000, c) pb=15000, d) pb=20000, e) pb=25000, f) pb=30000, g) pb=35000, h) pb=50000.

8. Conclusion

This work focused on the design and verification of a test rig for the investigation and research of supersonic ejectors. The main design objective is to be able to design a working model of the test rig and verify that it is functioning as intended by numerical simulation. The test rig is designed such that specific parts are universal and can be reused for testing different ejector configurations. The parts have been manufactured and experimental verification is recommended to further expand the study.

The analytical solution initially used a one-dimensional, isentropic, steady state approach as adapted from the works [6] and [7]. Losses in the primary nozzle, secondary nozzle, mixing chamber, and diffuser were accounted for using data obtained from the numerical simulation. Results show that the efficiency of the ejector is significantly increased by the presence of a diffuser and is decreased when losses were accounted for. The values for entrainment ratio and critical back pressure ratio display significant difference compared to the numerical solution. This can be attributed to the limitation of the analytical solution, which lies in the non-inclusion of the complex phenomenon of two streams mixing and shock waves occurring in the mixing chamber.

The numerical simulation was conducted using the commercial software ANSYS Fluent using default solvers for compressible fluid flow. Mesh quality is relatively poor, making the simulations very time consuming. Although convergence in terms of the mass balance was achieved, it cannot be confidently concluded that the result of the numeric simulation has a high accuracy because of the quality of the mesh. However, the results gave some valuable insight into the process occurring inside the ejector. A characteristic curve has been generated. It is

recommended to do more simulation for higher relative back pressure intervals to be able to give a higher resolution and see more clearly the dependence of the entrainment ratio to the back pressure at the sub-critical regime.

9. References

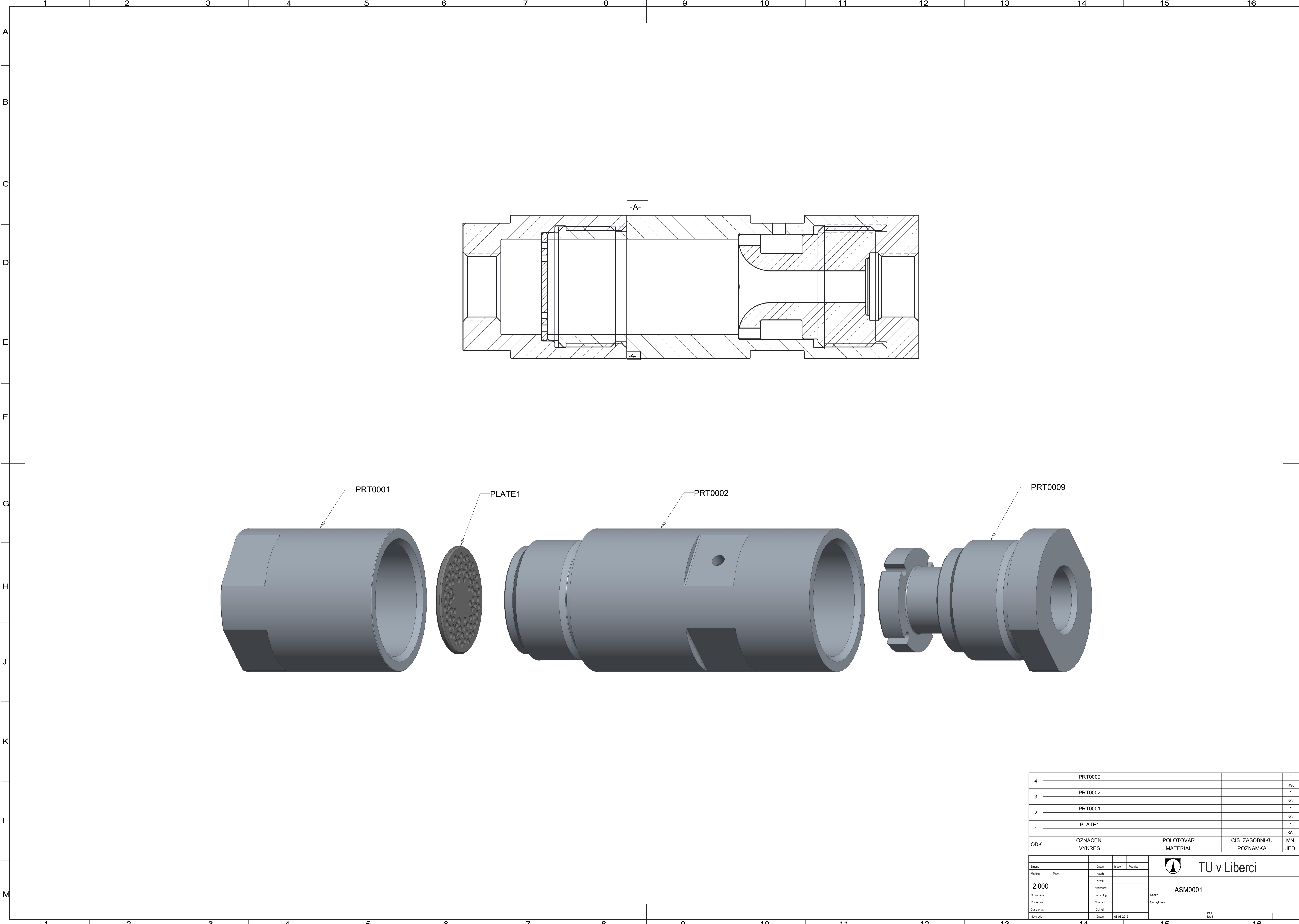
- [1] Sun, D.W., Eames I.W., 1995. Recent development in the design theories and applications of ejector – a review. *J. Inst. Energy*, 68, 1995, 65-79.
- [2] Keenan, J.H., Neumann E.P., A simple air ejector. *J. Applied Mechanics, Trans ASME*, 64, 1942, A75-A81.
- [3] Keenan J.H., Neumann, E.P., Lustwerk F., An investigation of ejector design by analysis and experiment. *J. Applied Mechanics, Trans ASME*, 72, 1950, 299-309.
- [4] Bartosiewicz, Y., Aidoun, Z., Desevaux, P., Mercadier, Y., Numerical and experimental investigations on supersonic ejectors. *International Journal of Heat and Fluid Flow*, 26, 2005, 56-70.
- [5] Dutton, J.C., Mikkelsen, C.D., A theoretical and experimental investigation of the constant area, supersonic-supersonic ejector. *AIAA Journal*, Vol.20, No.1, 1982, 1392-1400.
- [6] Kracik, J., Dvorak, V., Development of an Analytical Method for Predicting Flow in a Supersonic Air Ejector. *EPJ Web of Conferences*, 114, 2016, 02059.
- [7] Dvorak, V., Introduction to Flow of Compressible Fluids, Reference text, 2016.
- [8] Hedges, K.R., Hill, P.G., Compressible flow ejectors. Part I – Development of a finite-difference flow model, *J Fluids Eng, Trans ASME*, 94, 1974, 407-416.
- [9] Kolar, J., Dvorak, V., Verification of k- ω SST Turbulence model for supersonic internal flows. *International Journal of Mechanical, Aerospace, Industrial, Mechatronic and Manufacturing Engineering*, Vol. 5, No. 9, 2011, 1715-1719.
- [10] Marzkirich, W., *Flow Visualization*, Academic Press, New York, 1977.

- [11] Ristic, S., Flow visualization techniques in wind tunnels – optical methods (Part II), Scientific Technical Review, ISSN 206: 2007, 1820.
- [12] McKeon, B., Engler, R., Pressure Measurement Systems. Reference work entry – Springer Handbook of Experimental Fluid Mechanics, 2007, 179-214.
- [13] McKeon B.J., Smits, A.J., Static pressure correction in high Reynolds number fully developed turbulent pipe flow, Measurement Science and Technology, Institute of Physics Publishing, 13, 2002, 1608-1614.
- [14] Chue, S.H., Pressure probes for fluid measurement. Prog. Aerospace Sci., Vol 16, No.2, 1975, 147-223
- [15] INTERNATIONAL ORGANIZATION FOR STANDARDIZATION, Measurement of fluid flow by means of pressure differential devices inserted in circular-cross section conduits running full. ISO 5167-2:2003. Geneva: International Organization for Standardization, 2003.
- [16] Punmia, B.C., Jain, A.K., Jain, A.K., Mechanics of Materials. Firewall Media, 2002, 814-815.
- [17] Technical information for Free-Cutting Brass UNS C36000 website: <http://www.ezlok.com/TechnicalInfo/MPBrass.html>, published on: 2015-03-11, accessed on: 2016-01-30.
- [18] Gagan, J., Smierciew, K., Butrymowicz, D., Karwacki, J., Comparative study of turbulence models in application to gas ejectors. International Journal of Thermal Sciences, 78, 2014, 9-15.

- [19] Chow, W.L., Addy, A. L., Interaction between Primary and Secondary Streams of Supersonic Ejector Systems and Their Performance Characteristics. AIAA Journal, Vol. 2, No. 4, 1964, 686-695.
- [20] Gan, G., Riffat, S.B., Pressure loss characteristics of orifice and perforated plates. Experimental Thermal and Fluid Science, 14, 1995, 160-165.
- [21] Malavasi, S., Messa, G., Fratino, U., Pagano, A., On the pressure losses through perforated plates. Flow Measurement and Instrumentation, 28, 2012, 57-66.
- [22] Kumar, V., Singhal, G., Subbarao, P.M.V., Study of supersonic flow in a constant rate of momentum change (CRMC) ejector with frictional effects. Applied Thermal Engineering, 60, 2013, 61-71.
- [23] ANSYS Fluent Users Guide.
- [24] Matsuo, K., Miyazato, Y., Kim, H., Shock train and pseudo-shock phenomena in internal gas flows. Progress in Aerospace Sciences, 35, 1999, 33-100.

Appendix

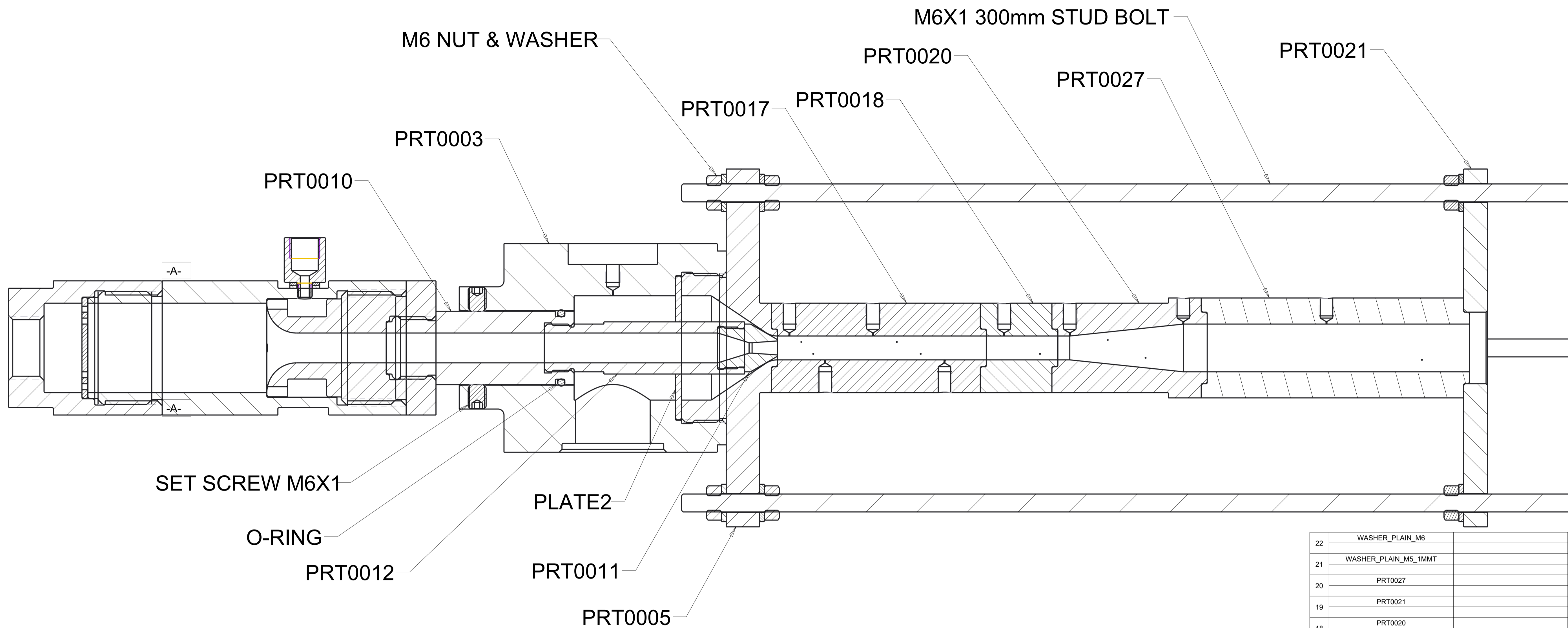
Assembly and part drawings



4	PRT0009				1
					ks.
3	PRT0002				1
					ks.
2	PRT0001				1
					ks.
1	PLATE1				1
					ks.
ODK	OZNACENI	POLOTOVAR	CIS. ZASOBNIKU	MN.	
	VYKRES	MATERIAL	POZNAMKA	JED.	

Zmena		Datum	Index	Popis	
Merklo	Pozn.	Nechf			
		Kreslil			
		Prepracoval			
		Technik			
		Normaliz.			
		Schválil			
		Datum	08-03-2016		

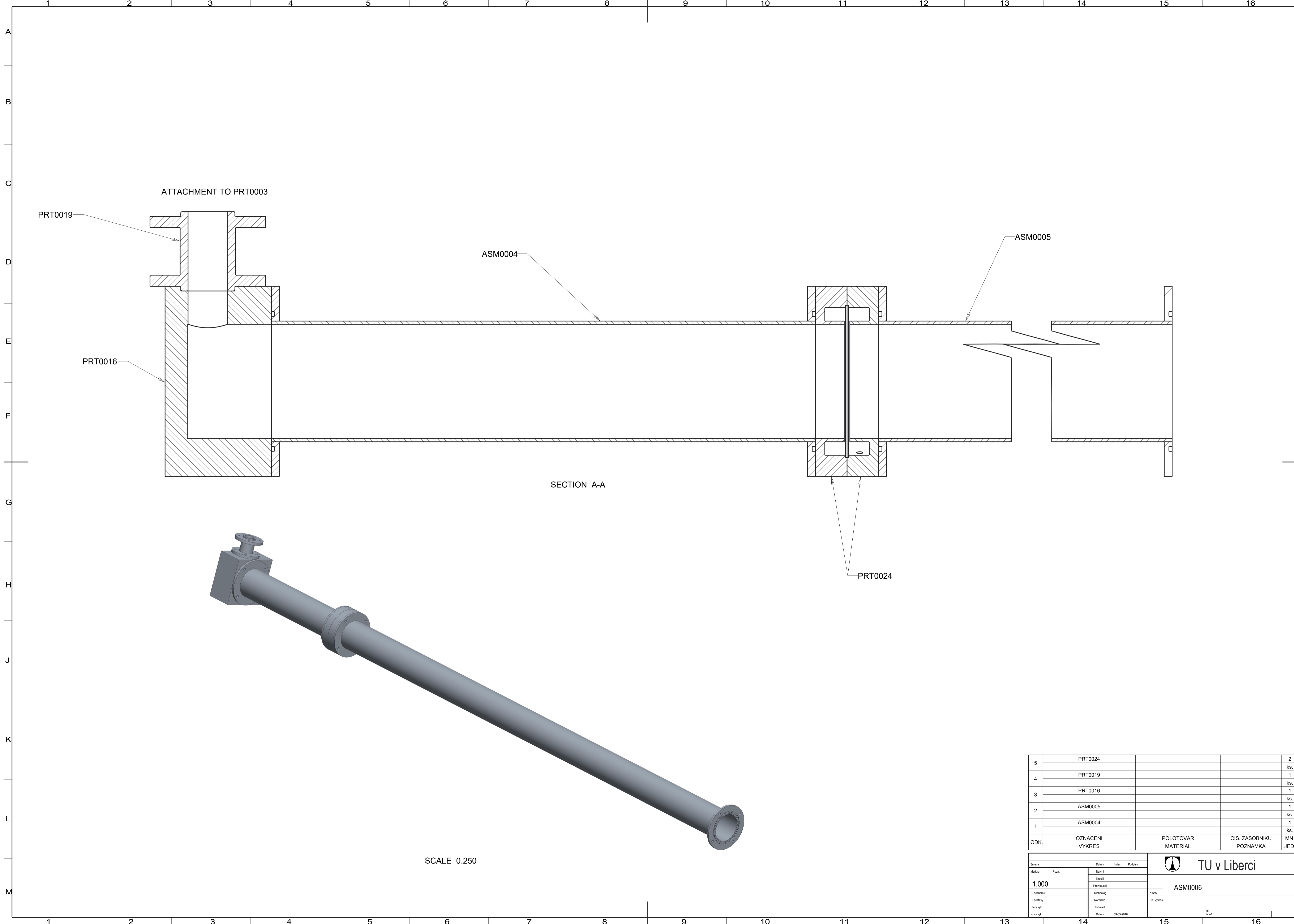
TU v Liberci	
ASM0001	
Str. 1 z 1	



SECTION XSEC0002-XSEC0002

22	WASHER_PLAIN_M6			12
				ks.
21	WASHER_PLAIN_M5_1MMT			2
				ks.
20	PRT0027			1
				ks.
19	PRT0021			1
				ks.
18	PRT0020			1
				ks.
17	PRT0018			1
				ks.
16	PRT0017			1
				ks.
15	PRT0012			1
				ks.
14	PRT0011			1
				ks.
13	PRT0010			1
				ks.
12	PRT0009			1
				ks.
11	PRT0005			1
				ks.
10	PRT0003			1
				ks.
9	PRT0002			1
				ks.
8	PRT0001			1
				ks.
7	PLATE2			1
				ks.
6	PLATE1			1
				ks.
5	NUT_M6			12
				ks.
4	NPA21_2_03			1
				ks.
3	MSSFS6-8_2_03			4
				ks.
2	BOLT_STUD_M6_300MM			4
				ks.
1	ADAPTER_M10X1_PART2A			1
				ks.
ODK	OZNACENI	POLOTOVAR	CIS. ZASOBNIKU	MN.
	VYKRES	MATERIAL	POZNAMKA	JED.

Zmena	Datum	Index	Podpis	 TU v Liberci
1.400				
C. sestavy	Technicky			Nazev
C. sestavy	Normaliz.			Ch. vyřesku
Stary vřt.	Schvalil			
Novy vřt.	Datum	06-04-2015		Str 1 z 1



ATTACHMENT TO PRT0003

PRT0019

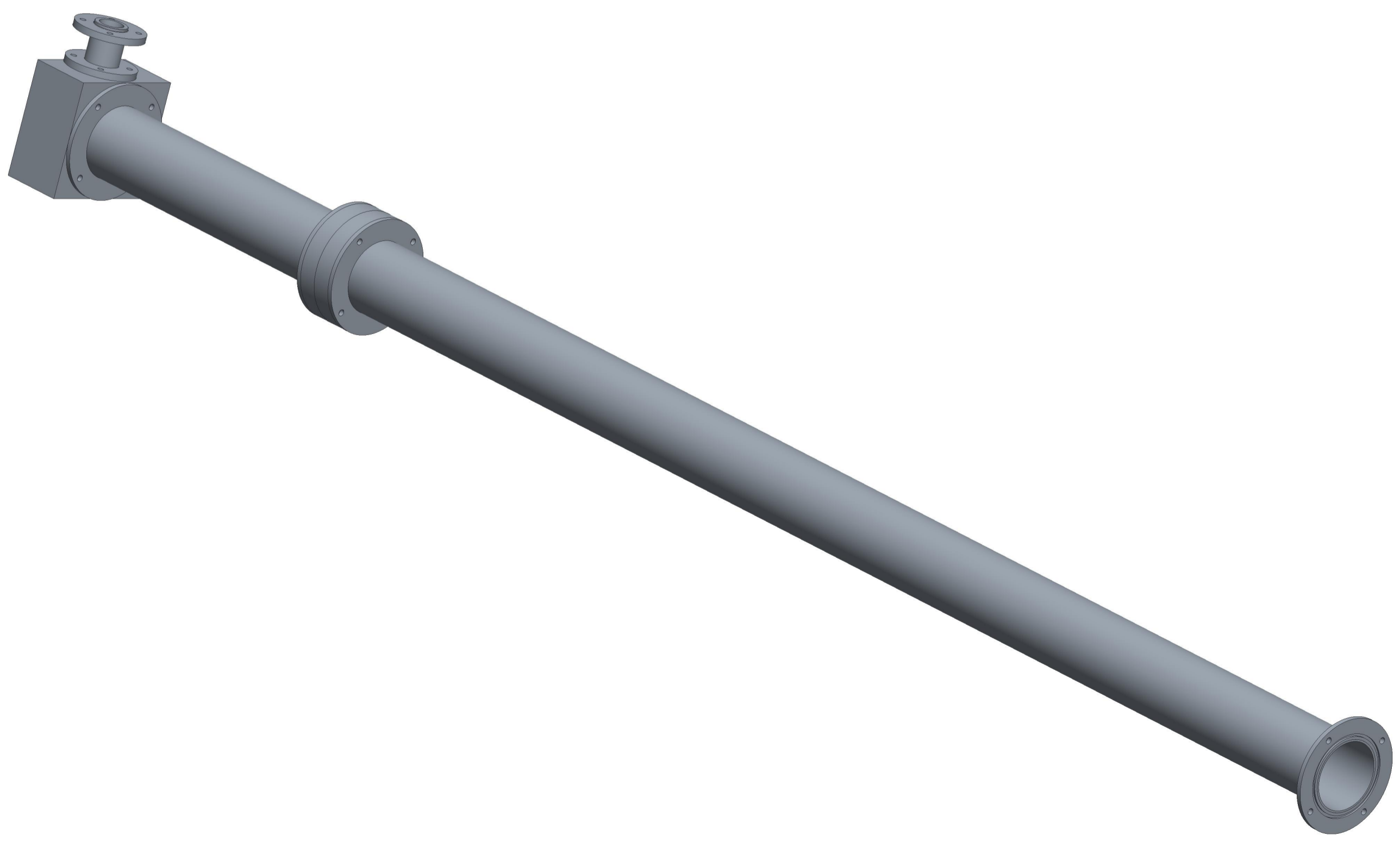
ASM0004

ASM0005

PRT0016

SECTION A-A

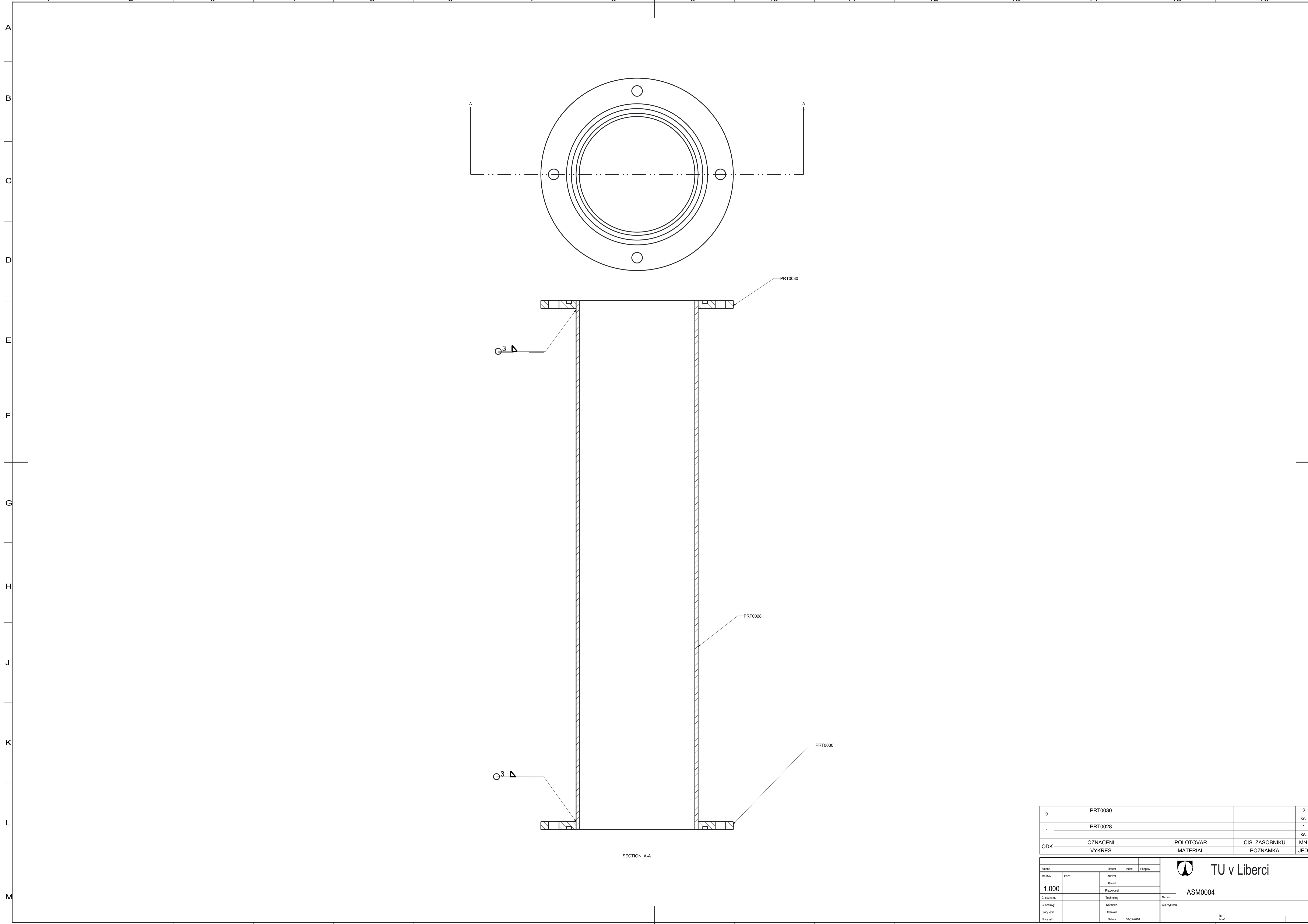
PRT0024



SCALE 0.250

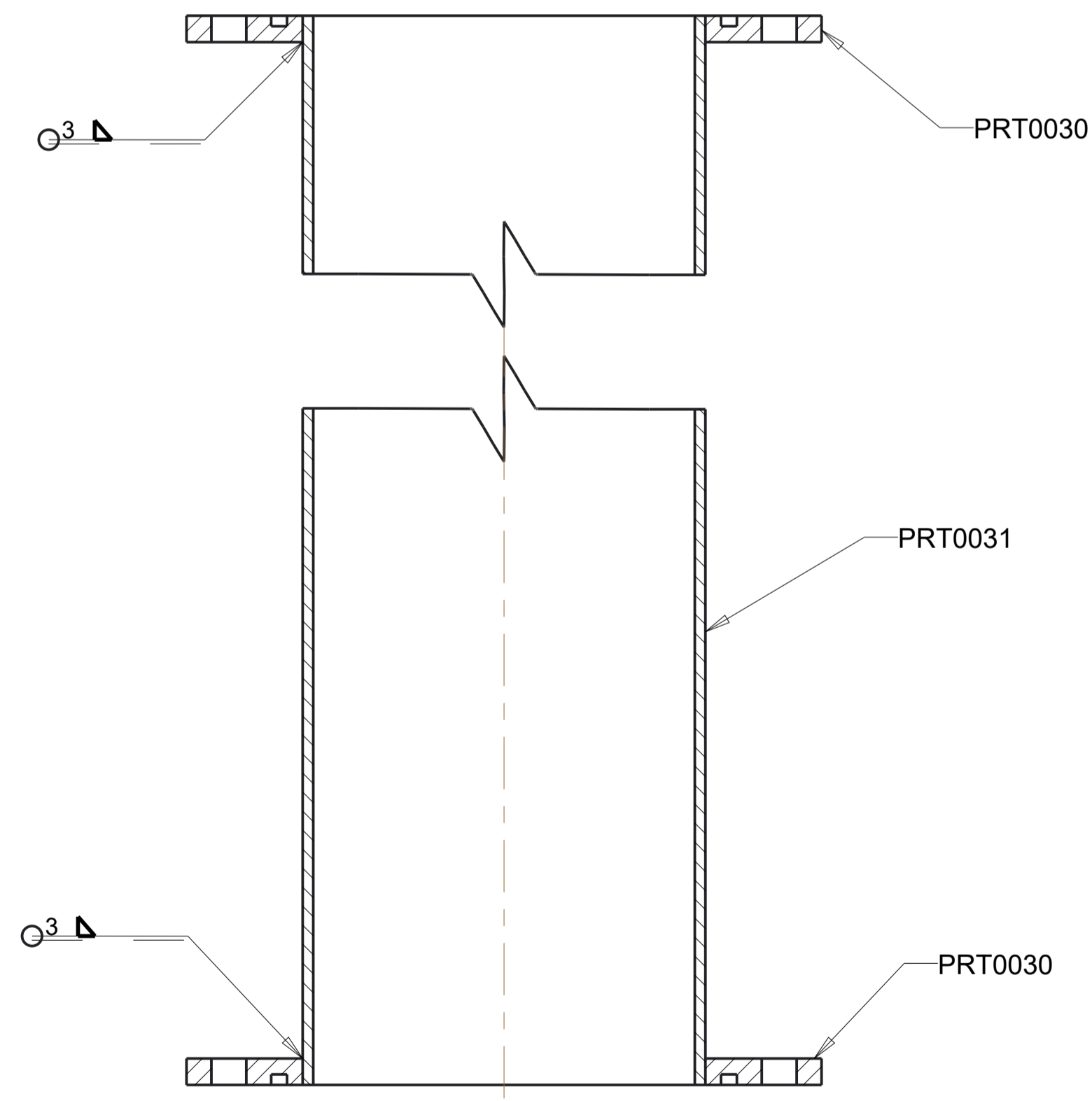
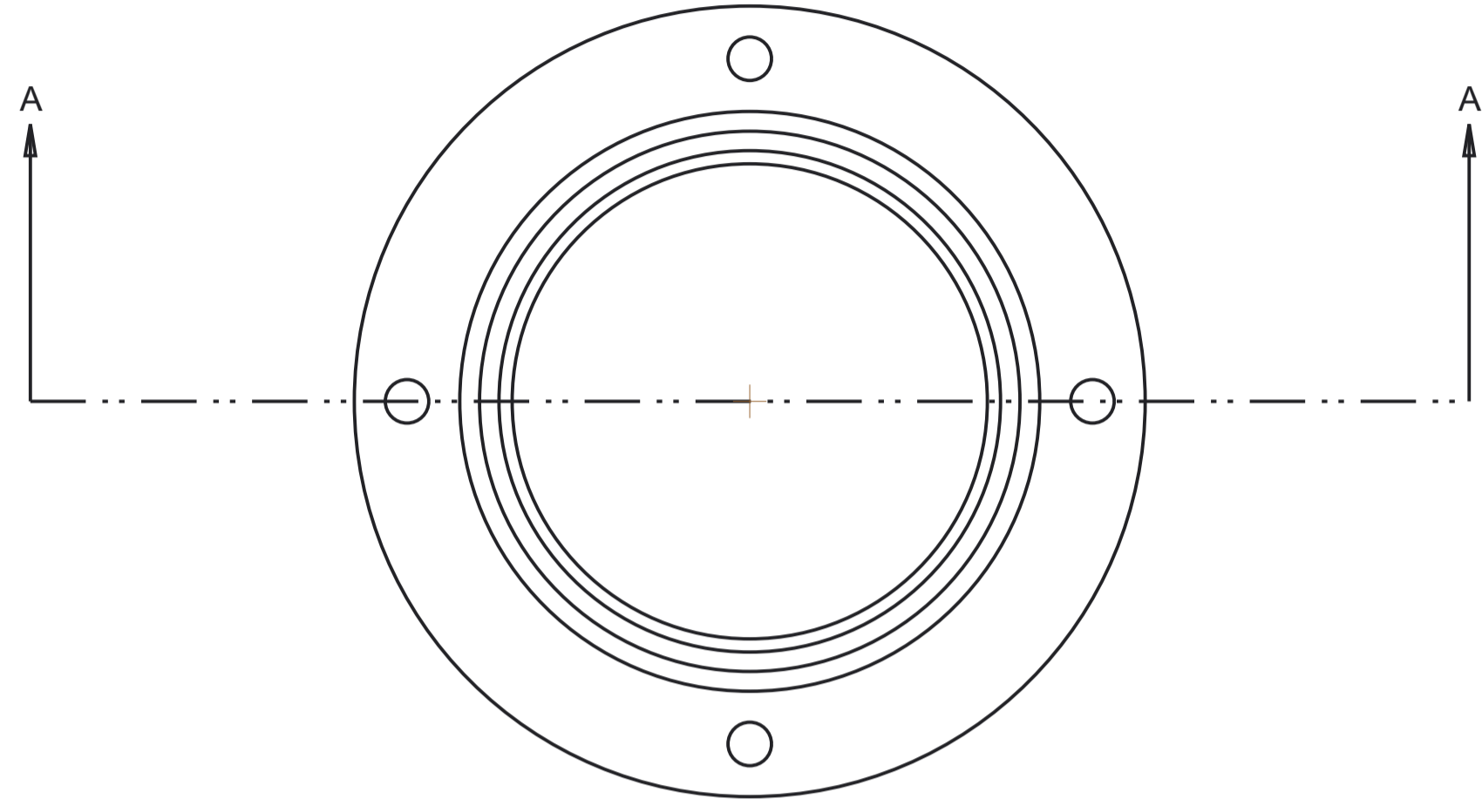
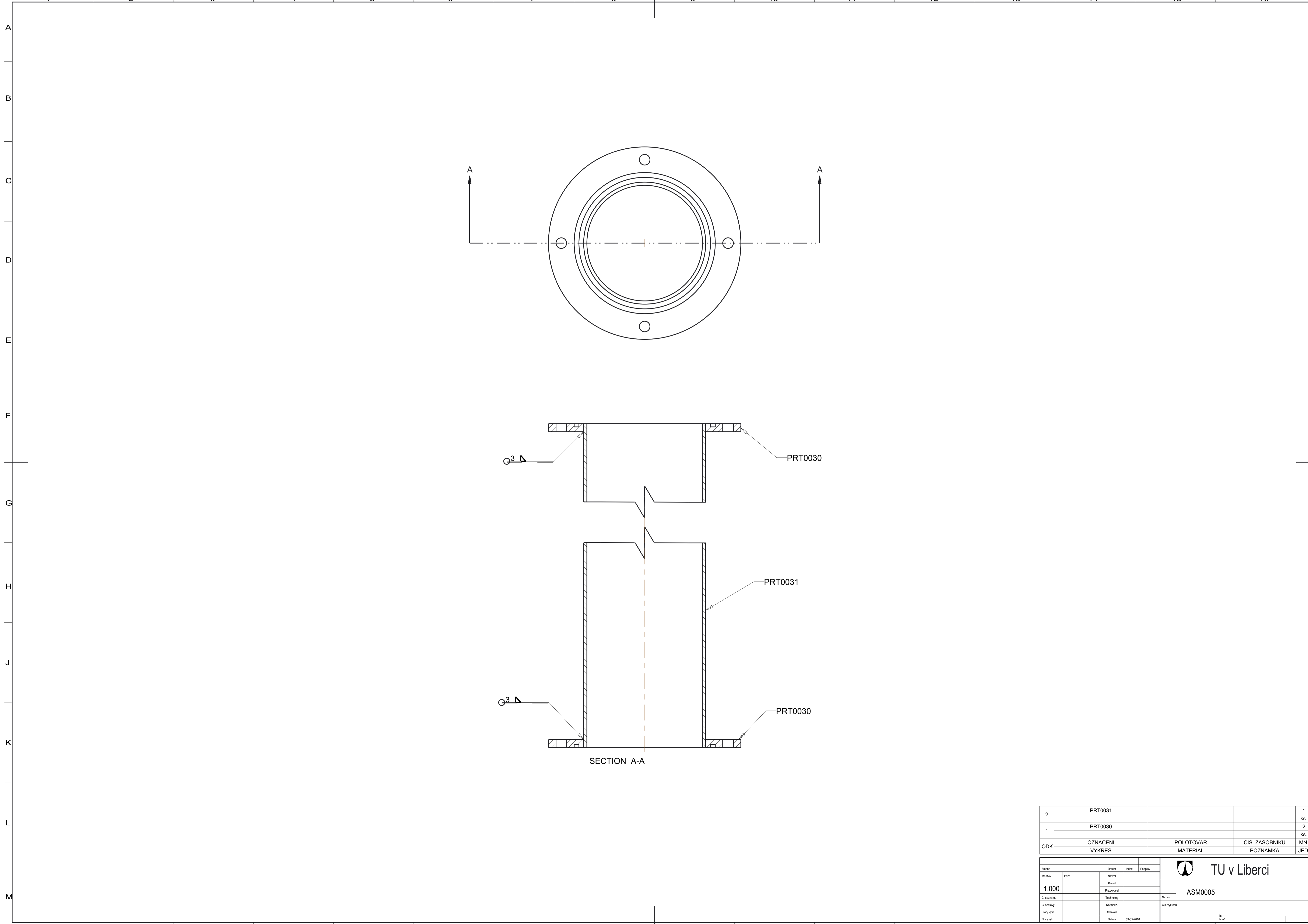
5	PRT0024			2
				ks.
4	PRT0019			1
				ks.
3	PRT0016			1
				ks.
2	ASM0005			1
				ks.
1	ASM0004			1
				ks.
ODK	OZNACENI	POLOTOVAR	CIS. ZASOBNIKU	MN.
	VYKRES	MATERIAL	POZNAMKA	JED.

Zmena		Datum	Index	Podpis	 TU v Liberci
Merklo	Prizn.	Nacrhl			
		Kreslil			ASM0006
		Prepracoval			
C. sestava		Technicky			Nazev
C. sestavy		Normaliz.			Obj. vyřetku
Stary vylt.		Schvalil			
Novy vylt.		Datum	04-05-2016		
					Str 1
					Str 1



2	PRT0030			2
				ks.
1	PRT0028			1
				ks.
ODK	OZNACENI	POLOTOVAR	CIS. ZASOBNIKU	MN.
	VYKRES	MATERIAL	POZNAMKA	JED.

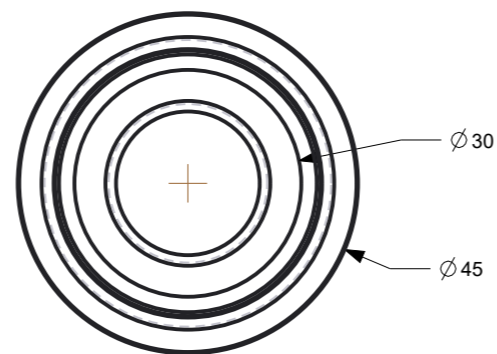
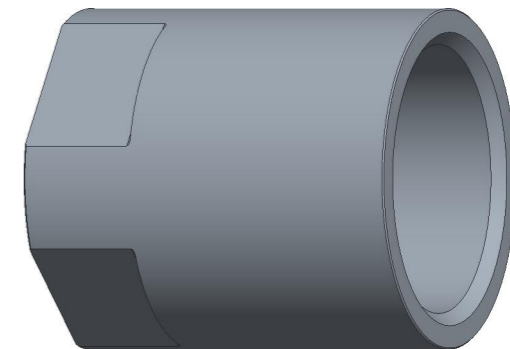
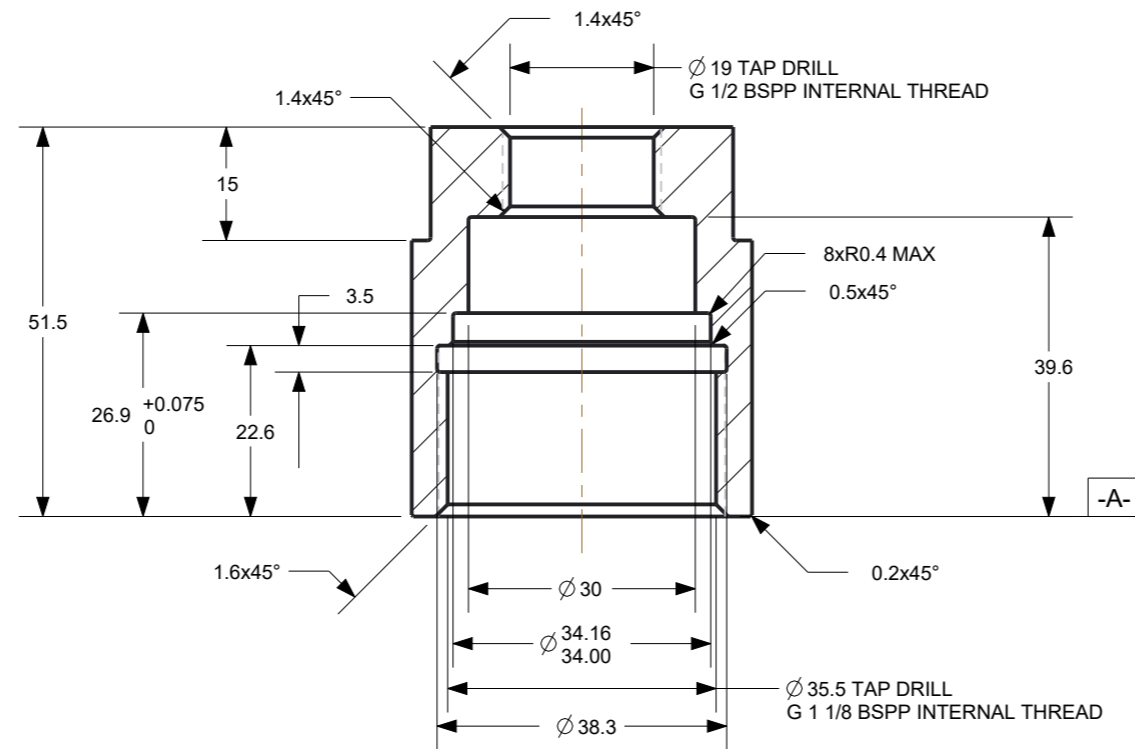
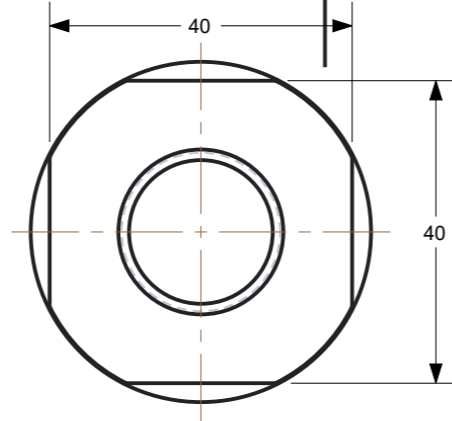
Zmena		Datum	Index	Podpis	 TU v Liberci ASM0004
Merklo	Prizn.	Nacrth			
		Kresli			
		Preclousel			
C. sestavy		Technickij			Nazev
C. sestavy		Normaliz.			Obj. vyřesku
Stary vylt.		Schvalil			
Novy vylt.		Datum	10-05-2016		Str 1
					Str 1



SECTION A-A

2	PRT0031			1
				ks.
1	PRT0030			2
				ks.
ODK	OZNACENI	POLOTOVAR	CIS. ZASOBNIKU	MN.
	VYKRES	MATERIAL	POZNAMKA	JED.

Zmena		Datum	Index	Popis	 TU v Liberci
Merka	Prizn.	Nacrhl	Kreslil	Prepracoval	
1.000					Nazev ASM0005
C. sestavy		Technicky			Cis. vykresu 1
Stary vzh.		Normaliz.			
Novy vzh.		Schválil			
		Datum	20-05-2015		



NOTES:
 1. BREAK ALL SHARP EDGES UNLESS OTHERWISE SPECIFIED.
 2. ALL CORNER FILLET R0.4 MAX
 3. MATERIAL:BRASS
 4. DIMENSIONING AND TOLERANCING ACCORDING TO ASME Y14.5

GENERIC TOLERANCE:
 XX ± 0.125
 XX.X ± 0.075
 XX.XX ± 0.050
 XX° ± 0.01

Roz. -Polot.				Mater.		Tr. odp		Presnos Tolerovani	
		c)		C. hm		Hr. hm.			
		b)							
		a)							
Zmena		Datum		Index		Podpisy			
Meritko		Pozn.		Navrhl		Kreslil			
1.000				A. GUANLAO				Nazev PRT0001	
C. seznamu				Prezkousel				Cis. vykresu	
C. sestavy				Technolog					
Stary vykr.				Normaliz.					
Novy vykr.				Schvallil					
				Datum		06-03-2016		list 1 listu1	

1 2 3 4 5 6 7 8

A

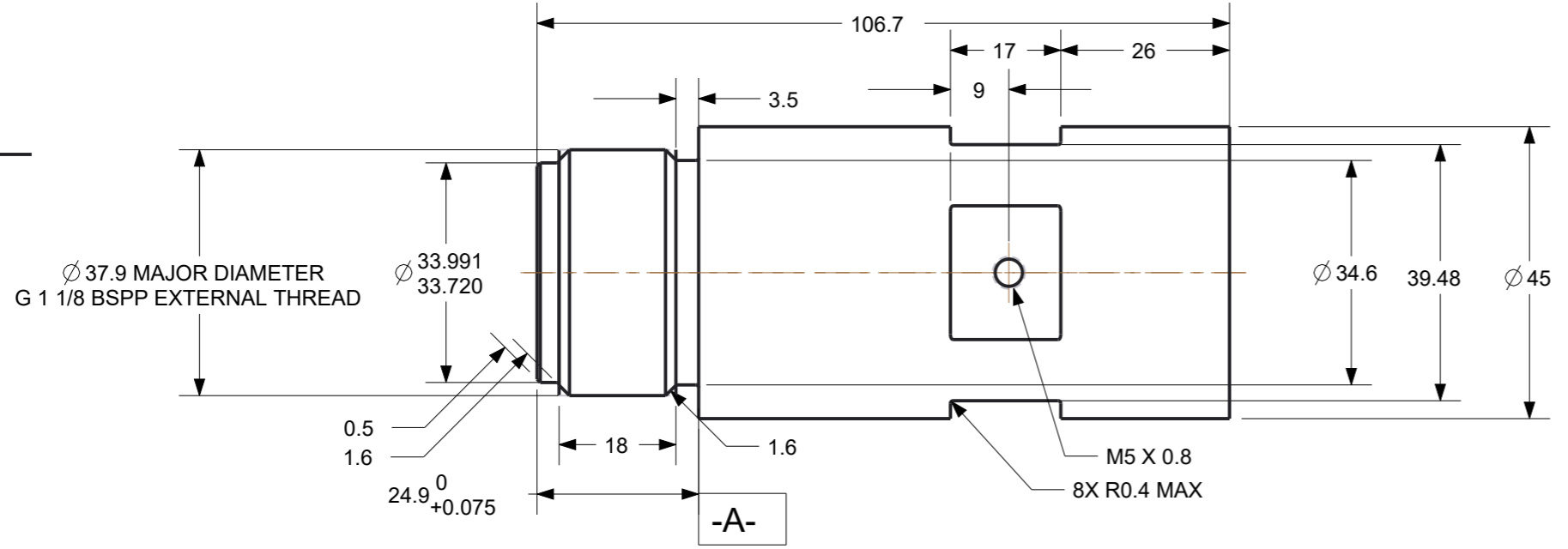
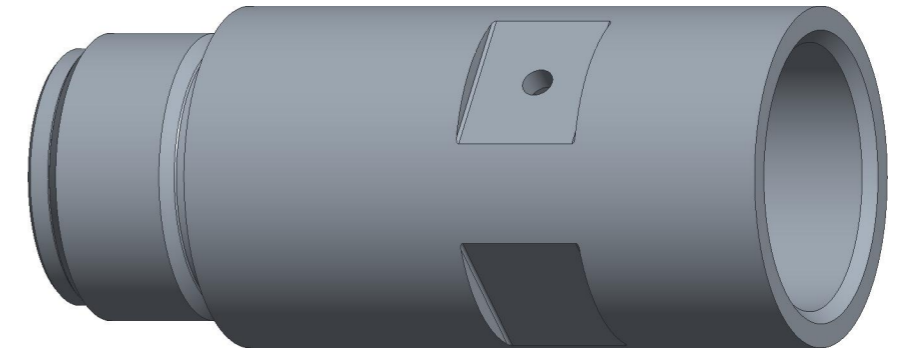
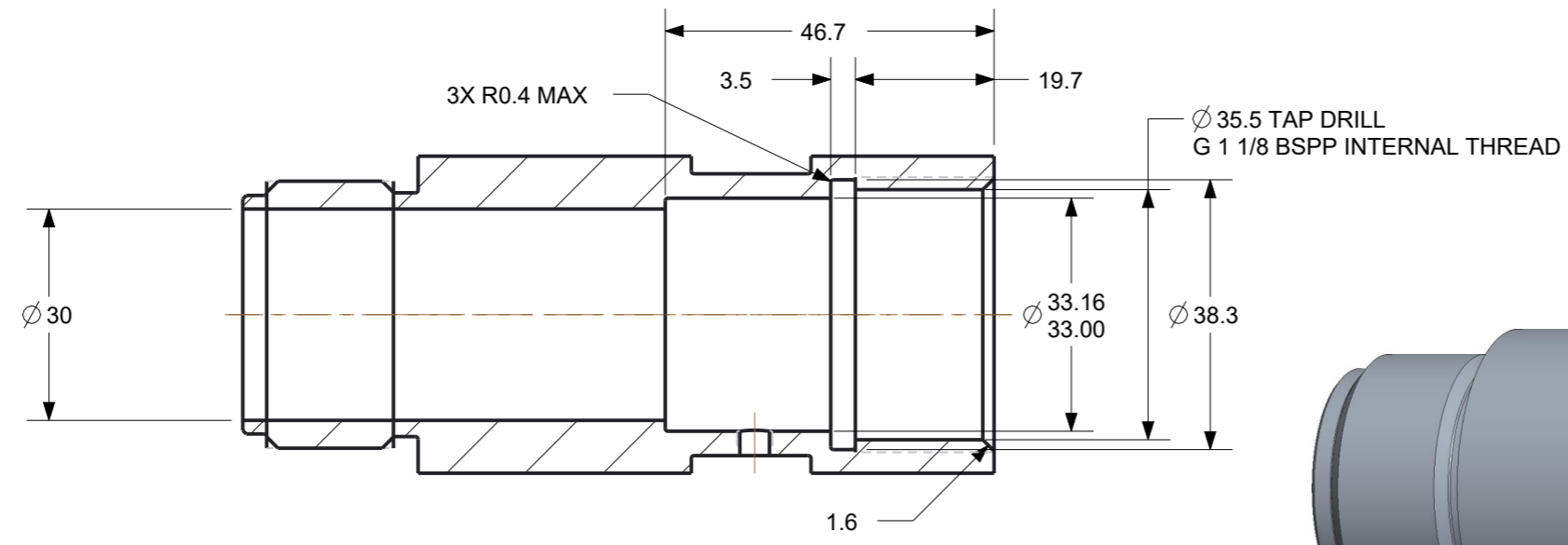
B

C

D

E

F

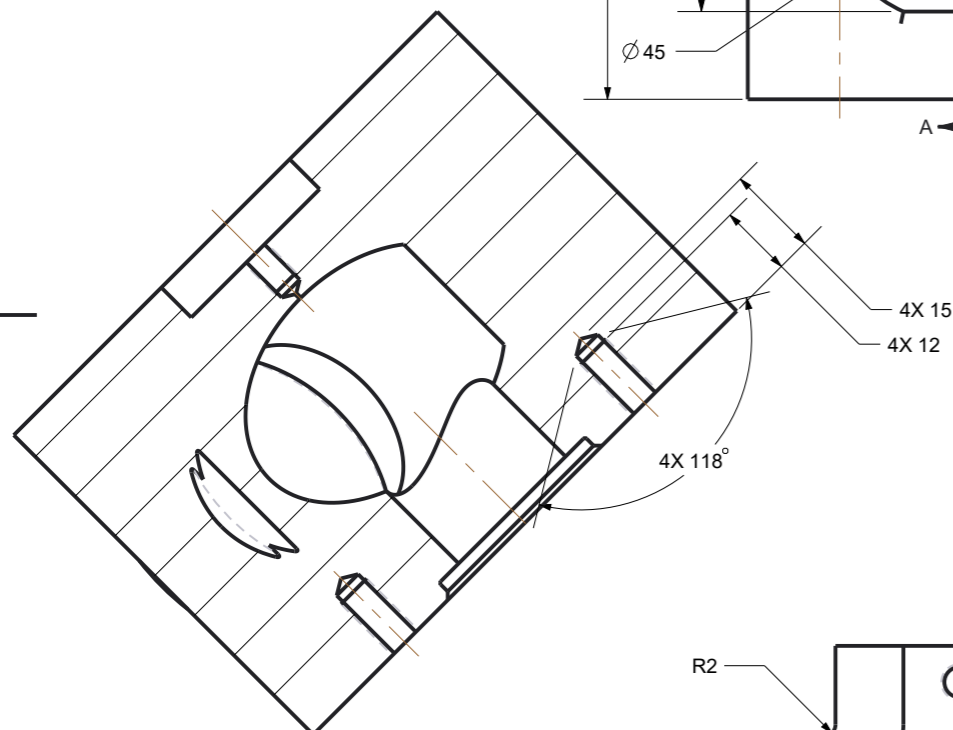
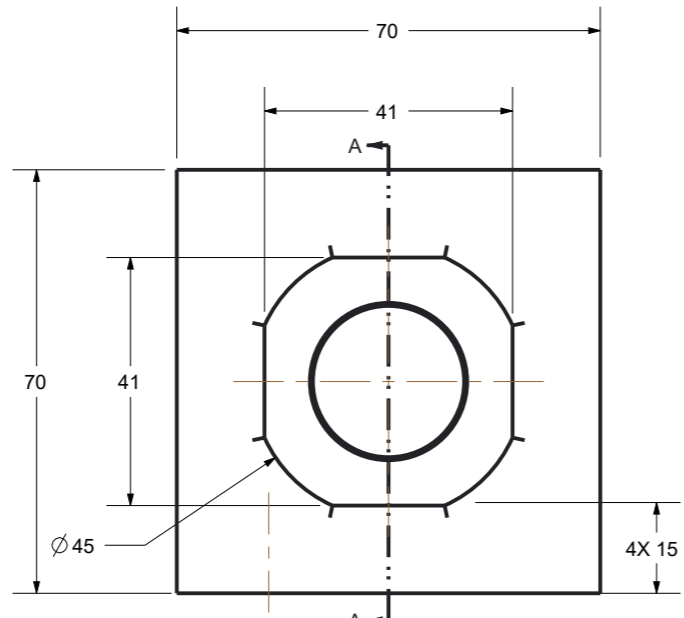
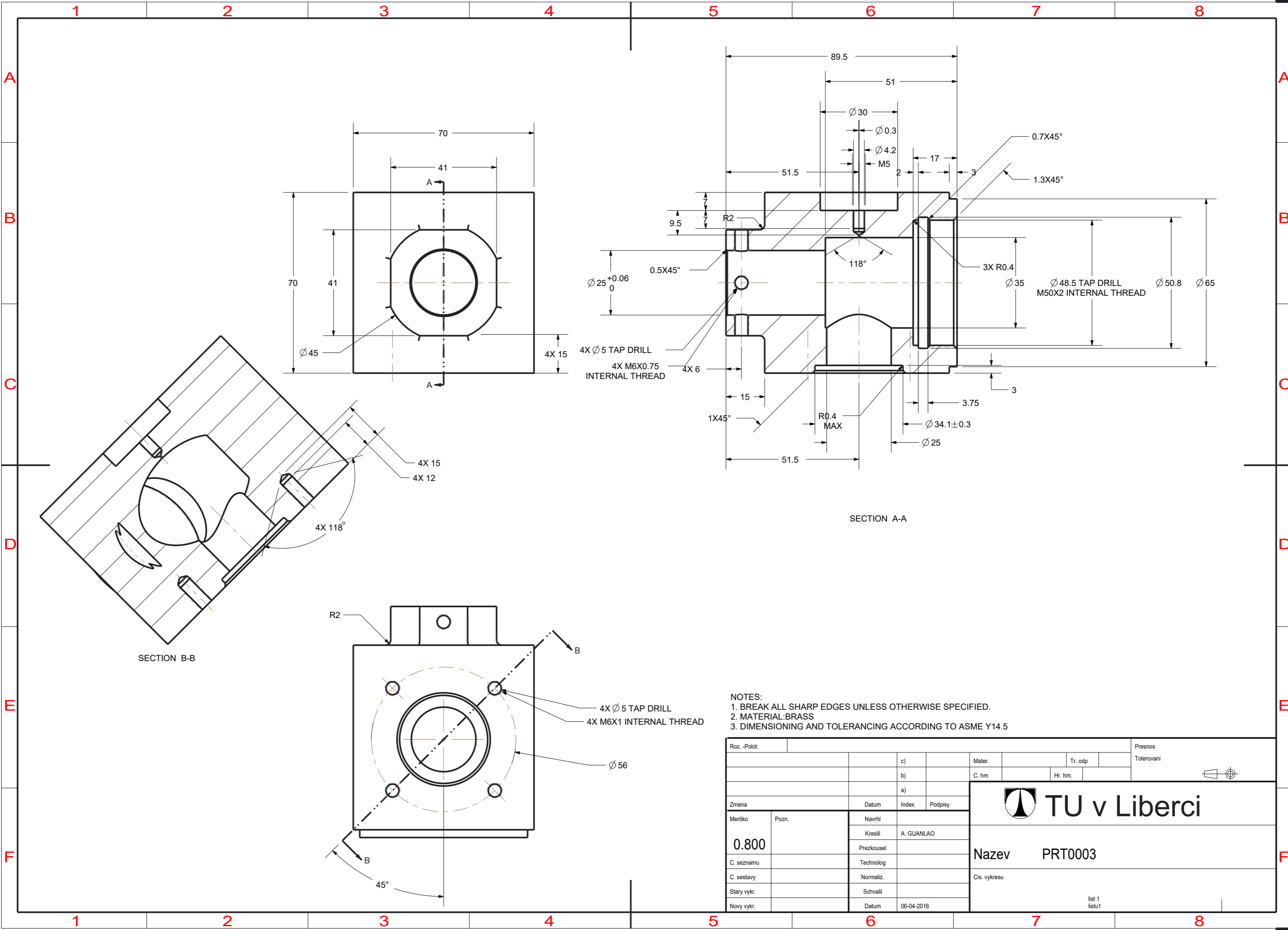


NOTES:
 1. BREAK ALL SHARP EDGES UNLESS OTHERWISE SPECIFIED.
 2. ALL CORNER FILLET R0.4 MAX
 3. MATERIAL:BRASS
 4. DIMENSIONING AND TOLERANCING ACCORDING TO ASME Y14.5

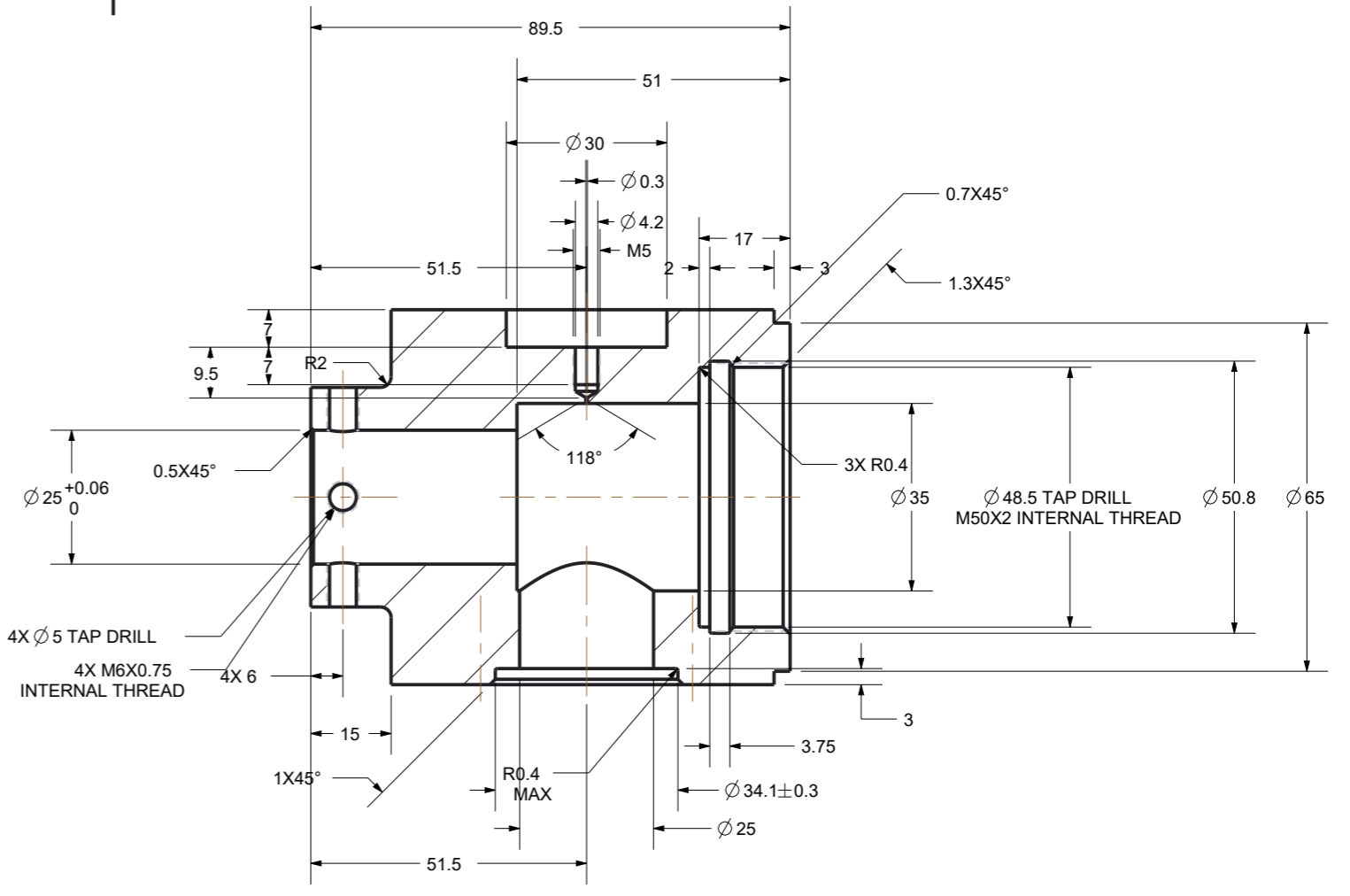
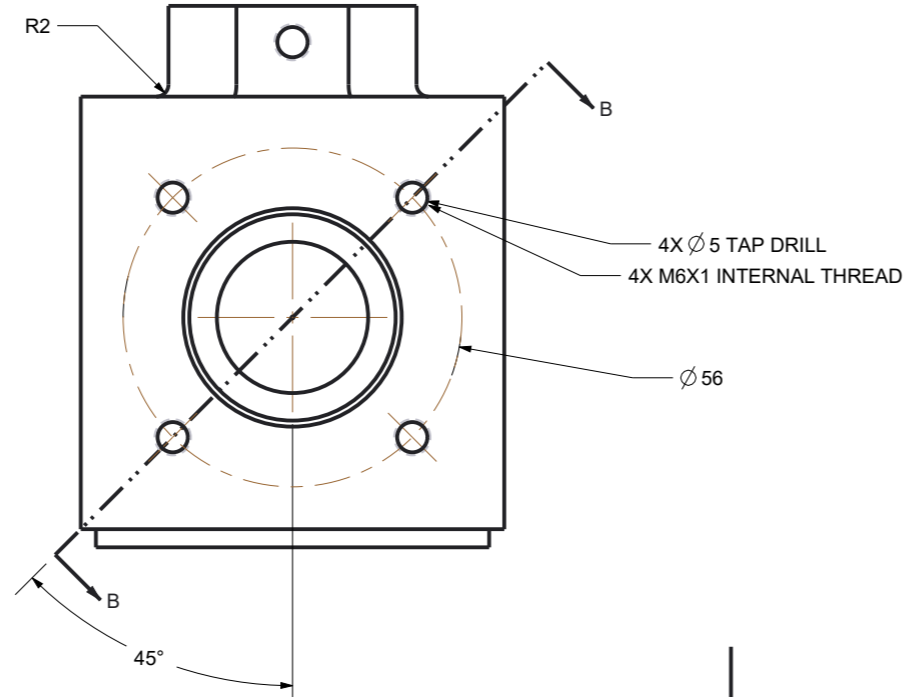
GENERIC TOLERANCE:
 XX ± 0.125
 XX.X ± 0.075
 XX.XX ± 0.050
 XX^o ± 0.01

Roz. -Polot.				Presnos Tolerovani	
		c)		Mater.	Tr. odp
		b)		C. hm	Hr. hm.
		a)			
Zmena	Datum	Index	Podpisy	 TU v Liberci Nazev PRT0002 Cis. vykresu list 1 listu1	
Meritko	Pozn.	Navrhil			
1.000		Kresilil	A.GUANLAO		
C. seznamu		Prezkousel			
C. sestavy		Technolog			
Stary vykr.		Normaliz.			
Novy vykr.		Schvallil			
		Datum	06-03-2016		

1 2 3 4 5 6 7 8



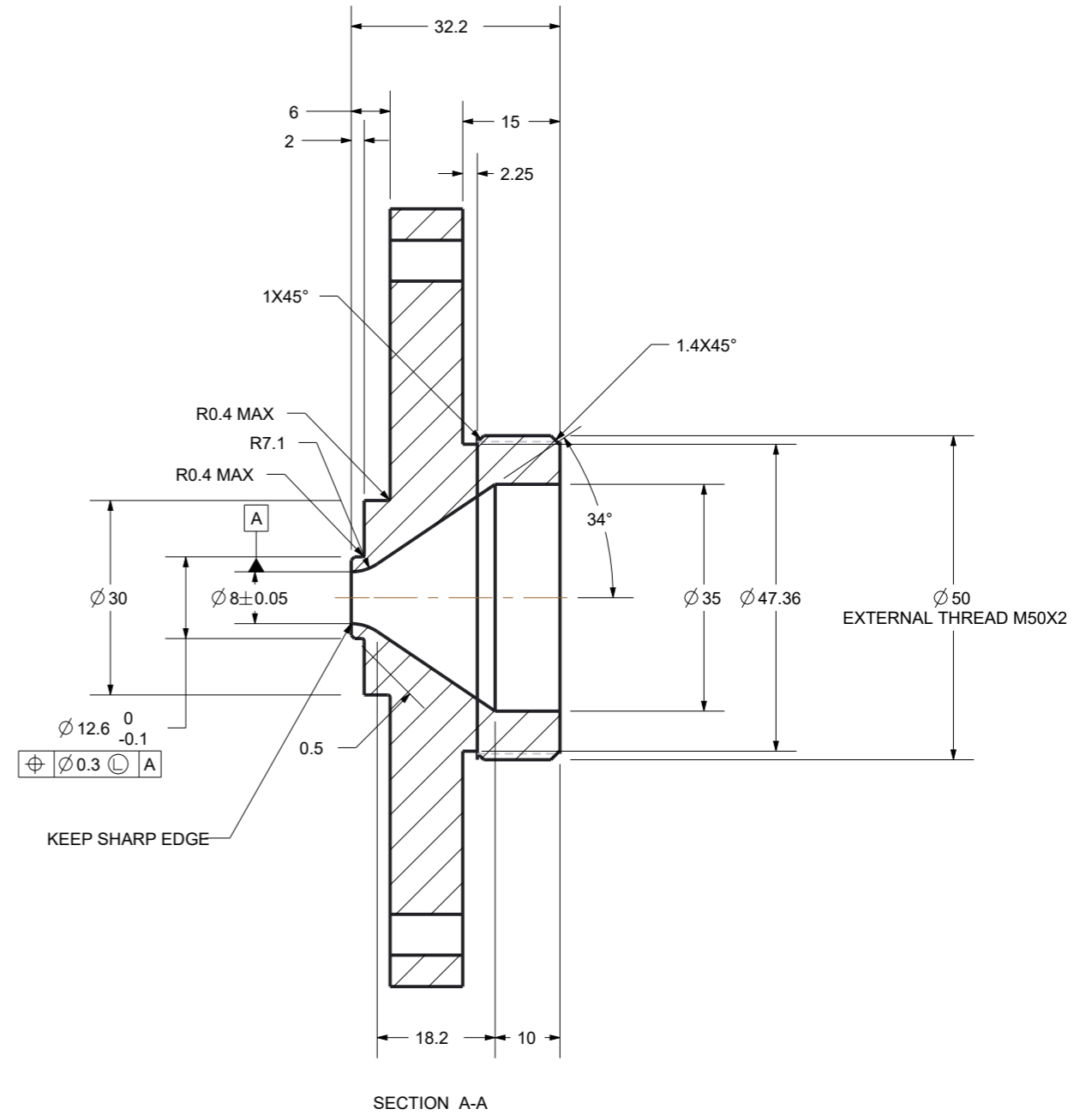
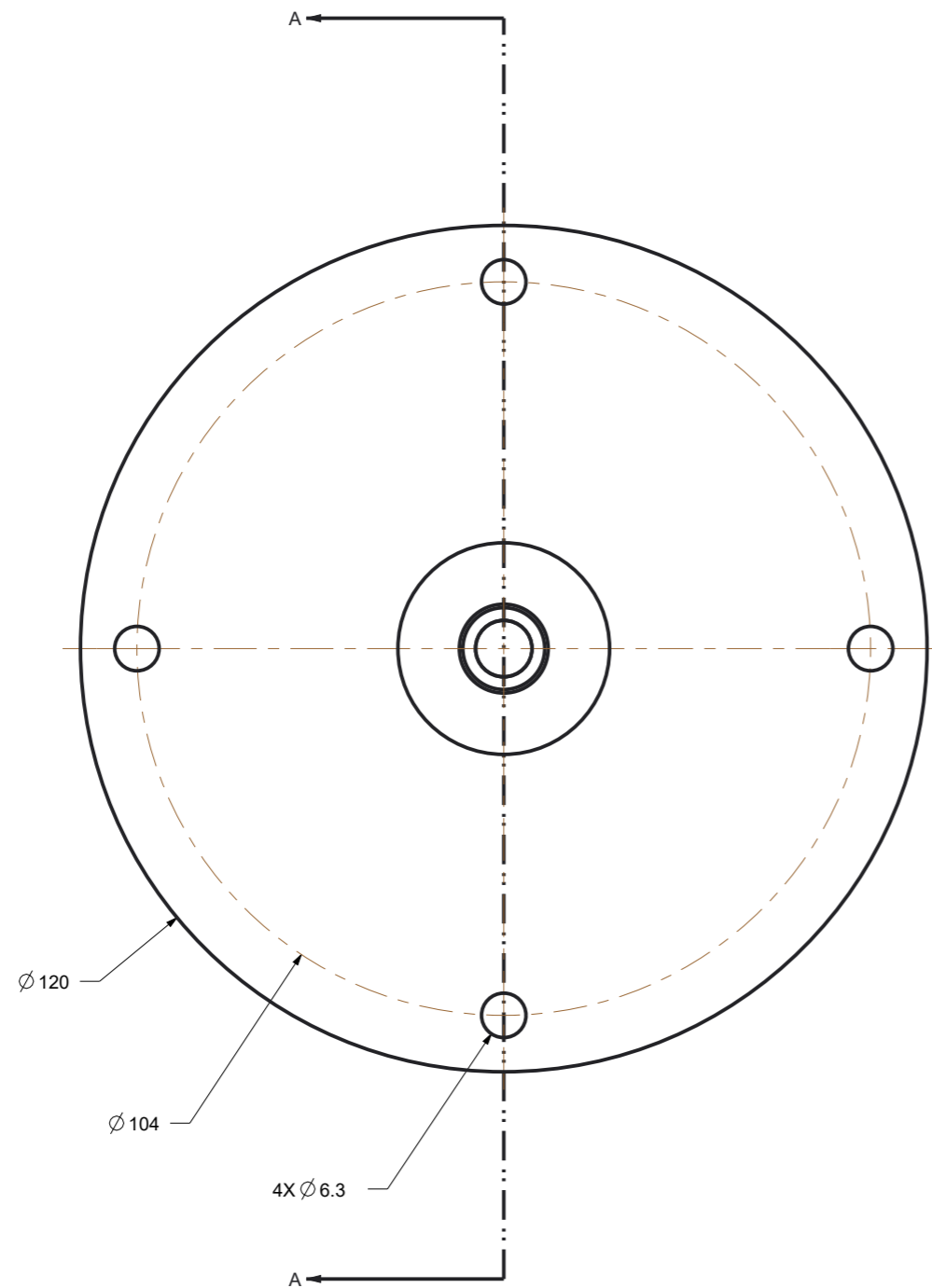
SECTION B-B



SECTION A-A

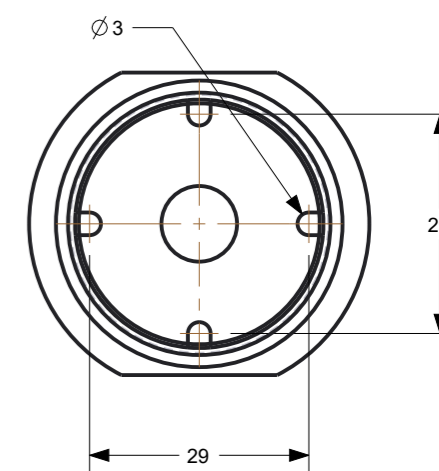
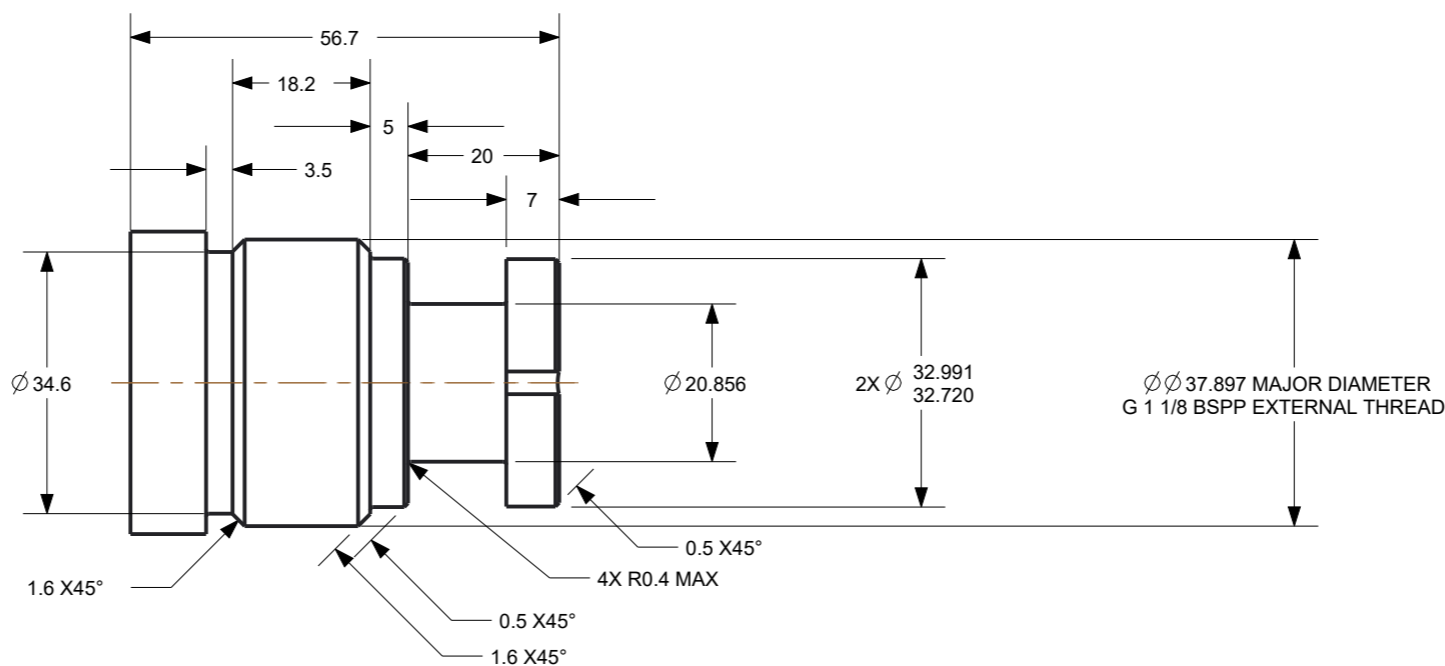
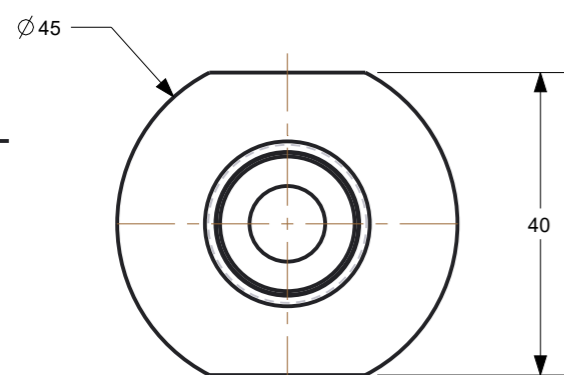
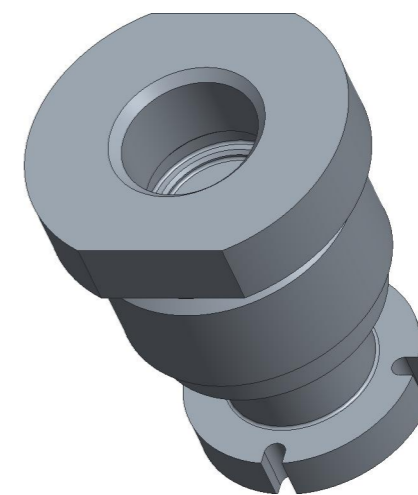
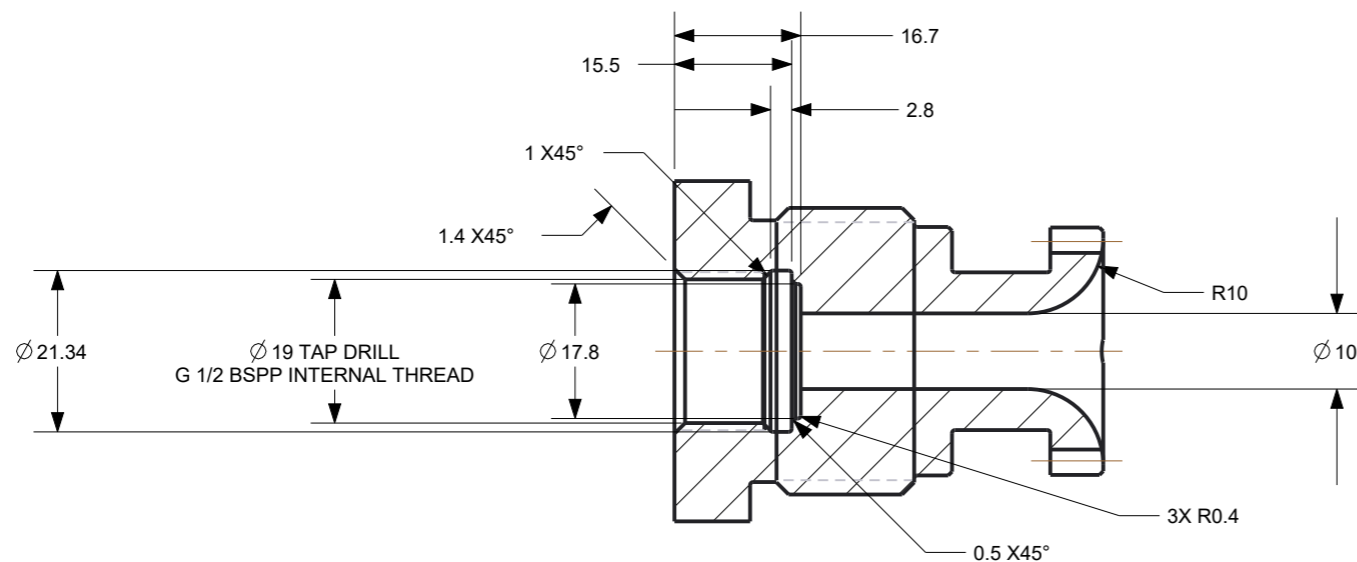
NOTES:
 1. BREAK ALL SHARP EDGES UNLESS OTHERWISE SPECIFIED.
 2. MATERIAL: BRASS
 3. DIMENSIONING AND TOLERANCING ACCORDING TO ASME Y14.5

Roz. -Polot.				Presnos Tolerovani					
				c) Mater.		Tr. odp			
				b) C. hm		Hr. hm.			
				a)					
Zmena		Datum		Index		Podpisy			
Meritko	Pozn.	Navrhl		TU v Liberci Nazev PRT0003 Cis. vykresu list 1 listu 1					
0.800		Kreslil						A. GUANLAO	
C. seznamu		Prezkousel							
C. sestavy		Technolog							
Stary vykr.		Normaliz.							
Novy vykr.		Schvallil				Datum			
		06-04-2016							



- NOTES:
 1. BREAK ALL SHARP EDGES UNLESS OTHERWISE SPECIFIED.
 2. MATERIAL:BRASS
 3. DIMENSIONING AND TOLERANCING ACCORDING TO ASME Y14.5

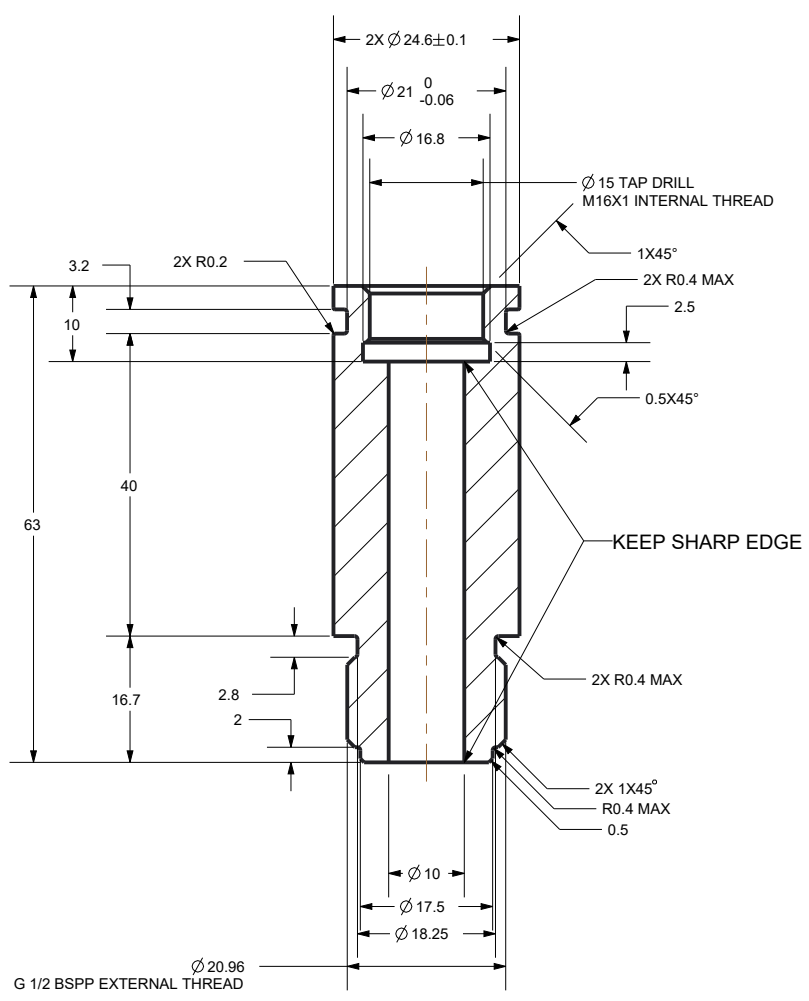
Roz. -Polot.				Presnos Tolerovani	
		c)		Mater.	Tr. odp
		b)		C. hm	Hr. hm.
		a)			
Zmena		Datum	Index	Podpisy	
Meritko	Pozn.	Navrhl			
1.000		Kresil	A.GUANLAO		
C. seznamu		Prezkousel			
C. sestavy		Technolog			
Stary vykr.		Normaliz.			
Novy vykr.		Schvail			
		Datum	05-04-2016		
				Nazev PRT0005 Cis. vykresu list 1 listu1	



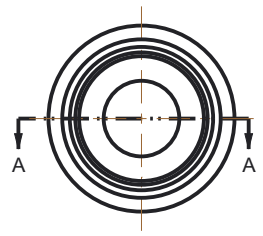
- NOTES:
 1. BREAK ALL SHARP EDGES UNLESS OTHERWISE SPECIFIED.
 2. ALL CORNER FILLET R0.4 MAX
 3. MATERIAL:BRASS
 4. DIMENSIONING AND TOLERANCING ACCORDING TO ASME Y14.5

GENERIC TOLERANCE:
 XX ± 0.125
 XX.X ± 0.075
 XX.XX ± 0.050
 XX° ± 0.01

Roz. -Polot.				Presnos Tolerovani	
		c)		Mater.	Tr. odp
		b)		C. hm	Hr. hm.
		a)			
Zmena	Datum	Index	Podpisy	 TU v Liberci Nazev PRT0009 Cis. vykresu list 1 listu1	
Meritko	Pozn.	Navrhl			
1.000		Kreslil	A. GUANLAO		
C. seznamu		Prezkousel			
C. sestavy		Technolog			
Stary vykr.		Normaliz.			
Novy vykr.		Schvallil			
		Datum	06-03-2016		

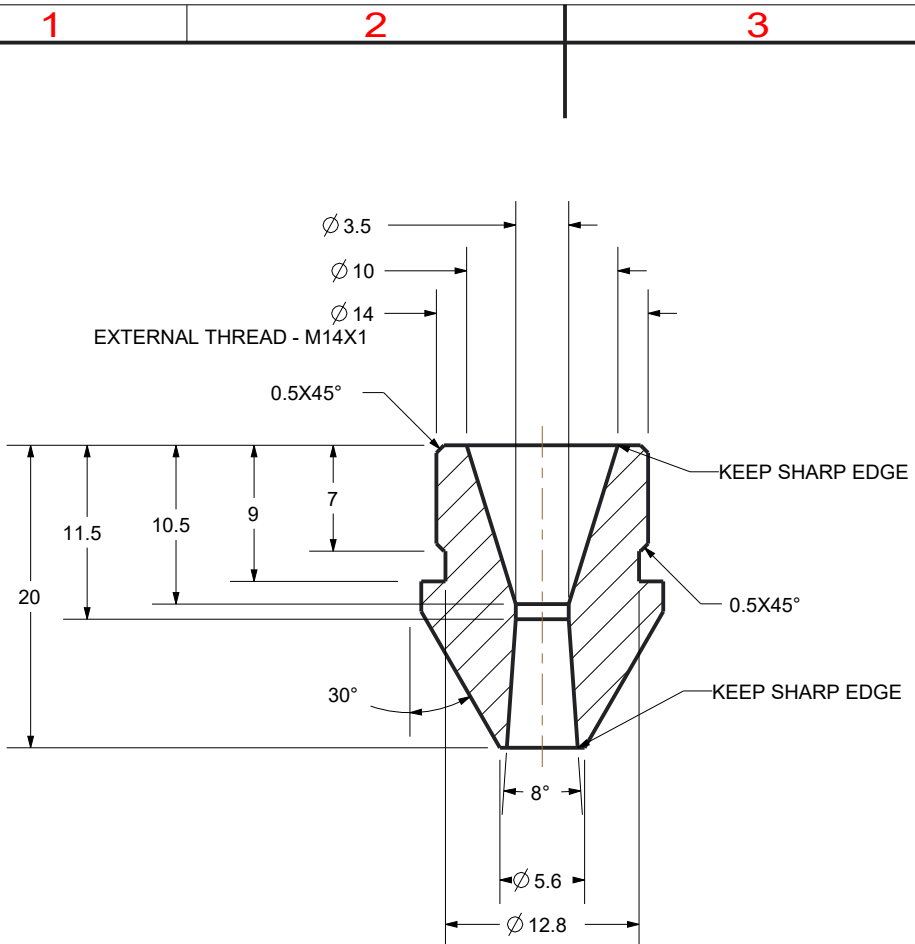


SECTION A-A

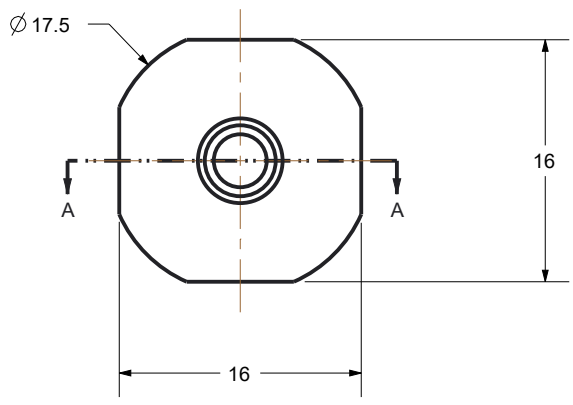


- NOTES:
 1. BREAK ALL SHARP EDGES UNLESS OTHERWISE SPECIFIED.
 2. MATERIAL:BRASS
 3. DIMENSIONING AND TOLERANCING ACCORDING TO ASME Y14.5

Roz. -Polot.				Mater.		Tr. odp		Presnos Tolerovani	
		c)		C. hm		Hr. hm.			
		b)							
		a)							
Zmena		Datum		Index		Podpisy		<h1>TU v Liberci</h1> <p>Nazev PRT0010</p> <p>Cis. vykresu</p> <p>list 1 listu 1</p>	
Meritko		Pozn.		Navrhl		A. GUANLAO			
1.000				Kreslil					
C. seznamu				Prezkousel					
C. sestavy				Technolog					
Stary vykr.				Normaliz.					
Novy vykr.		Datum		Schvallil					
				Datum		28-03-2016			



SECTION A-A



- NOTES:
 1. BREAK ALL SHARP EDGES UNLESS OTHERWISE SPECIFIED.
 2. MATERIAL:BRASS
 3. DIMENSIONING AND TOLERANCING ACCORDING TO ASME Y14.5

Roz. -Polot.				Mater.		Tr. odp		Presnos Tolerovani	
		c)		C. hm		Hr. hm.			
		b)							
		a)							
Zmena		Datum		Index		Podpisy		 TU v Liberci Nazev PRT0011 Cis. vykresu	
Meritko		Pozn.		Navrhl		A. GUANLAO			
2.000				Kreslil					
C. seznamu				Prezkousel					
C. sestavy				Technolog					
Stary vykr.				Schvallil					
Novy vykr.		Datum		05-04-2016				list 1 listu 1	

1 2 3 4

A

A

B

B

C

C

D

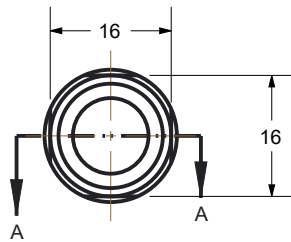
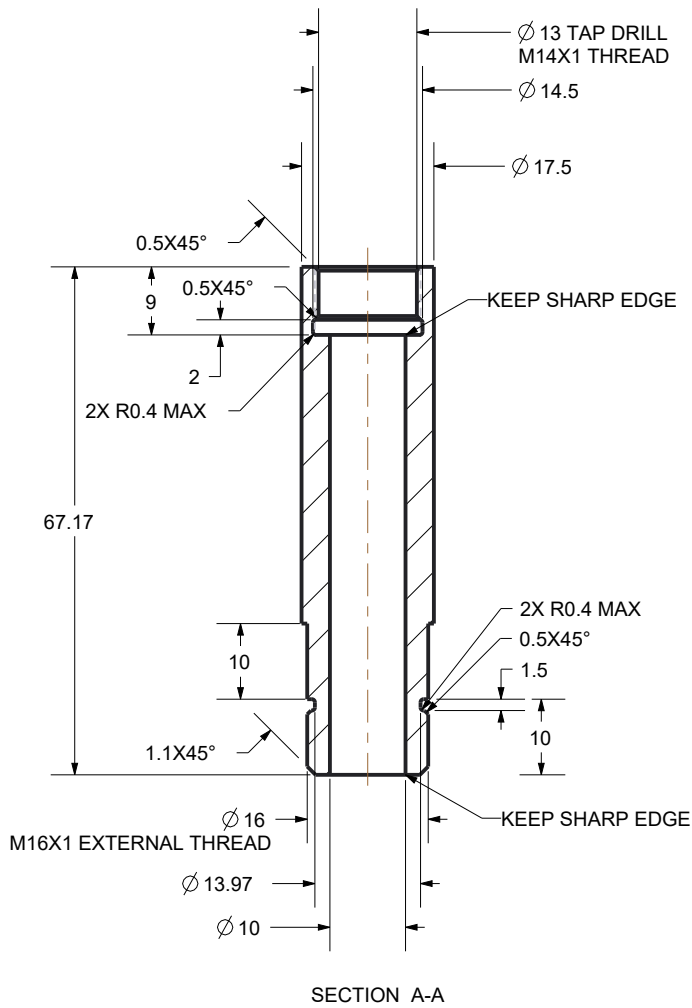
D

E

E

F

F

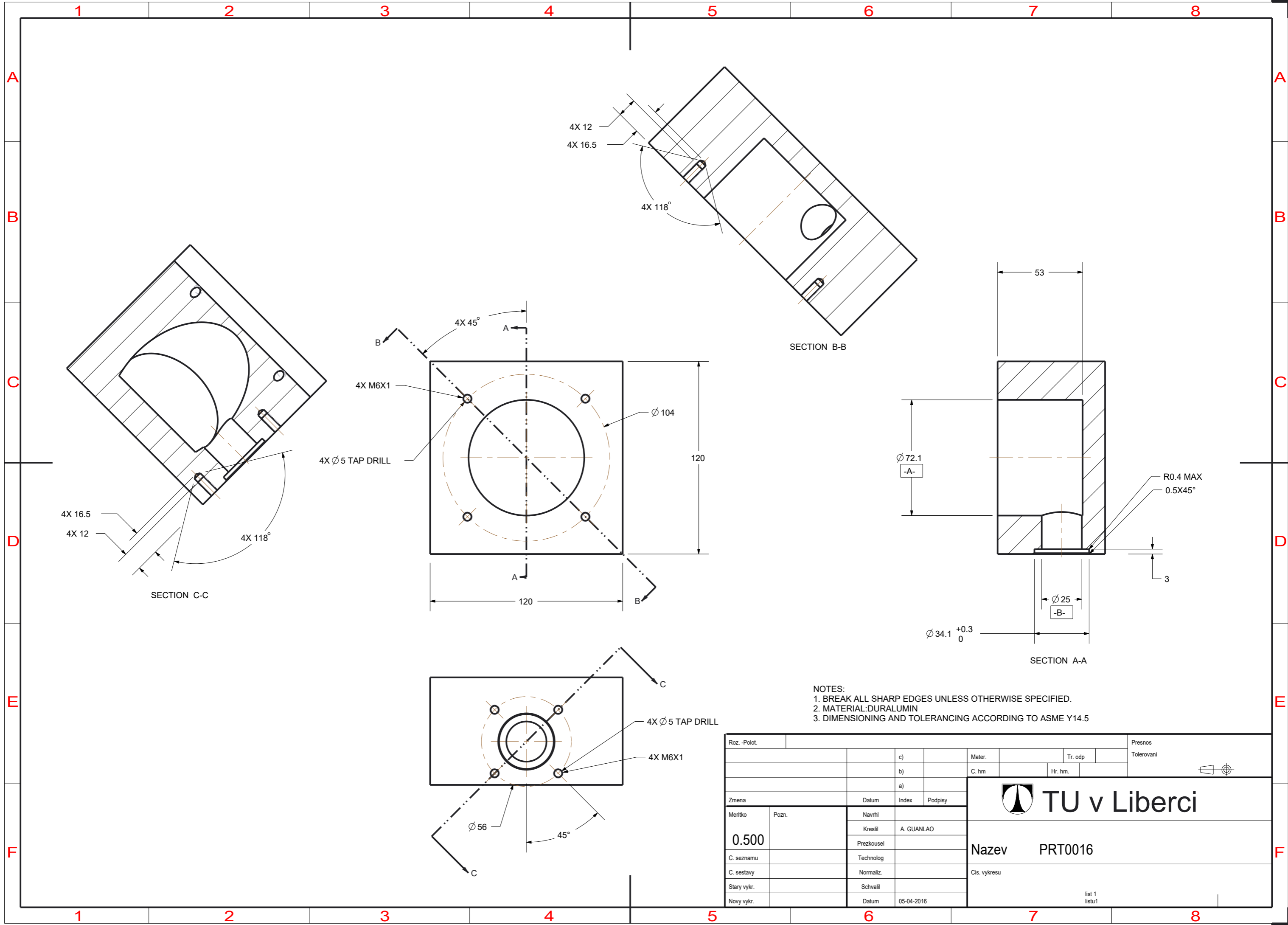


NOTES:

1. BREAK ALL SHARP EDGES UNLESS OTHERWISE SPECIFIED.
2. MATERIAL:BRASS
3. DIMENSIONING AND TOLERANCING ACCORDING TO ASME Y14.5

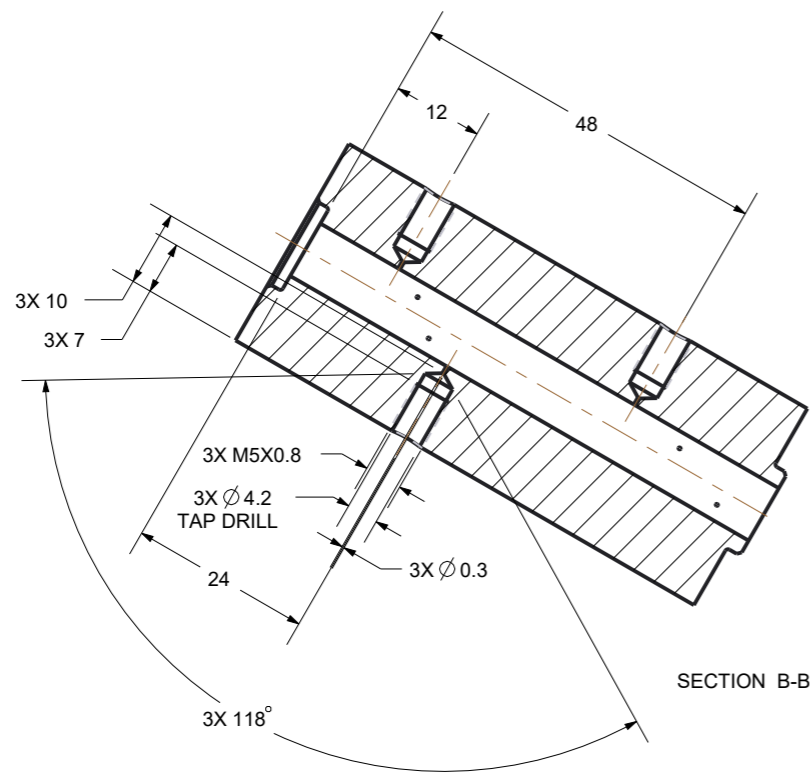
Roz. -Polot.				Mater.		Tr. odp		Presnos	
		c)		C. hm		Hr. hm.		Tolerovani	
		b)							
		a)							
Zmena		Datum		Index		Podpisy		<p>TU v Liberci</p> <p>Nazev PRT0012</p> <p>Cis. vykresu</p> <p>list 1 listu 1</p>	
Meritko		Navrh		Kreslil		A.GUANLAO			
1.000		Prezkousel							
C. seznamu		Technolog							
C. sestavy		Normaliz.							
Stary vykr.		Schvallil							
Novy vykr.		Datum		28-03-2016					

1 2 3 4

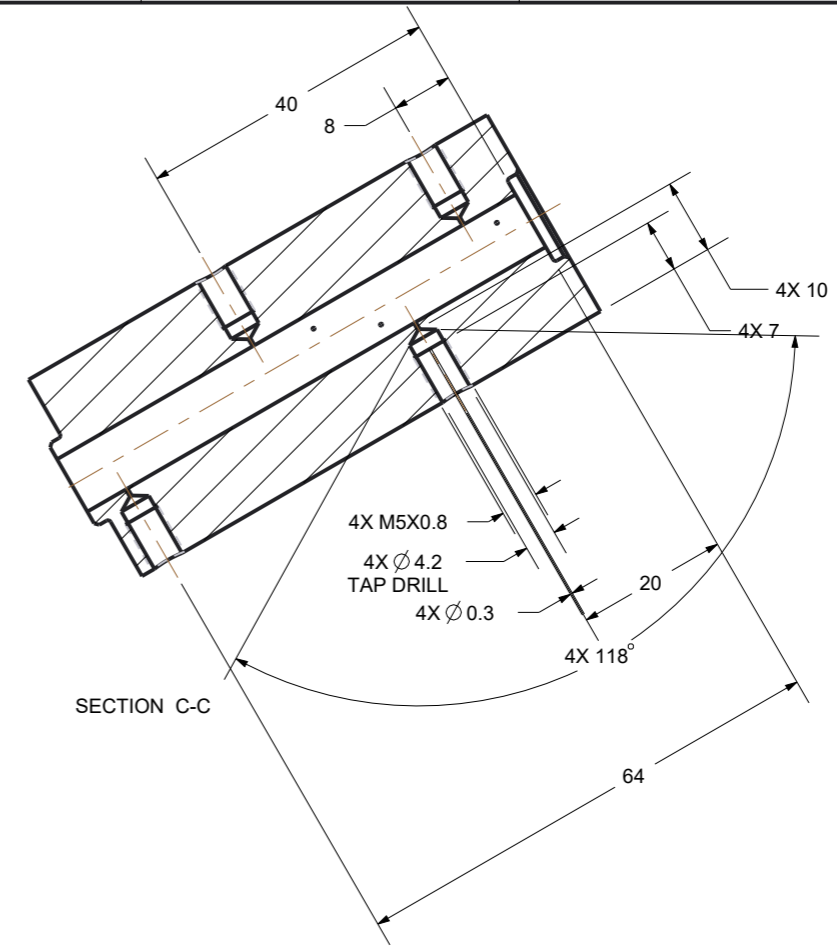
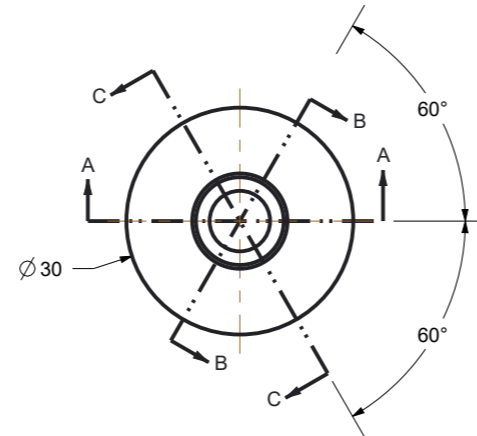


NOTES:
 1. BREAK ALL SHARP EDGES UNLESS OTHERWISE SPECIFIED.
 2. MATERIAL: DURALUMIN
 3. DIMENSIONING AND TOLERANCING ACCORDING TO ASME Y14.5

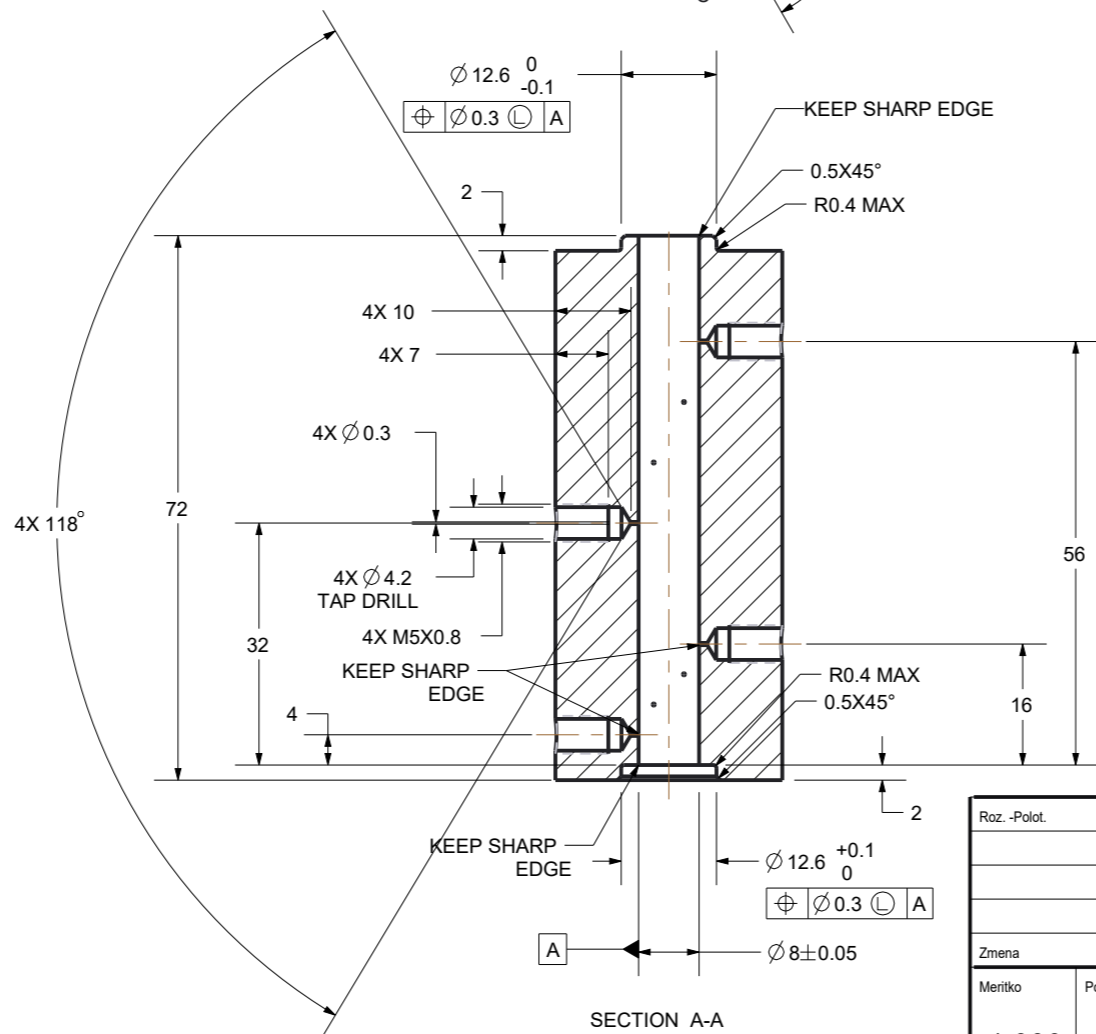
Roz. - Polot.				Presnos Tolerovani	
		c)		Mater.	Tr. odp
		b)		C. hm	Hr. hm.
		a)			
Zmena		Datum	Index	Podpisy	
Meritko	Pozn.	Navrhl			
0.500		Kreslil	A. GUANLAO		
C. seznamu		Prezkousel			
C. sestavy		Technolog			
Stary vykr.		Normaliz.			
Novy vykr.		Schvallil			
		Datum	05-04-2016		
				Nazev PRT0016	
				Cis. vykresu	
				list 1 listu1	



SECTION B-B




SECTION C-C



SECTION A-A

- NOTES:
 1. BREAK ALL SHARP EDGES UNLESS OTHERWISE SPECIFIED.
 2. MATERIAL:BRASS
 3. DIMENSIONING AND TOLERANCING ACCORDING TO ASME Y14.5

Roz. -Polot.		c)		Mater.	Tr. odp		Presnos
		b)		C. hm	Hr. hm.		Tolerovani
		a)					
Zmena	Datum	Index	Podpisy	 TU v Liberci Nazev PRT0017 Cis. vykresu list 1 listu1			
Meritko	Pozn.	Navrhl					
1.000		Kresil	A.GUANLAO				
C. seznamu		Prezkousel					
C. sestavy		Technolog					
Stary vykr.		Normaliz.					
Novy vykr.	Datum	Schvallil					
	04-04-2016	Datum					

1

2

3

4

A

A

B

B

C

C

D

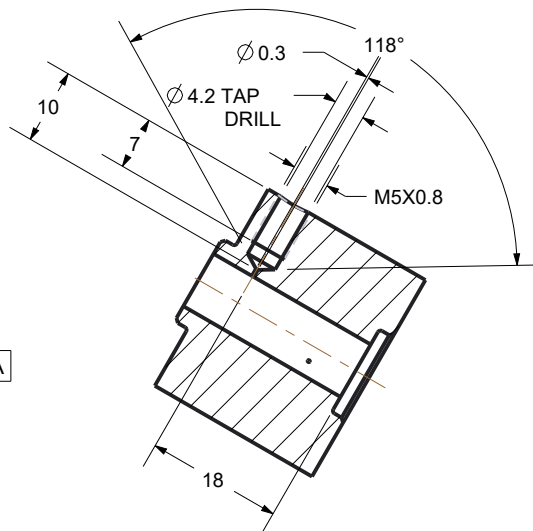
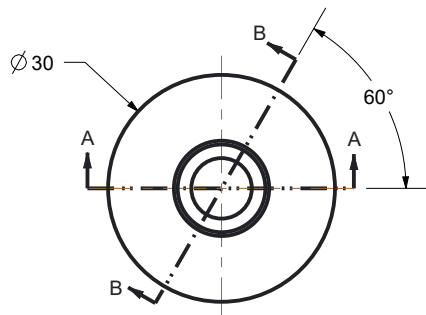
D

E

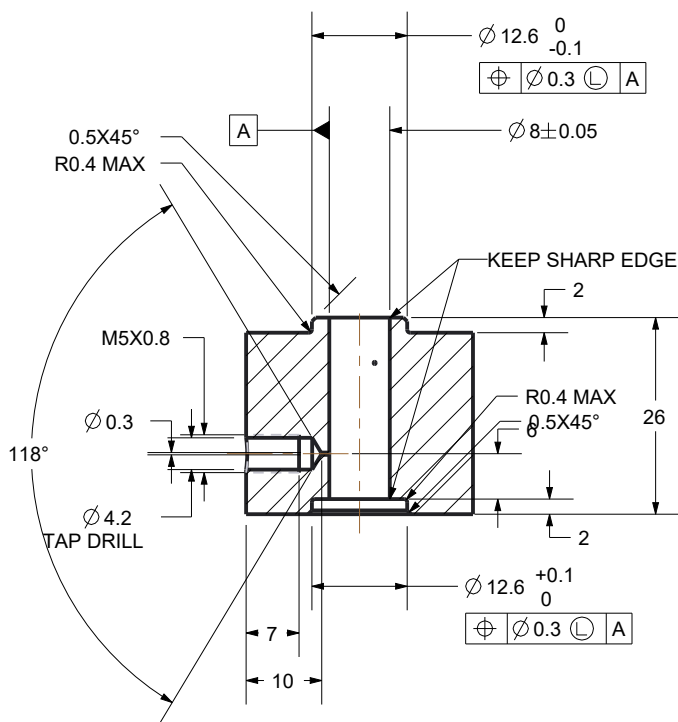
E

F

F



SECTION B-B



SECTION A-A

NOTES:

1. BREAK ALL SHARP EDGES UNLESS OTHERWISE SPECIFIED.
2. MATERIAL: BRASS
3. DIMENSIONING AND TOLERANCING ACCORDING TO ASME Y14.5

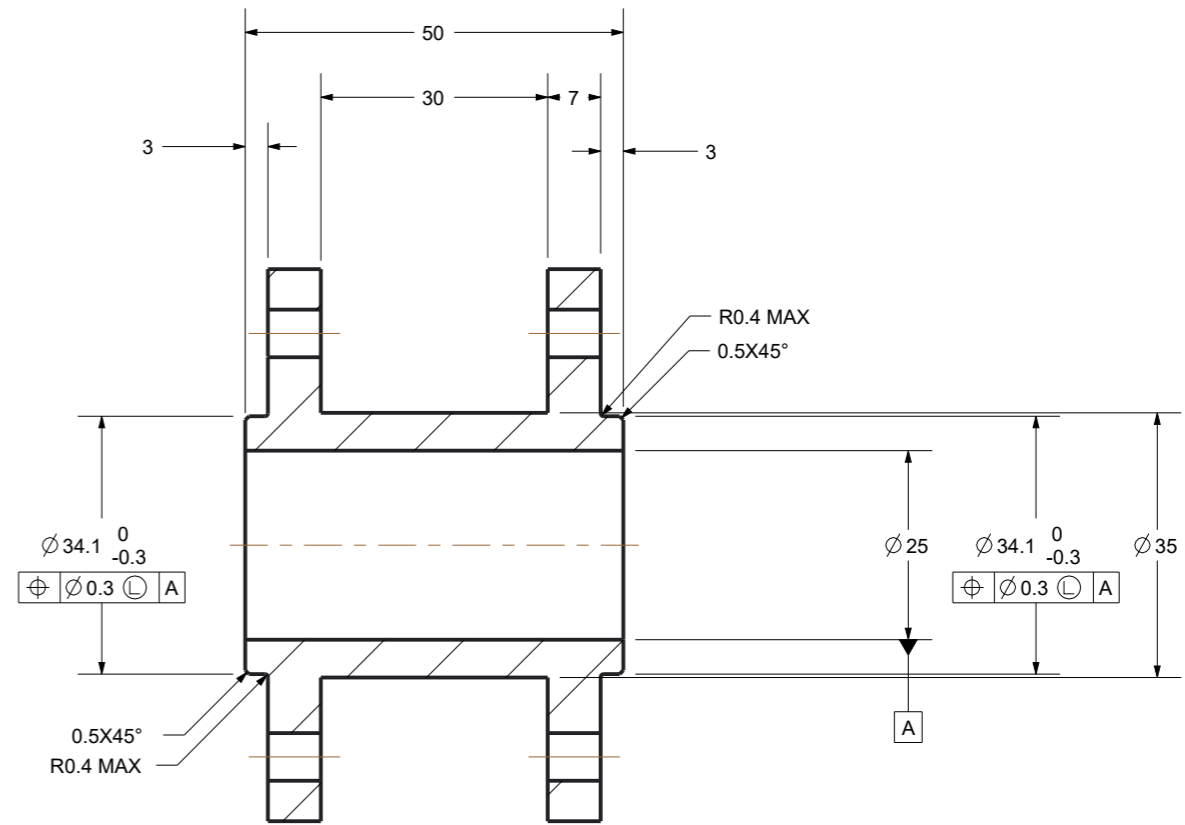
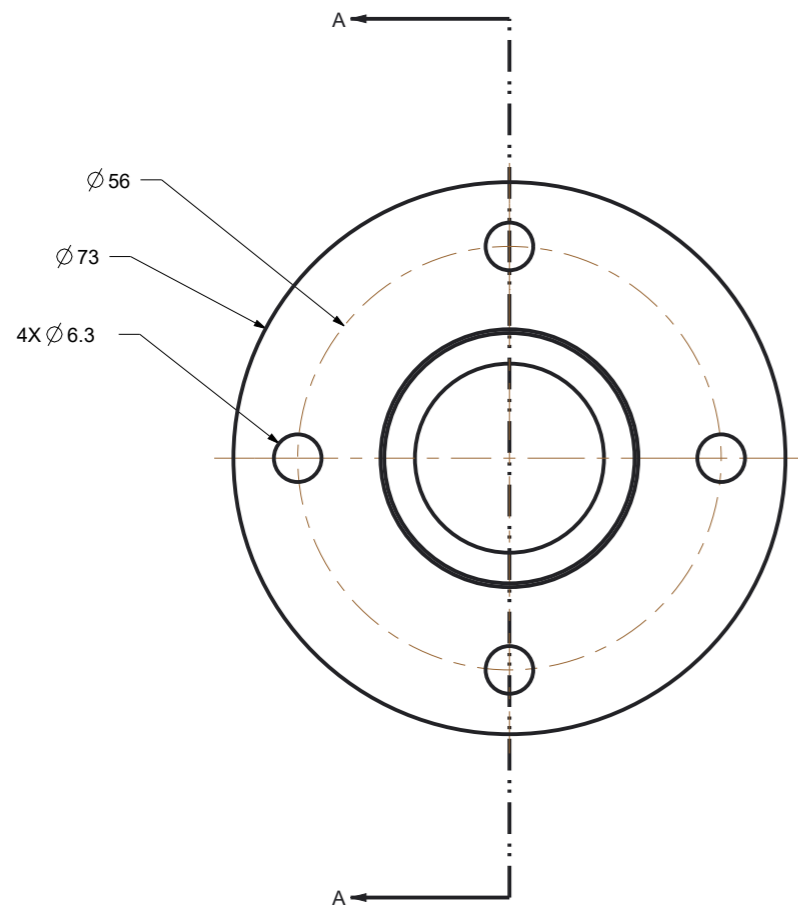
Roz. -Polot.				Mater.		Tr. odp.		Presnos Tolerovani	
		c)		C. hm		Hr. hm.			
		b)							
		a)							
Zmena		Datum		Index		Podpisy		 TU v Liberci Nazev PRT0018 Cis. vykresu	
Meritko		Navrhl		Kreslil		A.GUANLAO			
1.000		Prezkousel		Technolog					
C. seznamu		Normaliz.		Schvallil					
C. sestavy		Datum		03-04-2016					
Stary vykr.									
Novy vykr.								list 1 listu 1	

1

2

3

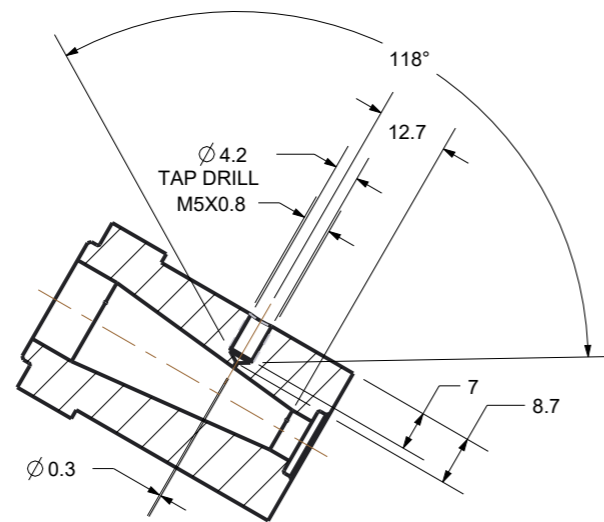
4



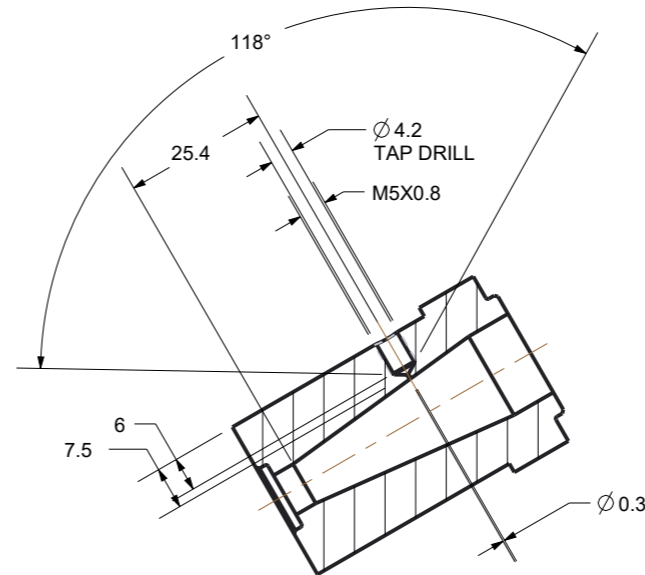
SECTION A-A

- NOTES:
 1. BREAK ALL SHARP EDGES UNLESS OTHERWISE SPECIFIED.
 2. MATERIAL:DURALUMIN
 3. DIMENSIONING AND TOLERANCING ACCORDING TO ASME Y14.5

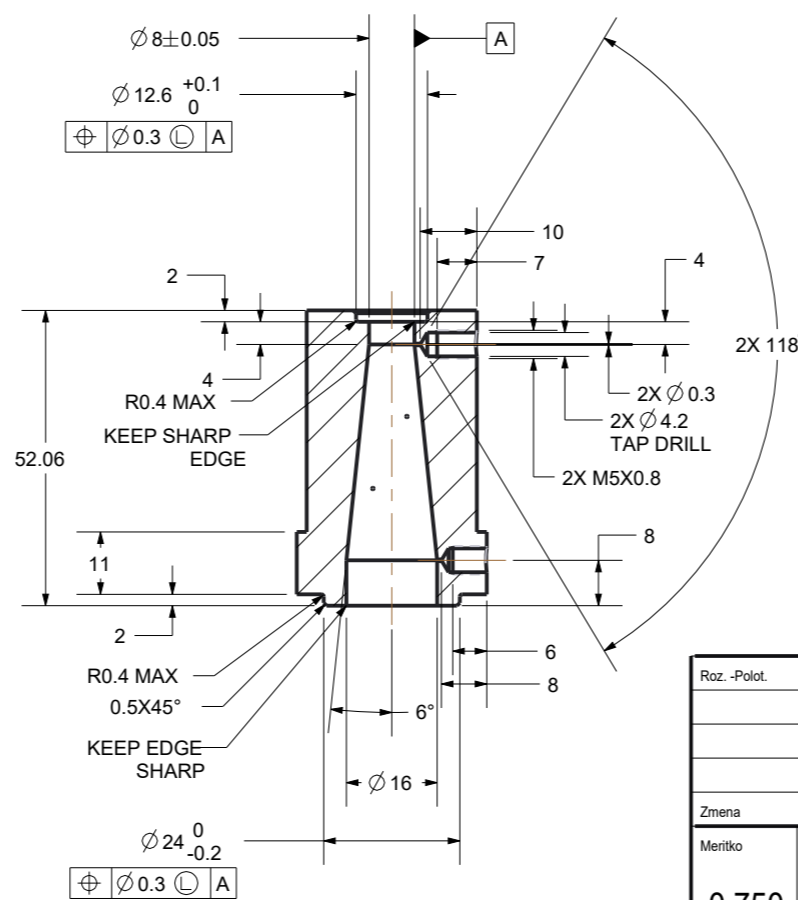
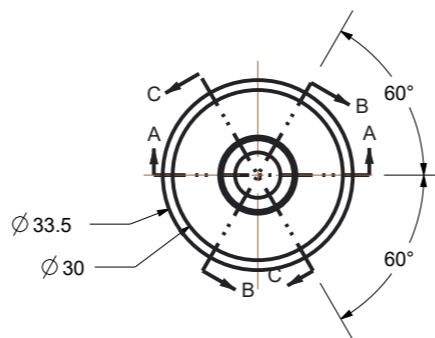
Roz. -Polot.				Presnos Tolerovani	
		c)		Mater.	Tr. odp
		b)		C. hm	Hr. hm.
		a)			
Zmena	Datum	Index	Podpisy	 TU v Liberci Nazev PRT0019 Cis. vykresu list 1 listu1	
Meritko	Pozn.	Navrhl			
1.000		Kreslil	A. GUANLAO		
C. seznamu		Prezkousel			
C. sestavy		Technolog			
Stary vykr.		Normaliz.			
Novy vykr.		Schvalil			
		Datum	05-04-2016		



SECTION B-B



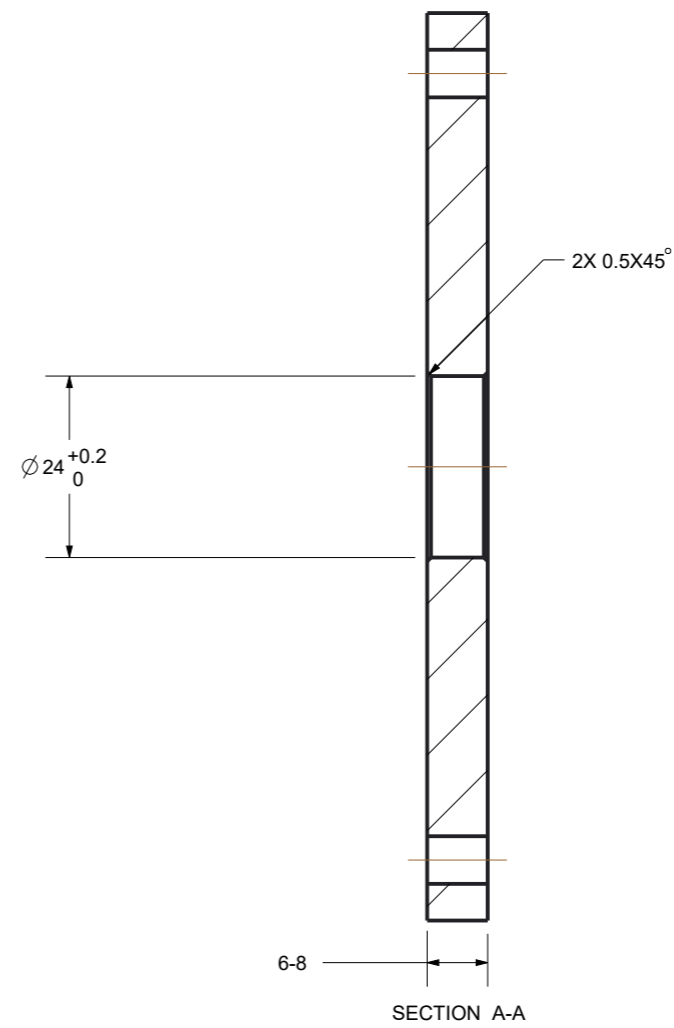
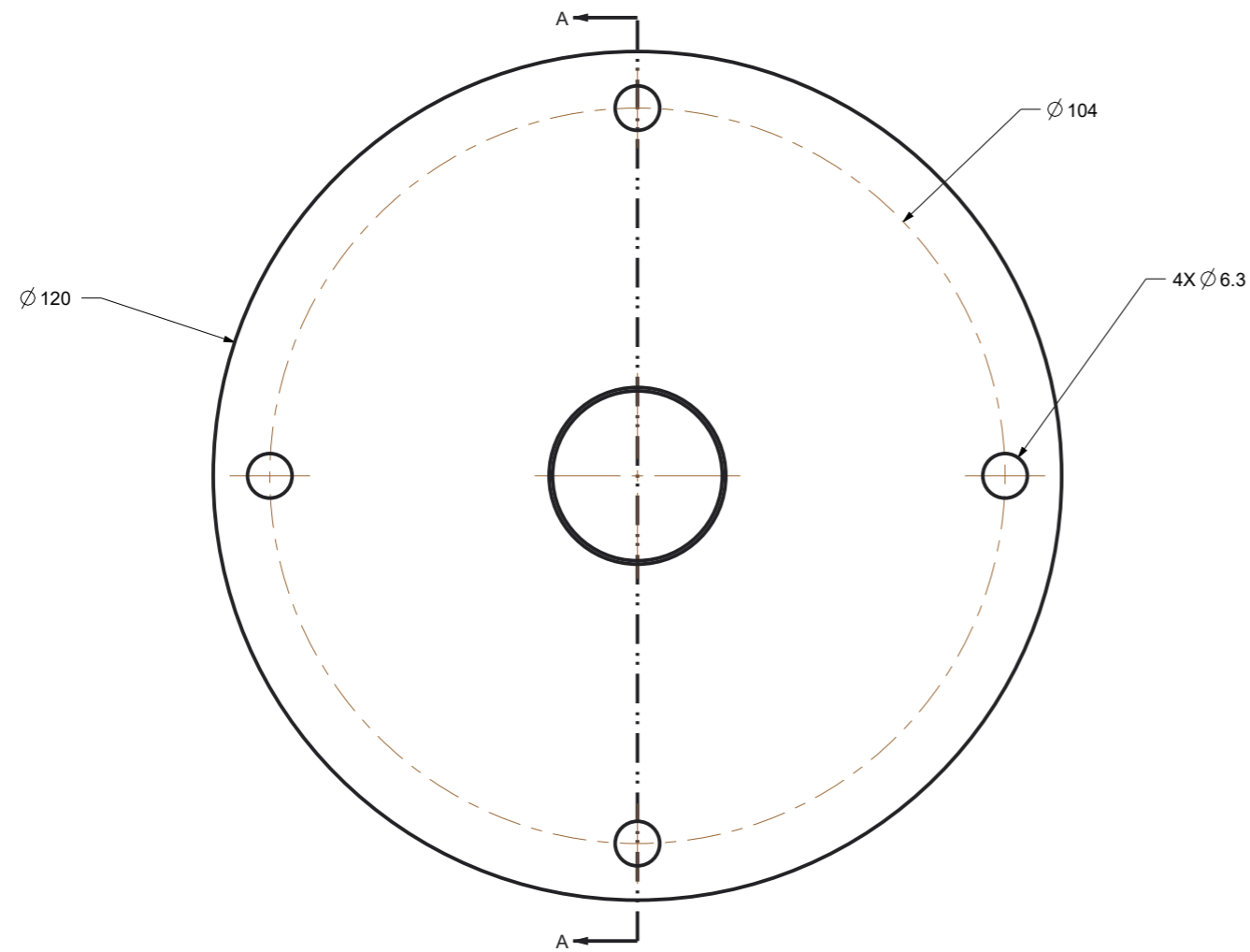
SECTION C-C



SECTION A-A

- NOTES:
 1. BREAK ALL SHARP EDGES UNLESS OTHERWISE SPECIFIED.
 2. MATERIAL:BRASS
 3. DIMENSIONING AND TOLERANCING ACCORDING TO ASME Y14.5

Roz. -Polot.		c)		Mater.	Tr. odp		Presnos
		b)		C. hm	Hr. hm.		Tolerovani
		a)					
Zmena	Datum	Index	Podpisy				
Meritko	Pozn.	Navrhl					
0.750		Kresil	A.GUANLAO				
C. seznamu		Prezkousel					
C. sestavy		Technolog		Nazev	PRT0020		
Stary vykr.		Normaliz.		Cis. vykresu			
Novy vykr.		Schvallil					
		Datum	04-04-2016				list 1 listu1



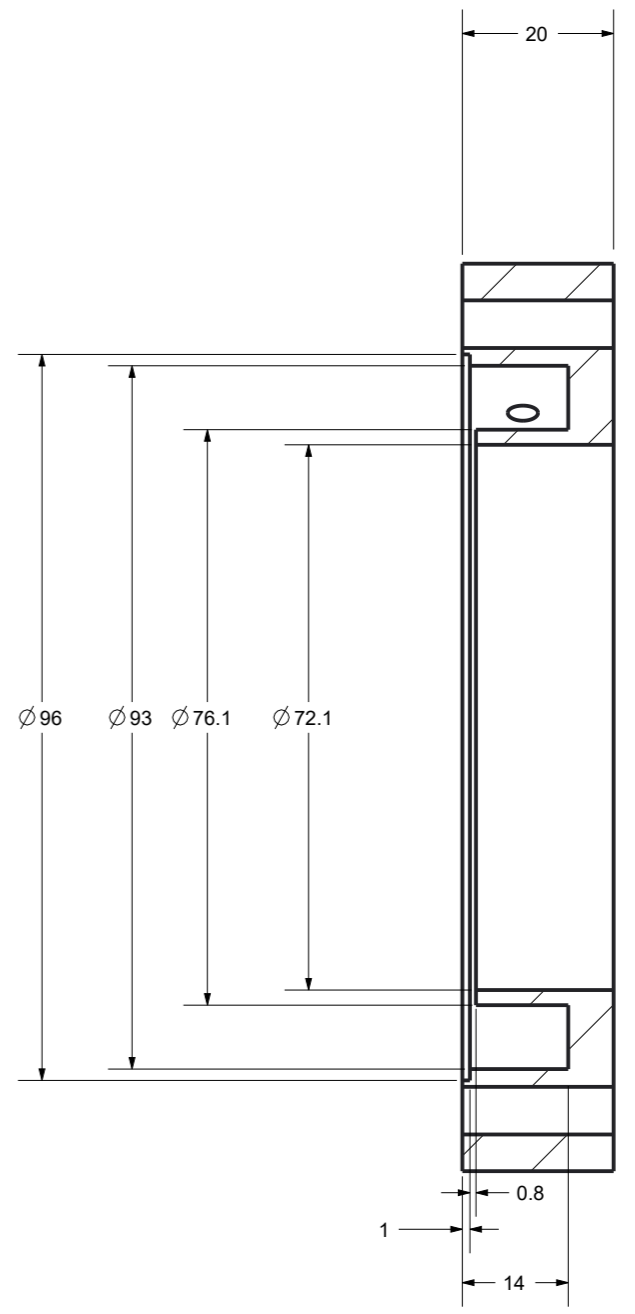
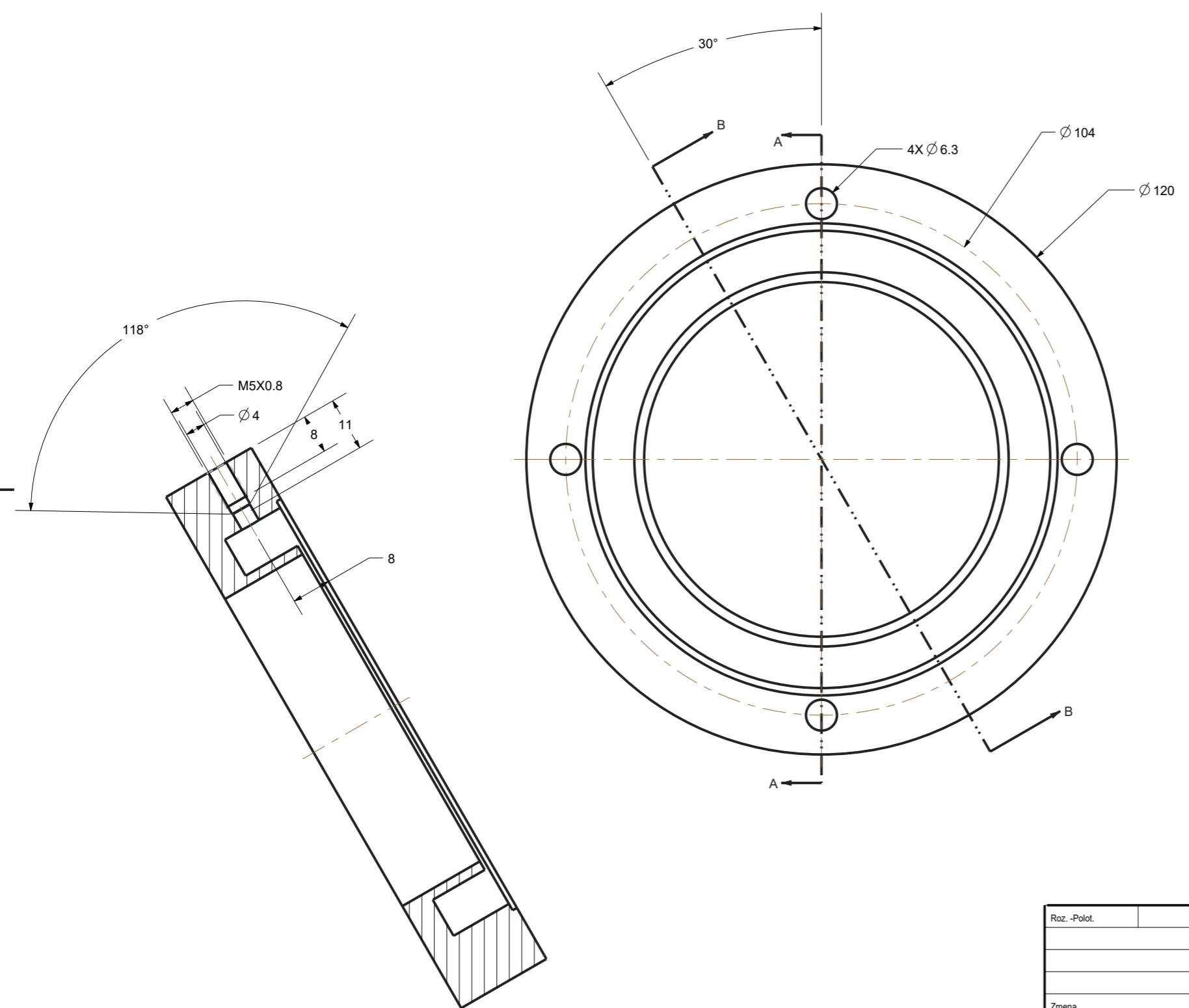
- NOTES:
 1. BREAK ALL SHARP EDGES UNLESS OTHERWISE SPECIFIED.
 2. MATERIAL:BRASS
 3. DIMENSIONING AND TOLERANCING ACCORDING TO ASME Y14.5

Roz. -Polot.				Presnos Tolerovani	
		c)		Mater.	Tr. odp
		b)		C. hm	Hr. hm.
		a)			
Zmena	Datum	Index	Podpisy	 TU v Liberci Nazev PRT0021 Cis. vykresu list 1 listu1	
Meritko	Pozn.	Navrhil			
1.000		Kresilil	A. GUANLAO		
C. seznamu		Prezkousel			
C. sestavy		Technolog			
Stary vykr.		Normaliz.			
Novy vykr.		Schvalil			
		Datum	05-04-2016		

1 2 3 4 5 6 7 8

A
B
C
D
E
F

NOTES:
 1. BREAK ALL SHARP EDGES UNLESS OTHERWISE SPECIFIED.
 2. MATERIAL: DURALUMIN
 3. DIMENSIONING AND TOLERANCING ACCORDING TO ASME Y14.5

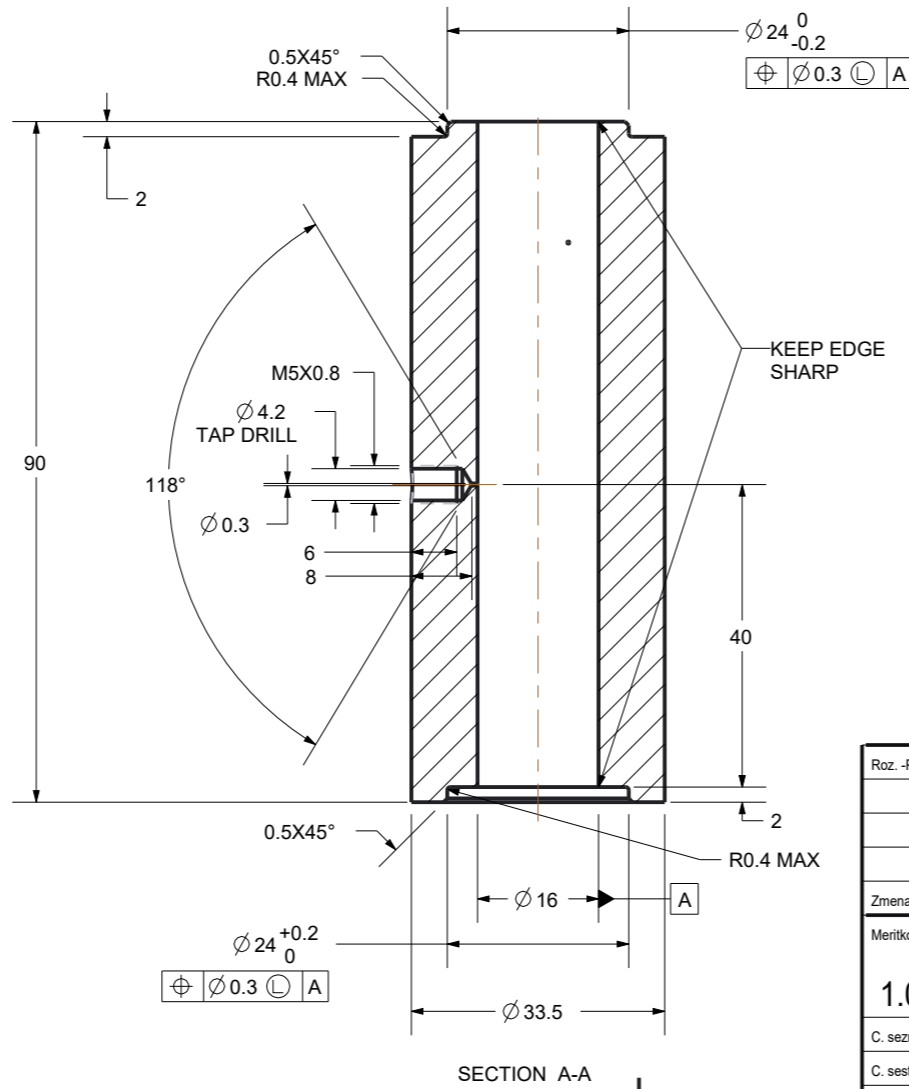
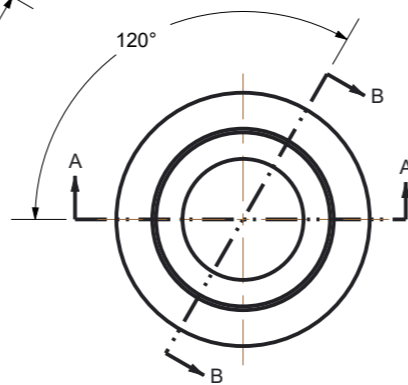
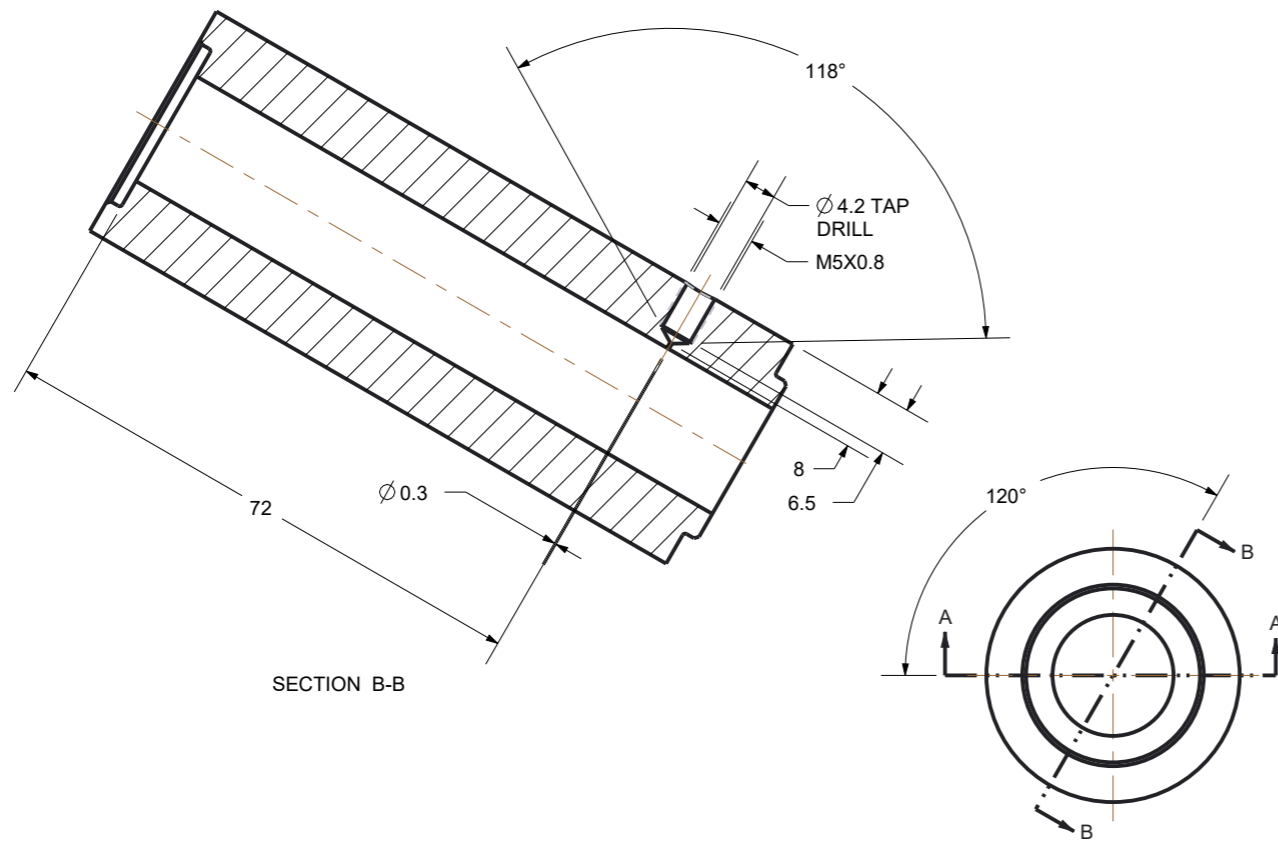


SECTION A-A

SECTION B-B

Roz. - Polot.		c)		Mater.	Tr. odp		Presnos
		b)		C. hm	Hr. hm.		Tolerovani
		a)					
Zmena	Datum	Index	Podpisy				
Meritko	Pozn.	Navrhil					
1.000		Kresilil	A. GUANLAO				
C. seznamu		Prezkousel					
C. sestavy		Technolog		Nazev	PRT0024		
Stary vykr.		Normaliz.		Cis. vykresu			
Novy vykr.		Schvallil					
		Datum	05-04-2016				list 1 listu 1

1 2 3 4 5 6 7 8



- NOTES:
 1. BREAK ALL SHARP EDGES UNLESS OTHERWISE SPECIFIED.
 2. MATERIAL:BRASS
 3. DIMENSIONING AND TOLERANCING ACCORDING TO ASME Y14.5

Roz. -Polot.				Presnos Tolerovani	
		c)		Mater.	Tr. odp
		b)		C. hm	Hr. hm.
		a)			
Zmena	Datum	Index	Podpisy	 TU v Liberci Nazev PRT0027 Cis. vykresu list 1 listu1	
Meritko	Pozn.	Navrhil			
1.000		Kresilil			
C. seznamu		Prezkousel			
C. sestavy		Technolog			
Stary vykr.		Normaliz.			
Novy vykr.	Datum	Schvallil			
		Datum	14-04-2016		

1

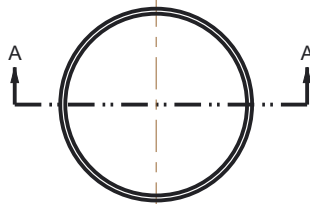
2

3

4

A

A



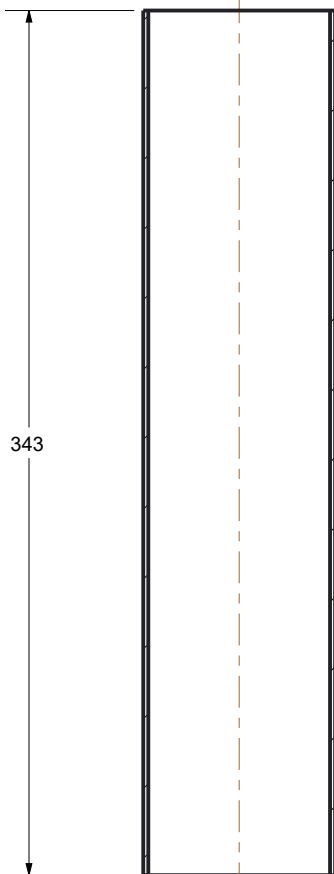
B

B

PIPE STOCK MATERIAL:
76.1X2.0 MM EN 1.4301(AISI304)

C

C



SECTION A-A

D

D

E

E

Roz. -Polot.						Presnos		
		c)		Mater.		Tr. odp	Tolerovani	
		b)		C. hm		Hr. hm.		
		a)						
Zmena		Datum	Index	Podpisy	TU v Liberci			
Meritko	Pozn.	Navrhl						
0.333		Kreslil			Nazev PRT0028			
C. seznamu		Prezkousel						
C. sestavy		Technolog			Cis. vykresu			
Stary vykr.		Normaliz.						
Novy vykr.		Schvalll			list 1 listu1			
		Datum	09-05-2016					

1

2

3

4

F

F

1

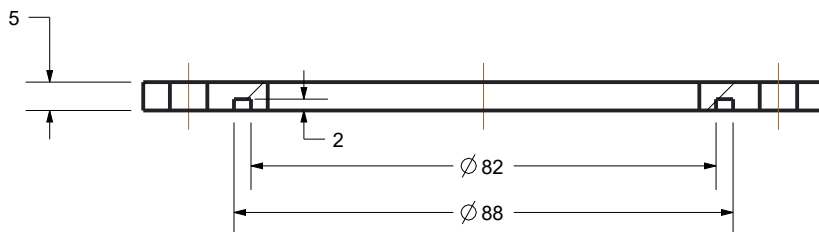
2

3

4

A

A



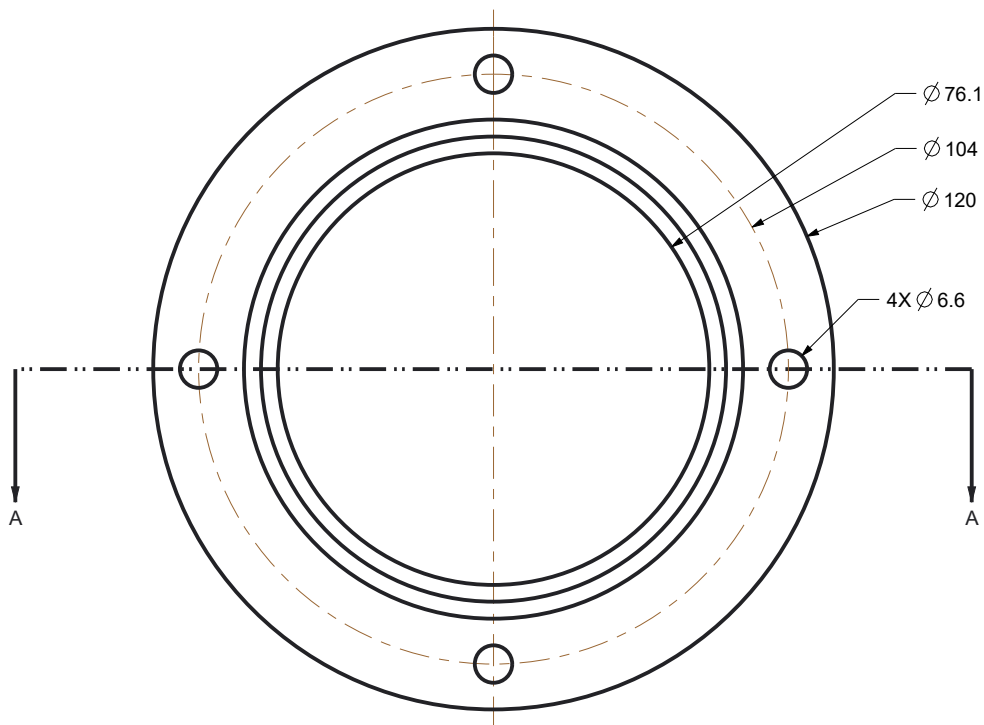
SECTION A-A

B

B

C

C



D

D

E

E

F

F

Roz. -Polot.						Presnos	
		c)		Mater.	AISI301/304	Tr. odp	Tolerovani
		b)		C. hm		Hr. hm.	
		a)					
Zmena		Datum	Index				
Meritko	Pozn.	Navrhl	Podpisy	TU v Liberci			
0.750		Kreslil		Nazev PRT0030			
C. seznamu		Prezkousel		Cis. vykresu			
C. sestavy		Technolog					
Stary vykr.		Normaliz.					
Novy vykr.		Schvallil					
		Datum	28-04-2016	list 1 listu 1			

1

2

3

4

1

2

3

4

A

A

B

B

C

C

D

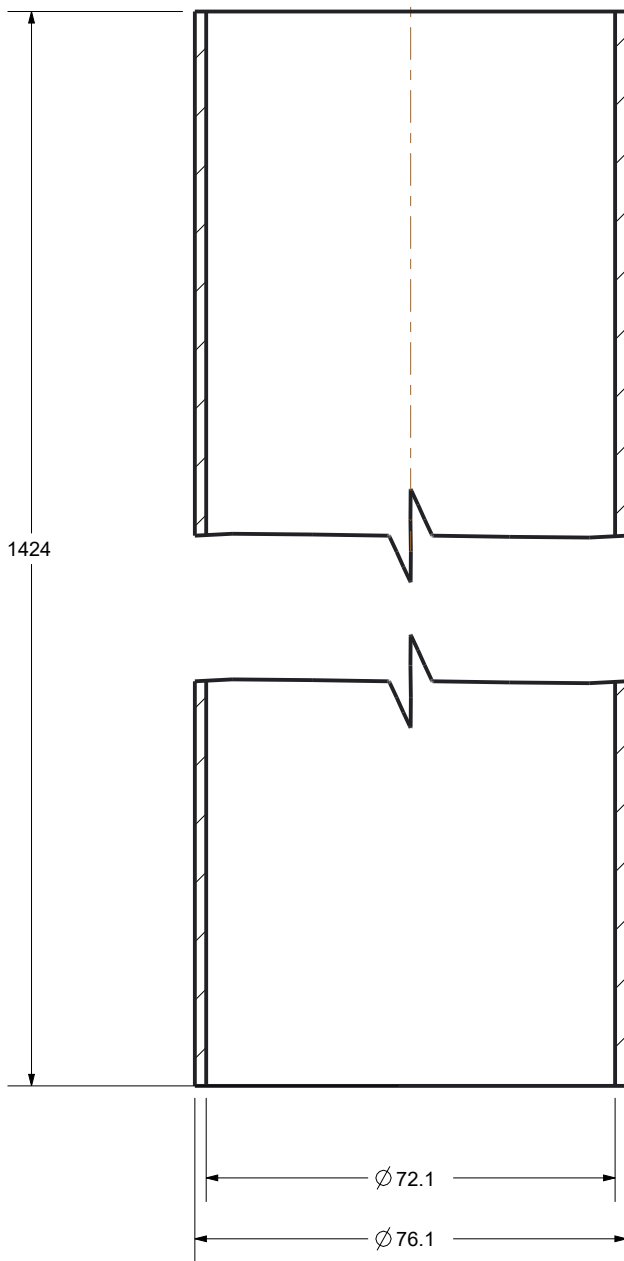
D

E

E

F

F



PIPE STOCK MATERIAL:
76.1X2.0 MM EN 1.4301(AISI304)

SECTION A-A

Roz. -Polot.						Presnos		
		c)			Mater.	Tr. odp		
		b)			C. hm	Hr. hm.		
		a)						
Zmena		Datum	Index	Podpisy				
Meritko	Pozn.	Navrhl						
0.750		Kreslil			Nazev PRT0031			
C. seznamu		Prezkousel						
C. sestavy		Technolog			Cis. vykresu			
Stary vykr.		Normaliz.						
Novy vykr.		Schvallil			list 1 listu1			
		Datum	09-05-2016					

1

2

3

4

1

2

3

4

A

A

B

B

C

C

D

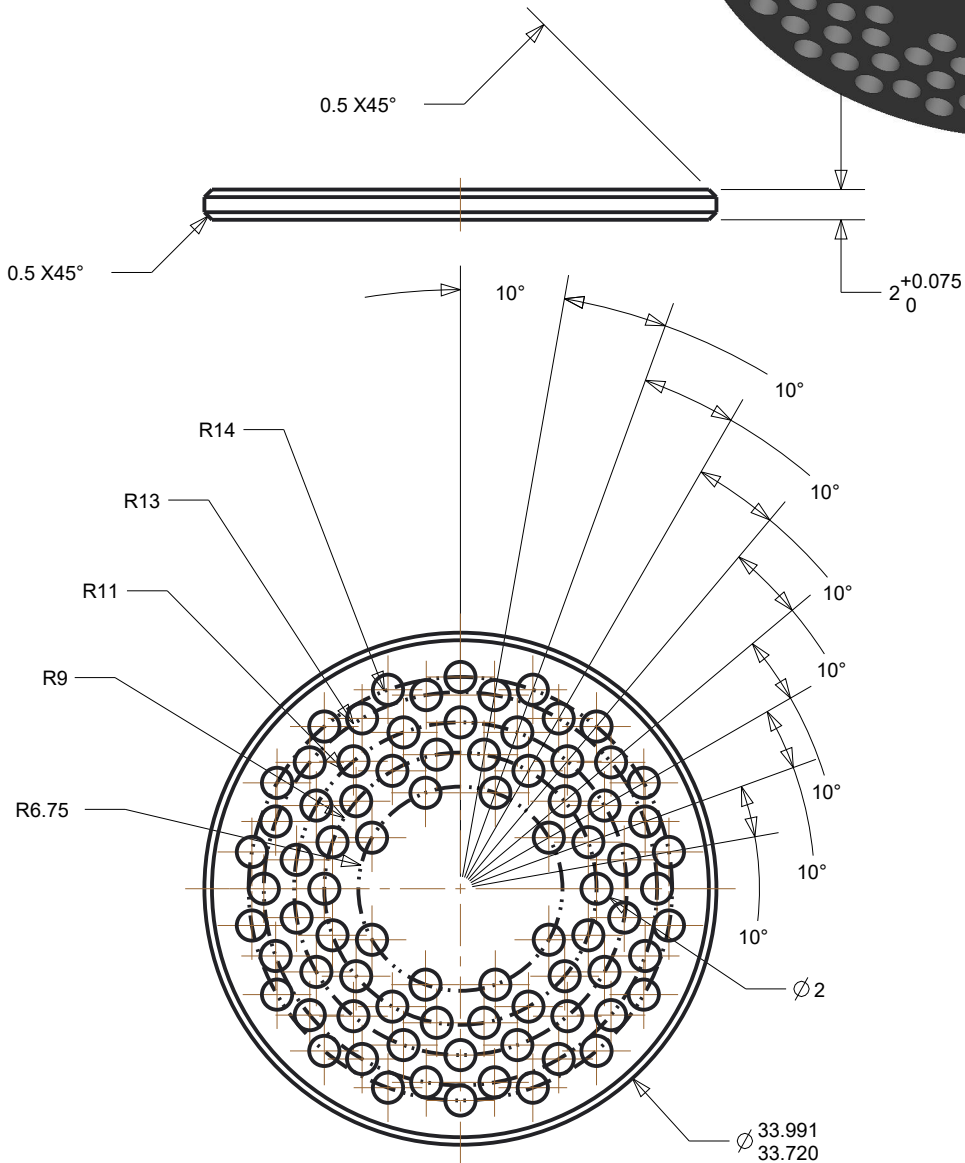
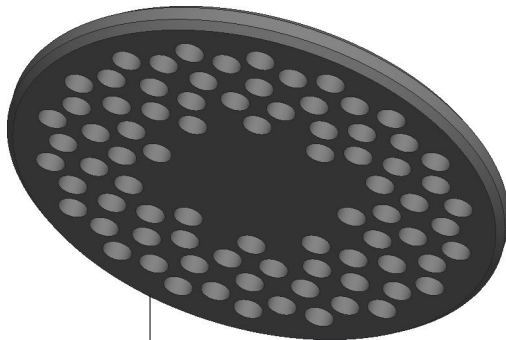
D

E

E

F

F



NOTES:

- 1. BREAK ALL SHARP EDGES UNLESS OTHERWISE SPECIFIED.
- 2. ALL CORNER FILLET R0.4 MAX
- 3. MATERIAL:BRASS
- 4. DIMENSIONING AND TOLERANCING ACCORDING TO ASME Y14.5

GENERIC TOLERANCE:

- XX ± 0.125
- XX.X ± 0.075
- XX.XX ± 0.050
- XX° ± 0.01

Roz. -Polot.						Presnos	
		c)		Mater.	Tr. odp		Tolerovani
		b)		C. hm	Hr. hm.		
		a)					
Zmena		Datum	Index	Podpisy			
Meritko	Pozn.	Navrhl					
2.000		Kreslil	A. GUANLAO				
C. seznamu		Prezkousel					
C. sestavy		Technolog					
Stary vykr.		Normaliz.					
Novy vykr.		Schvallil					
		Datum	02-03-2016				
						TU v Liberci	
				Cis. vykresu		list 1 listu1	

1

2

3

4

1

2

3

4

A

A

B

B

C

C

D

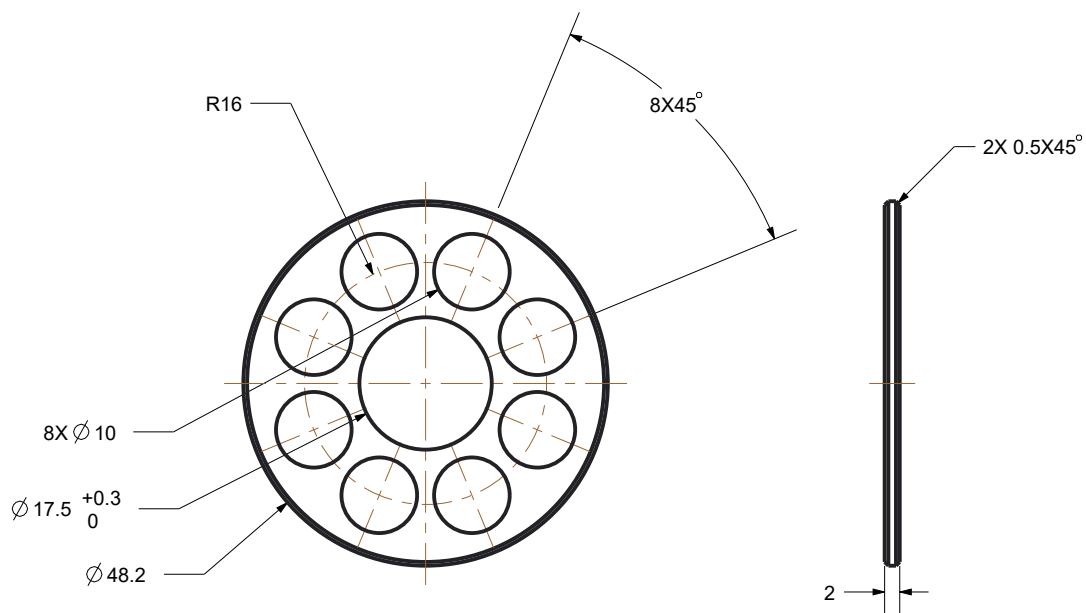
D

E

E

F

F



NOTES:

1. BREAK ALL SHARP EDGES UNLESS OTHERWISE SPECIFIED.
2. MATERIAL:BRASS
3. DIMENSIONING AND TOLERANCING ACCORDING TO ASME Y14.5

Roz. -Polot.						Presnos	
		c)		Mater.	Tr. odp		Tolerovani
		b)		C. hm	Hr. hm.		
		a)					
Zmena		Datum	Index				
Meritko	Pozn.	Navrhl	A.GUANLAO				
1.000		Kreslil	A. GUANLAO	Nazev PLATE2			
C. seznamu		Prezkousel					
C. sestavy		Technolog		Cis. vykresu			
Stary vykr.		Normaliz.					
Novy vykr.		Schvallil		list 1 listu1			
		Datum	28-03-2016				

1

2

3

4